dortmund university

Dissertation

The role of LIPG in regulating cholesterol homeostasis in cancer

Zur Erlangung des akademischen Grades des Doktors der Naturwissenschaften (Dr. rer. nat.)

Vorgelegt an der Fakultät für Chemie und Chemische Biologie an der Technischen Universität Dortmund

Von Zhwan Mahmoud

Dortmund, November 2024

Erstgutachter: Prof. Dr. Jan G. Hengstler

Zweitgutachter: Prof. Dr. Christoph van Thriel

IfADo LEIBNIZ RESEARCH CENTRE FOR WORKING ENVIRONMENT AND HUMAN FACTORS

Content

Für meine Familie

List of abbreviations

β-mCD	β-methyl-cyclodextrin
µL	microliter
µM	micromolar
ABCA1	ATP binding cassette subfamily A member 1
ABCG1	ATP binding cassette subfamily G member 1
Acetyl-CoA	acetyl coenzyme A
ACYL	ATP-citrate lyase
AKT	proteinkinase B
AMPK	AMP-activated proteinkinase
ApoA1	apolipoprotein A1
APS	ammoniumperoxodisulfate
ATP	adenosine triphosphate
BAD	Bcl-2-antagonist of cell death
BCA	bicinchoninic acid assay
cDNA	copy DNA
CD36	cluster of differentiation 36
CHL	Chinese Hamster Lung
COX2	cyclooxygenase 2
CTB	cell titer blue
CT-value	cycle threshold
DAG	diacylglyceride
DNA	deoxyribonucleic acid
dNTP	nucleic triphosphates
ECL	enhanced chemiluminescence
ECGS /H	Endothelial cell growth supplement with heparin
ECM	extracellular matrix
EDTA	ethylenaminetetraacetic acid
EGFR	epidermal growth factor receptor

EOC	epithelial ovarian cancer
ER	estrogen receptor
ErbB	receptor tyrosine kinases
ERK1/2	extra-cellular signal regulated kinase 1/2
ERK5	extra-cellular signal regulated kinase 5
FA	fatty acids
FAK	focal adhesion kinase
FASN	fatty acid synthase
FBS	fetal bovine serum
FM	full media
FRET	förster-resonance electron transfer
g	gram
GAP	GTPAse activating protein
GDI	guanosine nucleotide dissociation inhibitor
GDP	guanosine diphosphate
GEF	Guanine exchange factor
GSPx	glutathione peroxidase
GTP	guanosine triphosphate
h	hour
HDL	high-density lipoproteins
HER2	human epidermal growth factor receptor
HMG-CoA	3-hydroxy-3-methylglutaryl coenzym-A
HMGCR	3-hydroxy-3-methylglutaryl coenzym-A reductase
HRP	horse radish peroxidase
HSPGs	heparin-sulfate proteoglycans
HUVEC	human umbilical vein endothelial cells
ICAM1	intercellular adhesion molecule 1
IDL	Intermediate density lipoprotein
KD	knockdown
kDa	kilo dalton
LCAT	lecithin cholesterin acyltransferase
LDL	low-density lipoproteins

LDLR	LDL receptor
LIPG	endothelial lipase G
LPC	lysophosphatidylcholine
LPL	lipoprotein lipase
LXR	liver X receptor
mA	milliampere
MAPK	mitogen activated protein kinase
min	minute
mL	milliliter
mM	millimolar
mRNA	messenger RNA
NEAA	non-essential amino acids
NFκB	Nuclear factor kappa
nm	nanometer
OE	overexpression
PAF-AH	plasma platelet activating factor-acetylhydrolase
pAKT	phosphorylated proteinkinase B
PBS	phosphate buffered solution
PCR	polymerase chain reaction
PDZK	PDZ domain-containing adaptor protein
pERK1/2	phosphorylated extra-cellular signal regulated kinase 1/2
pERK5	phosphorylated extra-cellular signal regulated kinase 5
pFAK	phosphorylated focal adhesion kinase
PC	phosphatidylcholine
PGI2	prostacyclin
PgR	progesterone receptor
PI3K	phosphoinositide 3 kinase
PON1	paraoxonase 1
pPCs	proprotein convertases
PR	progesterone receptor

qPCR	quantitative polymerase chain reaction
RCT	Reverse cholesterol transport
RISC	RNA-induced silencing complex
RNA	ribonucleic acid
RT	room temperature
RT-PCR	real time-PCR
ROS	Reactive oxygen species
S1P	sphingosine-1-phosphate
SCARB1	scavenger receptor 1 gene
SDS-PAGE	sodiumdodecylsulfate-polyacrylamide gel electrophoresis
siRNA	single interference RNA
SOAT	sterol-O-acyltransferase
SR-BI	scavenger receptor 1 protein
SRC	non-receptor tyrosine kinase
SRE	sterol regulatory element
SREBP	sterol regulatory element binding protein
STAT3	signal transducer and activator of transcription 3
TAG	triglycerides
TEMED	tetraethylethylenamine
TGFβ	transforming growth factor β
TLR2	toll-like receptor 2
TME	Tumor microenviornment
TNBC	triple negative breast cancer
w/v	mass concentration
VCAM1	vascular cell adhesion molecule 1
v/v	volume percent

1. Abstract

In breast cancer, the endothelial lipase or lipase G (LIPG) is highly expressed in a limited subset of tumors and significantly associated with shorter metastasis-free survival in node-negative, untreated patients. [1] LIPG is a cell surface-associated protein with multiple actions on serum lipoproteins that influence the cellular lipid profile. It preferentially displays phospholipase A1 activity towards phosphatidylcholine present in high density lipoproteins (HDL). In addition, independently of its enzymatic activity it also functions as a bridging molecule, promoting the binding of lipoproteins to cells. In a previous study performed at IfADo, it was shown that LIPG supports the survival of tumor cells under oxidative stress *via* lipolysis of HDL, followed by uptake of released fatty acids that become incorporated into lipid droplets. [1] However, a role of LIPG in tumor cholesterol homeostasis *via* interactions with lipoproteins and a possible contribution of this process to metastasis has not been studied so far. LIPG was knocked down by silencing with siRNA oligos in MDA-MB-468 and HCC1954 cells. Cell adhesion assays, plating the cells to different components of the extracellular matrix, as well as cell-adhesion to endothelial cells and cell migration assays were performed. Gene expression changes were studied by real time qPCR and Western Blot. Human serum-derived native HDL and LDL were used for studying cholesterol exchange with cells. Total, free and esterified cholesterol was quantified with a cholesterol quantification kit. Silencing LIPG in breast cancer cells resulted in slower cell adhesion and migration, and this was accompanied by reduced expression/activation of the focal adhesion kinase (FAK). Loss of LIPG also led to expression changes in cholesterol and lipoprotein metabolism genes. Most prominent changes were observed for scavenger receptor 1 transcript (*SCARB1)* which was downregulated both at the mRNA and protein level. *SCARB1* encodes the main HDL-receptor scavenger receptor 1 (SR-BI) protein which mediates cholesterol exchange between cells and HDL particles. Thus, downregulation of this gene in LIPG silenced cells indicated compromised HDL-dependent cholesterol exchange mechanisms. Accordingly, free cholesterol levels in LIPG depleted cells were increased after incubation with HDL. In addition, HDL-triggered cell signaling events were altered in the absence of LIPG.

In conclusion, this study has identified a role for LIPG in tumor cholesterol homeostasis *via* regulation of cellular cholesterol exchange with lipoproteins and lipoprotein-

dependent signaling processes. Since cholesterol metabolism contributes to tumor cell metastasis, LIPG may promote processes related to metastasis, like cell adhesion and migration *via* regulation of optimal cellular cholesterol levels or cholesterol trafficking processes.

1. Zusammenfassung

Die endothelilale Lipase G (LIPG) ist hoch exprimiert in einer bestimmten Subgruppe in Brustkrebs. Eine hohe LIPG-Expression ist mit einer kürzeren, metastasefreien Überlebensrate bei unbehandelten Patienten, ohne Lymphknotenbefall, assoziiert. [1] LIPG ist ein zelloberflächen-assoziiertes Protein mit mehrfachem Einfluss auf Lipoproteine im Serum, welches das zelluläre Lipidprofil beeinflusst. LIPG besitzt eine Phospholipase A1 Aktivität in Bezug auf Phosphatidylcholine in „*High-Density*" Lipoproteinen (HDL). Unabhängig von der enzymatischen Aktivität fungiert LIPG als Überbrückungsmolekül zwischen Lipoproteinen und der Zelloberfläche. Aus einer vorangegangenen Arbeit ging hervor, dass LIPG das Tumorwachstum unter oxidativem Stress fördert. Das Tumorwachstum wird gefördert durch die Lipolyse von HDL, der darauffolgenden Aufnahme freier Fettsäuren und der Einlagerung der Fettsäuren in Lipidtröpfchen. [1] Eine potenzielle Rolle von LIPG bei der Erhaltung der Cholesterolhomöostase über Interaktionen mit Lipoproteinen und deren Einfluss auf die Tumormetastasierung wurde noch nicht erforscht. Um dies zu untersuchen, wurde LIPG durch Interventionen mit siRNA Oligos in MDA-MB-468 und HCC1954Luc Zellen runterreguliert. Hierfür wurden Zelladhäsionsexperimente auf verschiedenen extrazellulären Matrix (ECM) Komponenten, sowie Zellmigrationsexperimente durchgeführt. Genexpressionsveränderungen wurden anhand von *real time* qPCR und *Western blot* untersucht. Humanes, natives LDL und HDL wurden zur Analyse des Cholesterolaustausches verwendet. Totales, freies und verestertes Cholesterol wurden quantifiziert durch die Verwendung eines Cholesterol Quantifizierungskits. Als Antwort auf die Herunterregulierung von LIPG in Brustkrebszellen wurden eine verlangsamte Zelladhäsion auf verschiedenen Matrixproteinen und eine reduzierte Zellmigration beobachtet. Dies wurde begleitet von einer verminderten Expression der Fokale Adhäsionskinase (FAK). Ein Verlust an LIPG-Expression resultierte ebenfalls in Expressionsveränderungen von Cholesterol- und Lipoproteinmetabolismus Genen. Die größte Veränderung wurde in der Expression von *SCARB1* beobachtet, welches sowohl auf mRNA und Proteinebene runterreguliert wurde. *SCARB1* kodiert den HDL Rezeptor SR-BI, welcher für den Cholesterolaustausch zwischen HDL und der Zelle zuständig ist. Als Folge dieser Veränderung zeigten Brustkrebszellen eine Akkumulation von freiem, zellulärem Cholesterol. Ebenfalls beeinträchtigt waren Signaltransduktionswege, die von HDL stimuliert werden.

Zusammenfassend hat diese Arbeit eine neue Rolle für LIPG in der Tumor-Cholesterolhomöostase durch die Regulierung des zellulären Cholesterolaustausches zwischen Tumorzellen und Lipoproteinen und lipoproteinabhängigen Signalprozessen identifiziert. Da der Cholesterolmetabolismus eine wichtige Rolle in der Tumorzellmetastasierung spielt, könnte LIPG tumorrelevante Metastasierungsprozesse, wie Zelladhäsion und Migration, über die Regulation optimaler, zellulärer Cholesterollevel steuern.

2. Introduction

2.1 Prevalence of breast cancer and ovarian cancer

In 2021 breast cancer was the second highest cause of death worldwide, after lung cancer, in woman. The last years the death rate was declining due to better therapeutics and screenings. Nevertheless, metastasis and reoccurring cancer is still contributing the most to cancer morbidity. [2] Breast cancer subtypes show different rates of overall metastasis, different metastasis sites and different overall survival rates. [3], [4]

Table 1: Breast cancer subtypes and survival rates after metastasis.

Classification	**Immunoprofile**	**Proliferation**	**Metastasis sites**	**Survival rate**
Luminal A	ER+/HER2-	Low	Bone	3rd poorest
Luminal B	ER+/HER2+	High	Bone	3rd poorest
TNBC	ER-/HER2-	High	Liver, Brain	poorest
HER2	ER-/HER2+	High	Lung, Liver	2nd poorest

In Table 1 the breast cancer subtypes are listed. The categorization is based on the expression of growth receptors: estrogen receptor (ER), progesterone receptor (PR) and human epidermal growth factor receptor 2 (HER2). Luminal cancer is the most common breast cancer subtype (64.3%), whereas triple negative breast cancer (TNBC) accounts for the poorest survival rate. This may be because of the aggressive clinical course and the lack of targeted therapy.

Ovarian cancer is attributing to 2.1% of overall cancer related death in 2021 for women. The survival rate of the diagnosed patients amounts to 50.9%. [5] This might be due to late diagnosis and lack of symptoms. It is a highly metastatic cancer and more than 70% of ovarian cancer patients are diagnosed with metastasis. Hereby epithelial ovarian cancer (EOC) is the most common and most lethal. The classification is based on histological morphology and different cancer-causing mutations (Table 2). [6] [7]

Table 2: Ovarian cancer subtypes.

Classification	Mutation	Site of mutation
High-grade serous	P53, Genome instability	Fallopian tube
Low-grade serous	MAPK	Fallopian tube
Endometrioid	ARID1A	Ectopic endometrium, endometriosis
Clear cell	ARID1A, PI3K	Ectopic endometrium, endometriosis
Mucinous	KRAS	ovary

Ovarian cancer predominantly metastasizes in the peritoneal cavity and through the pelvic lymph nodes. [8]

2.2 Tumorigenesis and metastasis in mammalian cancer

Tumor development is a multi-step process, in which mutations and epigenetic changes in normal cells lead to malignant cells. Regulatory mechanisms are altered during multistage tumor progression. The most important ones are the control of proliferation, the balance between cell survival and programmed cell death (apoptosis), the communication with neighboring cells and the extracellular matrix, the induction of tumor neovascularization (angiogenesis) and tumor cell migration, invasion and metastatic dissemination. [9] Tumorigenesis stages consist of initiation, promotion, progression and as the last step metastasis (Fig. 1). Initiation involves the alteration stage and the mutation of genes, which leads to multiple functional changes. In the promotion stage actively proliferating preneoplastic cells accumulate. Progression is the final stage of neoplastic transformation, where phenotypic changes and cell proliferation occur. Here, the tumor size will increase. Metastasis is the last step in tumorigenesis, where tumors spread from the primary tumor to distant organ sites. [10]

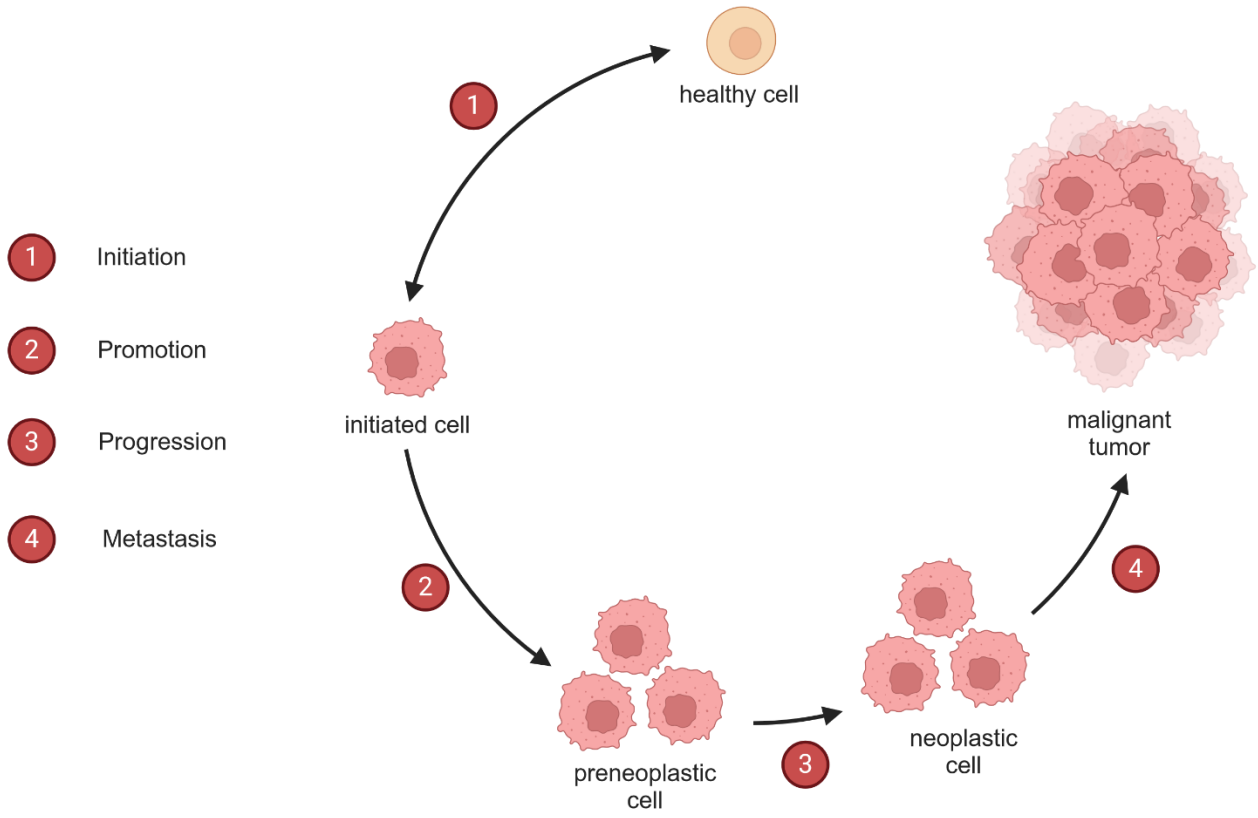

Figure 1: Visualized multi-step tumorigenesis. Healthy cells acquire genetic mutations, which leads to functional changes (Initiation). Mutated, preneoplastic cells accumulate (Promotion) and start cell proliferation (Progression). In the last step tumor cells spread to distant organ sites (Metastasis). [9] Illustrated with BioRender.

Metastasis is the primary cause of cancer morbidity and mortality. It is responsible for 90% of cancer related deaths worldwide. Nevertheless, most research does not involve metastasis analysis in *in vivo* experiments. [11] In the metastasis cascade primary cancer cells disseminate from the tumor and invade through surrounding extra-cellular matrix (ECM) and stromal cells (invasion) into the blood stream. They intravasate (intravasation) into the lumina of blood vessels and survive the blood stream. After transport through the circulation, tumor cells can be arrested in micro-vessels and extravasate into the tissue (extravasation). There, the cancer cells form micro-metastases. [12] During the metastatic cascade, changes in cell-cell and cell-ECM interactions and interactions with the tumor microenvironment (TME) are of importance. The process depends on the loss of cell-cell interactions of the primary cancer cells to disseminate. Further, metastasis relies on the cell ability to attain a motile phenotype *via* changes in cell to matrix interactions. [13]

2.3 The process of cell-adhesion and its cholesterol dependency

The metastatic capacity of tumor cells, that disseminate from the primary tumor, is dependent on mechanical factors like blood-flow, tumor size and capillary size to ensure a successful cell arrest. Moreover, the tumor growth ability is dictated by molecular interactions of the cells with the microenvironment. [14] Cell adhesion molecules have been shown to play an important role in the progression of colorectal cancer and its metastatic migration to the liver, especially in tumor cell attachment to distant tissue. [15] Various integrin heterodimers correlate with metastasis progression, while different integrins may contribute to different steps of the metastatic cascade. The interaction between *α*IIb*β*3 integrins on platelet and *α*v*β*3 on tumor cells facilitates tumor cell arrest in the vasculature and metastasis to various tissues. Tumor-associated vessels express αvβ3 and αvβ5, which contribute to the binding of the vasculature to the ECM. This enhances migration and invasion. [16]

2.3.1 Cell-adhesion to Extracellular-Matrix

The ECM is a three-dimensional network of non-cellular components that form a porous, physical scaffold in which cells can adhere. Not only does the ECM provide structural stability for the cells, but it also allows the diffusion of nutrients, oxygen, growth factors and waste products. Primary components are water, polysaccharides and proteins. In addition, the ECM is responsible for initiating signaling needed for tissue development, cell homeostasis and fundamental cell processes. Predominant proteins found in the ECM are collagen, laminin, fibronectin, vitronectin and elastin. [17] Cell adhesions are attachment structures between the ECM and the cells, or between cells and other cells. The most common cell adhesions are mediated mostly by integrin, which are linked to the cell cytoskeleton and are anchored by fibronectin, vitronectin or collagen (Figure 2). [18] Integrins are *α*-*β* heterodimers, and each subunit crosses the membrane once, with most of each polypeptide in the extracellular space. Eight *β*-subunits can assort with 18 *α*-subunits to form 24 distinct integrins. [19] Integrin interaction with specific ECM molecules and clustering leads to integrin activation and phosphorylation of the focal adhesion kinase (FAK), as well as the associated non-receptor tyrosine kinase (SRC). In turn, the activation of FAK and SRC modulate the activity of, Rho-GTPases, mitogen-activated protein kinase (MAPK) and phosphoinositide-3-kiase (PI3K)/ proteinkinase B (Akt) pathways. All this mediates cell proliferation, differentiation and migration. [20] Integrin activation and FAK

phosphorylation led to the recruitment of cytoskeleton components like vinculin, talin and α-actinin. Linking the focal adhesion complex to the F-actin cytoskeleton (Fig. 2). [21]

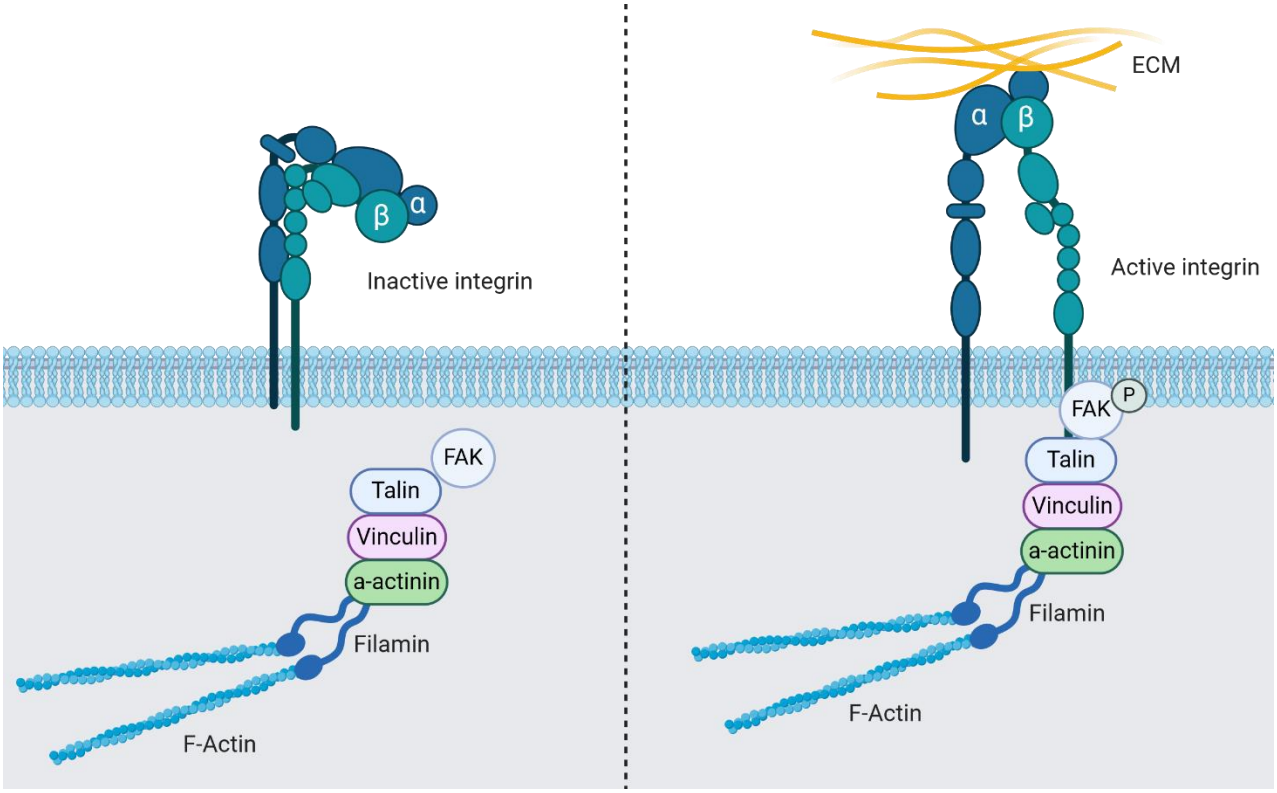

Figure 2: Integrin illustration in inactive and active conformation. Active Integrins bind to the ECM and phosphorylation of the FAK as well as the SRC. Activation of FAK and SRC leads to recruitment of cytoskeleton components like Talin, Vinculin and α-Actinin. The formation of the focal adhesion complex links Integrin to the actin cytoskeleton of the cell. [21] Illustrated with BioRender.

2.3.2 Cell-cell adhesion

Cell-cell adhesion is essential for epithelial morphology and function. Their structures assure necessary integrity and tensile strength. These adhesive structures are connected to intermediate filaments (desmosomes) or to microfilaments (adherens junctions, tight junctions). [22] Adherens junctions are formed by cadherin-dependent adhesion. Cadherins are single-pass transmembrane glycoproteins that link the actomyosin cytoskeleton of the cells they join together. This interaction is mediated through a group of intracellular anchor proteins called catenins. For some cells the adhesive properties rely on selectins. Selectins are cell-surface carbohydrate binding proteins that mediate cell-cell interactions in the bloodstream. [23] Interaction between the adherens junctions and the actomyosin cytoskeleton is regulated by mechanical forces and Rho-family of small GTPases. [24] Rho-family GTPases function as

molecular switches, cycling between an active guanosine triphosphate (GTP)-bound stage and an inactive guanosine triphosphate (GDP)-bound stage. The activation state is tuned by regulatory proteins like guanine nucleotide exchange factors (GEFs), which catalyze the exchange of GDP with GTP. Other regulatory proteins are GTPase activating proteins (GAPs), which increase the GTP hydrolysis rate and guanine dissociation inhibitors (GDIs), which inhibit the release of GDP. This regulation is necessary for facilitating coupling and detachment of cadherin-catenin complexes from the actomyosin cytoskeleton, allowing cell-cell separation, cell sorting and cell migration. [25]

2.3.3 The role of cholesterol in cell adhesion

Lipid rafts are cholesterol-enriched microdomains of the cell membrane and are involved in various cellular functions including the regulation of cell adhesion and membrane signaling. Cholesterol provides lipid rafts with correct structure, fluidity and membrane functioning. Removal of cholesterol leads to dissociation of most lipid raft associated proteins and renders them unfunctional. [26] Cell adhesion is mediated by the transmembrane protein integrin. Integrins attach to ECM compartments like fibronectin or collagen and assemble a focal adhesion complex to form a link to the cytoskeleton. Lipid rafts are involved in the integrin-mediated signaling as well as in integrin clustering at focal adhesion sites. [27] Lipid rafts regulate integrin signaling by partitioning activated integrins in microdomains where they form specific interactions with upstream and downstream signaling molecules. [28] The recruitment of integrins to lipid raft domains occurs during inside-out signaling upon binding to and activation by ECM ligands. Integrins are excluded from the lipid raft without stimulation and mobilized to the lipid raft after stimulation. [29] Lipid rafts might provide a more favorable membrane environment for activated integrins, since preferably activated integrins gather at the lipid raft membrane. [27]

2.4 Cellular cholesterol homeostasis and its deregulation in cancer

Cholesterol plays an important role in eukaryotic cells, being an essential component of the cell membrane, the precursor of steroid hormones, bile acids, fats and lipophilic vitamins. Cholesterol can be obtained through exogenous diet or through endogenous *de novo* synthesis. Due to its multiple cellular functions, altered cholesterol homeostasis leads to metabolic diseases and cardiovascular disorders. [30] Evidence suggests that hypercholesterolemia may be associated with the risk of developing

several types of tumors. [31] Excess cholesterol is toxic for the cells, therefore proper cholesterol levels must be maintained in cells. Cholesterol homeostasis is governed and regulated in accordance with the cellular needs by several mechanisms and lipoprotein trafficking plays an important role. The major pathways are intracellular *de novo* cholesterol synthesis, exogenous cholesterol uptake by cellular receptors, esterification and storage of cholesterol, cholesterol efflux by cellular exporters and cholesterol exchange primarily mediated by SR-BI (Fig. 3). [32]

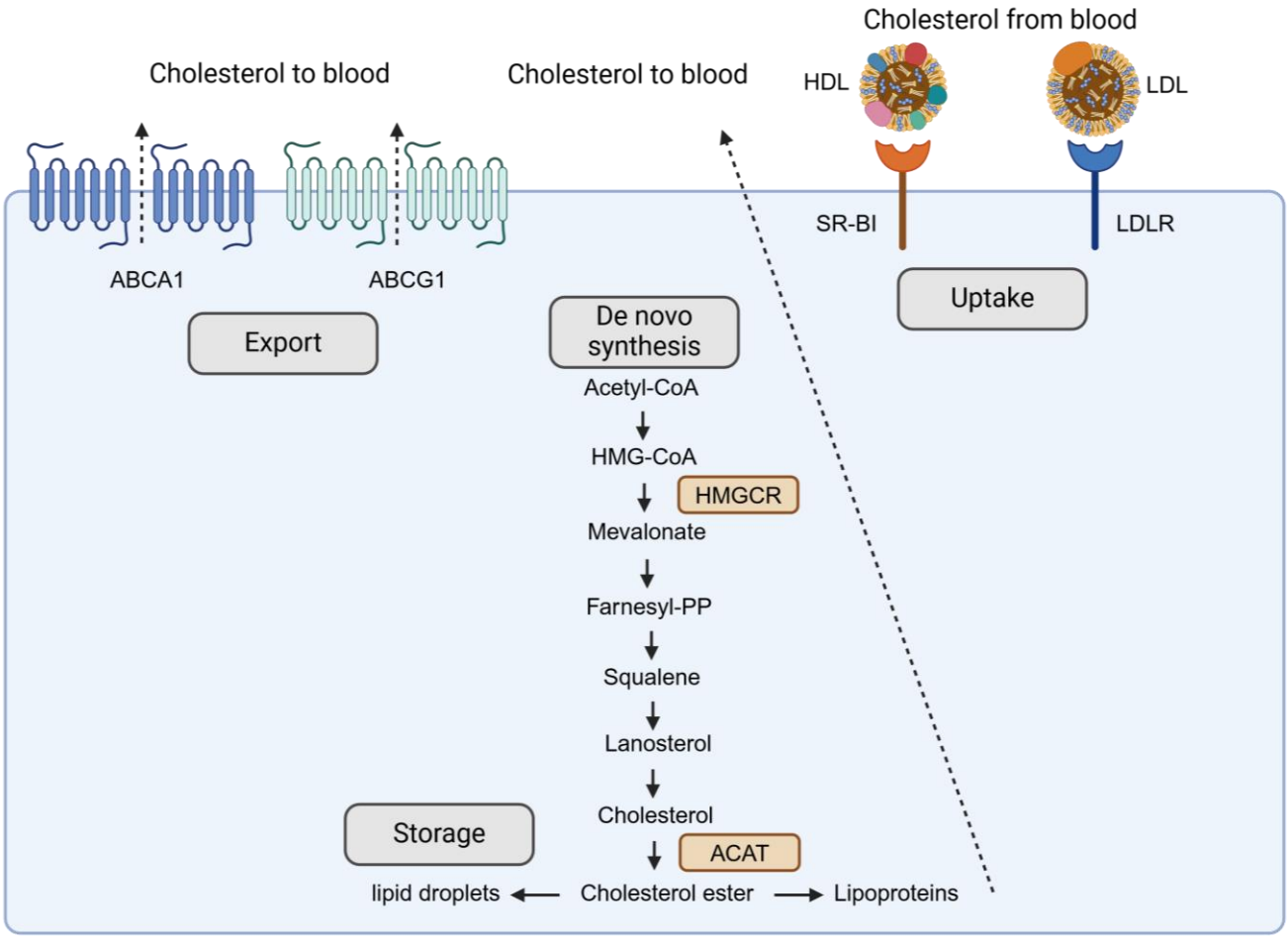

Figure 3: Illustration of cholesterol homeostasis. The uptake of cholesterol is accruing through binding of lipoproteins (HDL, LDL) to their respective receptors. Cholesterol accumulation leads to changes in the *de novo* synthesis which is tightly regulated by the rate limiting enzyme HMGCR. Excess cholesterol is esterified *via* ACAT and either stored in lipid droplets or used in the formation of lipoproteins. Cholesterol also gets transported out of the cell by ABCA1, ABCG1 and SR-BI. [32] Illustrated with BioRender.

2.4.1 Cholesterol synthesis

Acetyl-Coenzyme A (Acetyl-CoA) is a precursor of *de novo* cholesterol synthesis, which is taking place in the endoplasmic reticulum (ER). Acetyl-CoA is converted to 3-hydroxy-3methylglutaryl-CoA (HMG-CoA) by the acetyl-CoA-acetyltransferase (ACAT). The next reaction is a rate limiting step in cholesterol synthesis, catalyzed by the HMG-CoA reductase (HMGCR), which reduces HMG-CoA to mevalonate. Mevalonate is converted into isopentenyl pyrophosphate and afterwards into Squalene. Then Squalene is converted into cholesterol in a few steps initiated by the Squalene epoxidase. Cholesterol is in the end esterified by sterol-o-acetyl transferase (SOAT) into cholesterol ester and either stored in lipid droplets or transported out of the cell *via* ATP-binding Cassette Sub-family G Member 1 (ABCG1). [33]

Cholesterol regulates its own synthesis intracellularly using the sterol regulatory element binding protein (SREBP). SREBP senses cholesterol levels and binds to the sterol regulatory element (SRE) in the proximal region of the HMGCR promotor. The binding of SREPB triggers transcription of HMGCR and speeds up biosynthesis of cholesterol, when cholesterol levels drop. SREPB also binds to the SRE promotor region of low-density lipoprotein receptor (LDLR) and regulates low density lipoprotein (LDL) uptake in the liver. [34]

2.4.2 Extracellular cholesterol uptake

Cholesterol and triglycerides are transported through the circulation in association with proteins. Lipoproteins are complex particles that contain a cholesterol ester and triglyceride core and are surrounded by free cholesterol, phospholipids and apolipoproteins, which facilitate lipoprotein formation and function. Lipoproteins are divided into seven subclasses according to size, lipid composition and apolipoprotein type. [35], [36]

Table 3: List of lipoproteins and their composition.

Particle	Size [Å]	Cholesterol [%]	Triglyceride [%]	Phospho lipid [%]	Apoprotein [s]
Chylomicrons	800-5000	3	90	5	AI, AII, B, CI, CII, CIII
VLDL	300-800	10	70	10	BI, CI, CII, CIII, E
IDL	250-350	-	-	-	B, CIII, E
LDL	180-280	26	10	15	B
HDL	50-120	20	5	25	AI, AII

Apolipoproteins have four major functions: giving a structure, acting as ligands for lipoprotein receptors, guiding formation of lipoproteins and serving as regulators for enzymes involved in lipoprotein metabolism. [35]

Lipoprotein receptors are cell surface proteins, that bind lipoproteins with high affinity and specificity *via* interactions with certain apolipoproteins, resulting in a physiological response that affects the ligand and the cell. These receptors influence intracellular lipid and extracellular lipoprotein levels. [37]

There are several receptors that play a crucial role in lipoprotein uptake, like LDLR, cluster of differentiation 36 (CD36) and SR-BI. LDLR mediates the uptake of chylomicron remnants and intermediate density lipoprotein (IDL) but preferentially of LDL, which occurs through endocytosis. LDL is then internalized *via* clathrin-mediated endocytosis. [38], [39] Afterwards, the internalized coated LDL fuses with a lysosome and gets hydrolyzed. The protein is hydrolyzed into amino acids and the cholesterol esters are hydrolyzed by a lysosomal acid lipase. The resulting unesterified cholesterol crosses the lysosomal membrane and enters the cytoplasmic compartment (Fig. 4). [40] SR-BI mediates the selective uptake of cholesterol ester from HDL in the liver and here also HDL holo-particle uptake is possible, after which the HDL particle gets re-secreted into the plasma. [35]

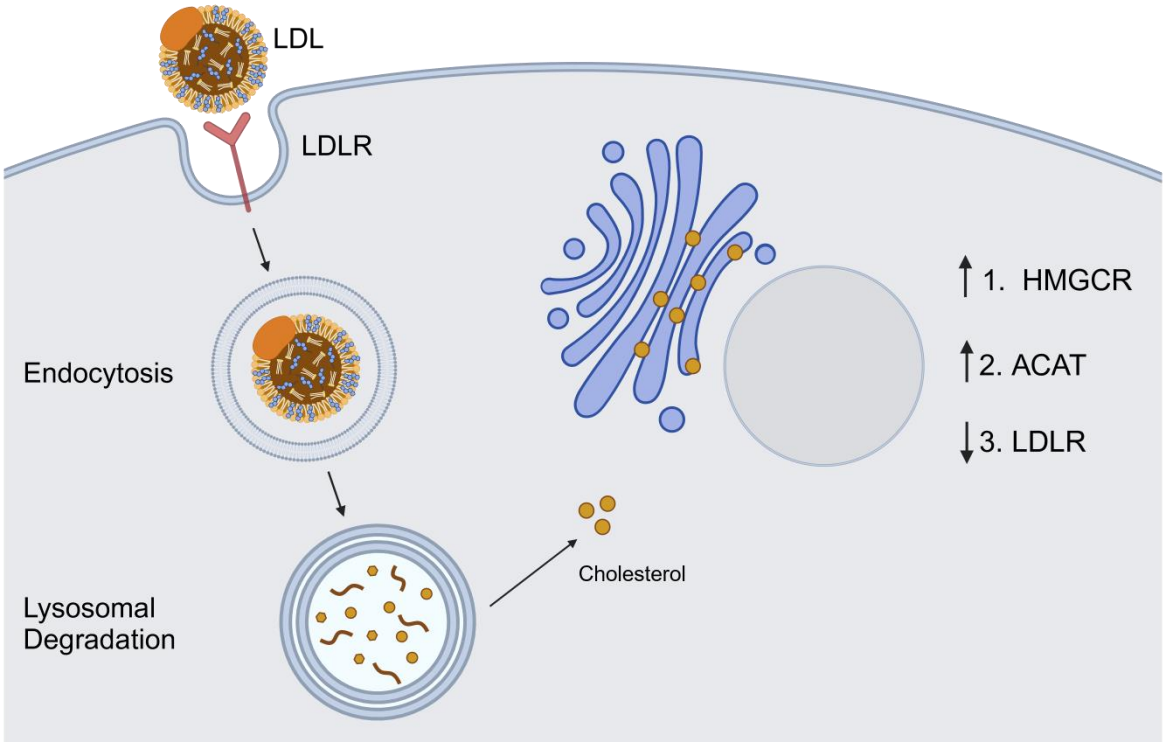

Figure 4: Illustration of LDL endocytosis by binding to LDLR. Internalization of LDL and lysosomal degradation of the lipoprotein into cholesterol, fatty acids and amino acids. Cholesterol accumulation in the cell leads to upregulation of HMGCR and ACAT. LDLR is downregulated after cholesterol uptake. [40] Illustrated with BioRender.

2.4.3 Cholesterol esterification

Accumulation of free cholesterol is toxic for the cell. Therefore, esterification of free cholesterol is needed to store and transport cholesterol. [41] The conversion of free cholesterol to cholesterol ester is catalyzed by the enzyme ACAT (Fig. 5). ACATs are membrane bound proteins, which use long-chain fatty acids and cholesterol as substrates. In most cell types, cholesterol esters are present in low levels, mainly as cytoplasmic lipid droplets. In plasma, cholesterol esters are part of the neutral cargo in chylomicrons and very low density lipoproteins (VLDLs). In mammals two isoenzymes ACAT1 and ACAT2 exist, encoded by two different genes, SOAT1 and SOAT2 respectively. [42]

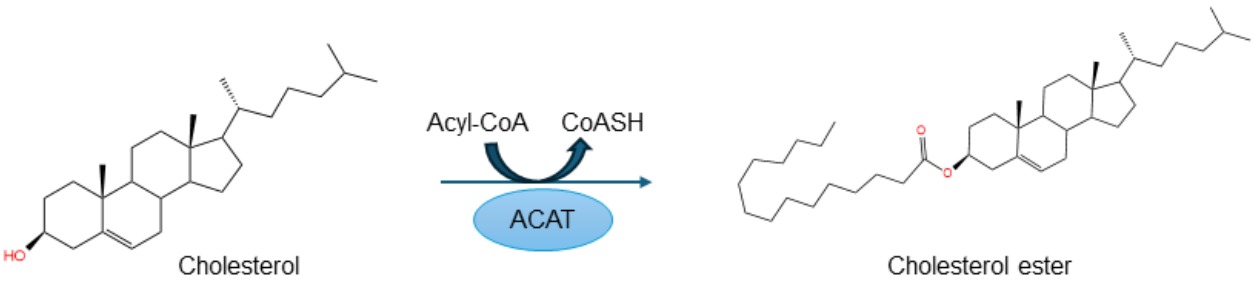

Figure 5: Illustration of Cholesterol esterification. ACAT is responsible for catalyzing the esterification of free Cholesterol into Cholesterol ester using Acyl-CoA as a substrate. Illustrated with ChemDraw and PowerPoint.

2.4.4 Cholesterol efflux

The efflux process involves cholesterol localized at the plasma membrane that in turn may derive from intracellular sites like the late endosomal/lysosomal compartment and from the Golgi-Apparatus. Mechanisms accounting for cholesterol efflux include passive diffusion, aqueous diffusion or meditated by SR-BI and active pathways mediated by ATP-binding Cassette Sub-family A Member 1 (ABCA1) and ABCG1 (Fig. 6). [43] ABCA1 is an ABC-Transporter in the cell membrane, which uses adenosine triphosphate (ATP) as an energy source to actively transport cholesterol across membranes. ABCA1 selectively mediates efflux of cholesterol to lipid-poor apolipoproteins, mainly apolipoprotein A1 (ApoA1). ABCA1 gene expression is regulated by liver X receptor (LXR), which senses cholesterol level and becomes stimulated by the cholesterol accumulation in the cell. ABCA1 has a floppase activity, which allows flipping of cholesterol and phospholipids from the inner leaflet of the membrane to the cell surface. [44] ABCA1 mediated generation of nascent HDL may promote further cholesterol efflux by ABCG1 and SR-BI to HDL particles. Similar to ABCA1, ABCG1 is also localized at the cell membrane and the expression is also regulated by LXR stimulation after cholesterol accumulation. ABCG1 is responsible for interactions with HDL and the resulting efflux of intracellular cholesterol. [45] SR-BI stimulates free cholesterol efflux to phospholipid enriched acceptors, such as mature HDL particles. [43] In contrast to ABCA1- and ABCG1-mediated efflux, SR-BI mediated efflux, which is enabled by the formation of a hydrophobic tunnel, does not require energy, and is a passive, concentration dependent process. In fact, it has been suggested that both efflux and influx of cholesterol occur, and that the direction of cholesterol flux may be ruled by various factors, including the availability of different

cholesterol acceptors and the composition of the cellular plasma membrane. [46] The efflux of cholesterol to apolipoproteins is the first step of reverse cholesterol transport. The lipidated apolipoprotein dissociates from the receptor and travels into the blood stream. The cholesterol will be delivered from non-hepatic tissues to the liver and then gets distributed to other tissues or removed from the body by the gallbladder. [47]

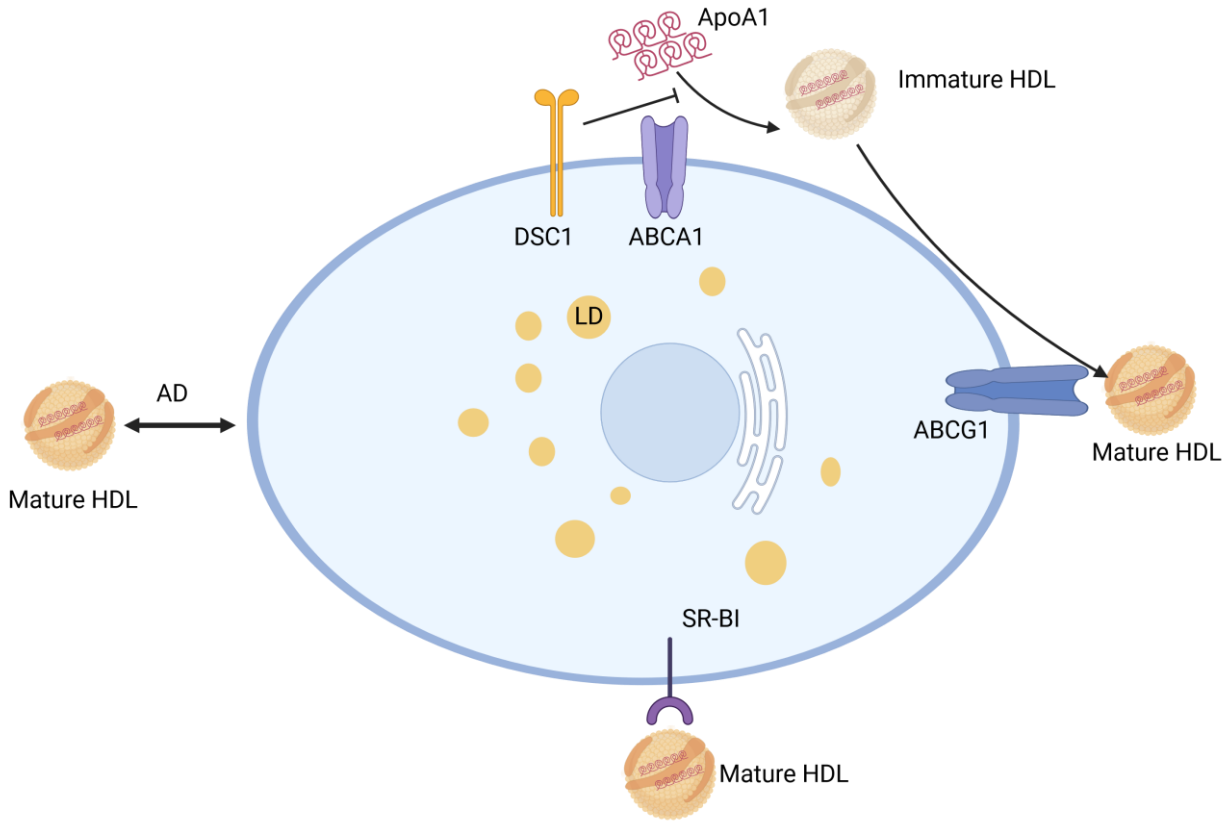

Figure 6: Four main cholesterol efflux pathways: ABCA1 facilitates efflux of phospholipids and cholesterol to apoA1 is called nascent HDL particle. *Via* the ABCG1-mediated efflux process, the nascent, immature HDL acquires additional cholesterol, thus becoming a mature HDL particle. SR-BI facilitates diffusion of cholesterol molecules between the plasma membrane and bound mature HDL particles. The extracellular domain of SR-BI forms a non-polar channel to mediate the cholesterol exchange. Passive aqueous diffusion (AD) is also possible and represents a simple diffusion process in which cholesterol moves down its concentration gradient. [48] Illustrated with BioRender.

2.4.5 Metabolic reprogramming and deregulated cholesterol homeostasis in cancer

Hanahan and Weinberg described metabolic reprogramming as a hallmark of cancer. Reprogramming of catabolic and anabolic metabolism and synthesizing biomass is critical for survival and cell growth of cancer cells. [49] To adapt to the increasing hypoxic and nutrient-poor environment, in addition to increasing glucose uptake and aerobic glycolysis, tumor cells also undergo lipid metabolism reprogramming to enhance their biological behaviors. [50] Highly proliferative cancer cells tend to have a high lipid content, which is important for providing energy, membrane synthesis and lipid signaling. Cancer cells show an enhanced ability to synthesize lipids and have a higher lipid uptake. In agreement with this, it was reported that cancer cells upregulate fatty acid and cholesterol related enzymes for tumor progression. [51] Tumor cells have a high demand of cholesterol to enhance membrane biosynthesis and oncogenic signaling. Their cholesterol content is increased by upregulating *de novo* cholesterol synthesis (HMGCR), increase cholesterol uptake (LDLR, ABCA1 and ABCG1), altering cholesterol efflux (SR-BI) or by increasing cholesterol storage. [52] Cancer metastasis into different organ sites is a process that relies on the constituents of the tumor microenvironment. The tumor microenvironment plays a key role in trapping tumor cells and forming secondary tumors. The organ site is also referred to as the pre-metastatic niche, whereby the organ site is primed and metabolically reprogrammed, providing metastatic tumor cells with a microenvironment suitable and supportive of their colonization (seed and soil hypothesis). [53] While it is important for tumor cells to quire survival mechanisms at the secondary sites, such as mitigating oxidative stress, for colonization they also need to adapt molecular strategies according to the metabolic nature of the target tissue. For example, breast cancer cells adapt to the lung, a pyruvate rich organ by upregulating pyruvate uptake. Breast cancer cells metastasizing to the brain with low availability of lipids, upregulate *de novo* fatty acid synthesis. Whereby, breast cancer cells in the peritoneum have high access to exogenous lipids and upregulate uptake of lipids. [54]

2.5 The importance of high-density lipoproteins in cholesterol homeostasis

HDL encompasses a diverse group of lipoproteins, characterized by a size of 8-10 nm. The composition of HDL comprises a core of cholesterol ester, enveloped by a single layer of phospholipids, free cholesterol and apolipoproteins. Among these apolipoproteins, ApoA1 and ApoA2 are the predominant ones. [55] HDL has been

correlated with a reduced risk of atherosclerosis, when found in high levels in the blood stream. Therefore, HDL was thought to have a protective function against atherosclerosis. One crucial protective function of HDL involves cholesterol excess removal from non-hepatic cells and its transport to the liver for its subsequent excretion *via* the bile. This process is termed “reverse cholesterol transport” (RCT). [43] In addition, HDL has important anti-oxidant and signaling properties, which will be described below. HDL has recently gained attention in understanding the development and progression of breast cancer. Commonly, HDL is inversely correlated to breast cancer incidence and unfavorable disease outcome. However, no correlation and positive correlations have been demonstrated as well. These controversies suggest that the amount of HDL detected in blood plasma is not enough to prove its role in cancer progression. Rather, differences in its composition may explain these controversies and may also help understand the contribution of HDL to breast cancer progression. HDL mediates cholesterol removal, limiting the cholesterol content which, in the tumor microenvironment context, may be necessary for tumor metastasis, and it counteracts oxidative and inflammatory stress that aggravates tumor biology. [56] Proteome analysis revealed dozens of proteins associated with various HDL subfractions, modulating different functional properties. [56]

2.5.1 Cholesterol efflux and reverse cholesterol transport

RCT is a pathway that transports cholesterol from extrahepatic cells and tissues to the liver and intestines for excretion. Accumulation of cholesterol in arteries is prevented by RCT, which could hinder atherosclerosis development. Cholesterol efflux is part of RCT and describes the secretion of cholesterol outside the cell by macrophages in the vessel. RCT starts in the liver by producing ApoA1 and releasing it into the plasma. Circulating ApoA1 interacts with serum phospholipids and forms nascent HDL. Nascent HDL particles then trigger cholesterol efflux in macrophages and fibroblasts in the subendothelial space and act as cholesterol acceptors. Externalized cholesterol is esterified by lecithin cholesterol acyltransferase (LCAT) with HDL. By this means, HDL gets enriched with cholesterol ester and triglycerides, which leads to an increase in size and HDL density. Triglycerides can be processed by a hepatic lipase, which decreases the HDL size and density. Finally, cholesterol enriched HDL particles transport the cholesterol esters to SR-BI in the liver, which get converted to bile salts and eliminated through the gastrointestinal tract. [57] Cholesterol efflux is taking place

by passive diffusion and by active pathways including the efflux receptors ABCA1, ABCG1 and the cholesterol exchange receptor SR-BI. [58]

2.5.2 Antioxidant function of high-density lipoprotein

Atherosclerosis development is dependent on LDL particle uptake by macrophages, leading to foam cell formation. LDL modification is necessary to induce this process, which includes aggregation, enzymatic digestion and oxidation. Normally, LDL gets internalized and endocytosed by LDLR, but oxidation of LDL by one-electron and two-electron oxidants increases its affinity to macrophage SR-BI receptors leading to rapid LDL uptake and fatty streak formation. [59] HDL exerts an antioxidative function which is crucial to protect from atherosclerotic plaque formation and development. This antioxidative function inhibits accumulation of primary and secondary peroxidation products. Different HDL-associated apolipoproteins and enzymes have been shown to contribute to its antioxidative capacity (e.g. paraoxonase-1 PON1; platelet activating factor acetylhydrolase PAF-AH; lecithin-cholesterol acyltransferase LCAT and glutathione peroxidase GSPx). [60] Removal of lipid hydroperoxides can also be mediated *via* ApoA1. Lipid hydroperoxides are transferred from LDL to HDL by lipid transfer proteins. Subsequently, lipid hydroperoxides get removed by SR-BI-mediated selective uptake in the liver. [61] Lipid peroxidation is a process, where oxidants, such as reactive oxygen species (ROS), oxidize lipids into lipoperoxyl radicals and lipo hydroperoxides. Lipid hydroperoxides decompose to form reactive aldehydes, which in turn act as second messengers of free radicals and diffuse across cell membranes. These aldehydes can bind to the deoxyribonucleic acid (DNA) and promote mutagenic effects. There is growing evidence that lipid peroxidation products are implicated in several pathological states such as inflammation, atherosclerosis, diabetes, neurodegenerative conditions, and importantly carcinogenesis. [62]

2.5.3 Signal transduction by high-density lipoprotein

Epidemiological studies demonstrate that high levels of HDL are associated with a reduced risk of atherosclerosis. [63] In addition to its direct role in RCT serving as a cholesterol donor and acceptor, evidence shows that an important mechanism of how HDL protects from atherosclerosis is related to its ability to trigger cell signaling. HDL has been shown to activate a broad set of complex cell signaling events in endothelial cells. [64] Some of them are triggered by the direct binding of the main apoprotein of

HDL (ApoA1) with the HDL receptor (SR-BI) or with cholesterol transporters (ABCA1), while others involved the interaction of bioactive molecules (sphingosine-1-phosphate, S1P) present in HDL with corresponding transmembrane receptors (S1P1, S1P2, S1P3). [64]

2.5.3.1 HDL-induced cell signaling mediated by scavenger receptor 1

HDL binding to SR-BI is leading to the recruitment of SRC to the C-terminal tail of SR-BI and activation of SRC. SRC phosphorylation is followed by phosphorylation and activation of AMP-activated protein kinase (AMPK). Phosphorylation of SRC and AMPK is critically dependent on the PDZ domain-containing adaptor protein (PDZK), which interacts with the C-terminal residues of SR-BI and is important for its stability in the plasma membrane. SRC and AMPK activation is followed by PI3K activation and simultaneous activation of AKT and the mitogen-activated protein kinase (MAPK). MAPK and AKT activation led to various biological functions like the regulation of hypoxia, angiogenesis, insulin sensitivity, vasodilation and reendothelialization (Figure 5). [65], [66] Furthermore, HDL signaling also results in migration and proliferation of endothelial cells and suppresses the expression of vascular cell adhesion molecule 1 (VCAM1) and intercellular adhesion molecule 1 (ICAM1). [65] These signaling events are illustrated in Figure 7.

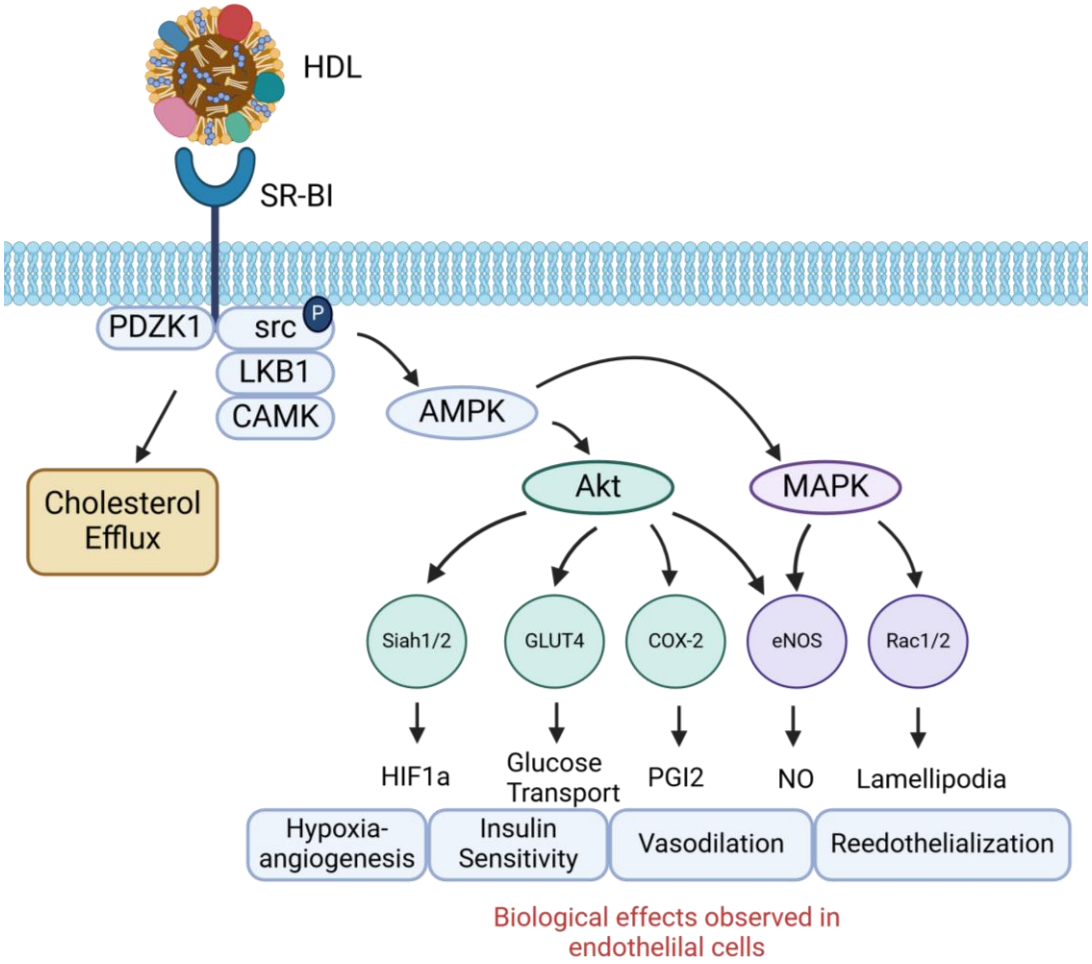

Figure 7: HDL signaling after binding to SR-BI. HDL binding to SR-BI leads to recruitment and phosphorylation of src. Src activates AMPK and AMPK activation leads to the phosphorylation of MAPK pathway resulting in various biological functions. [66] Illustrated with BioRender.

Although not shown in Figure 7, when the MAPK pathway becomes activated it transduces the signal to the extracellular signal regulated kinases 1/2 (ERK1/2), which are essential components of the MAPK pathway. [67] Although less well-studied, and so far, not directly linked to HDL signaling, the extracellular signal regulated kinase 5 (ERK5) is also a member of the MAPK cascade but is twice the size of the other MAPKs. ERK5 gets stimulated by mitogens and stress factors. [68] After receptor activation MEKK2 and MEKK3 get phosphorylated and in turn activate MEK5. MEK5 is phosphorylating ERK5, which is activating transcription factors responsible for differentiation, survival and proliferation. [69] ERK1/2 was reported to also phosphorylate ERK5. [70]

ERK5 activation was linked to FAK. Dominant negative-mutants of FAK were showing no ERK5 phosphorylation compared to the FAK wild-type control. Furthermore,

dominant negative ERK5 mutants showed no phosphorylation of ERK5 and FAK and showing less cell adhesion compared to their controls. Blocking various Integrin receptors also shows less phosphorylation of FAK and less cell adhesion. Therefore, this work shows a possible contribution of ERK5 activation to cell adhesion. [71]

2.5.3.2 HDL-induced signaling mediated by lipid sphingosine-1-phosphate

The bioactive lipid S1P carried in HDL is known to interact with five receptors (S1P1–5) which are G-protein-coupled receptors and regulate multiple cellular functions, such as proliferation, survival, cytoskeletal rearrangements, and cell migration. In blood vessels, these receptors regulate new vessel formation and the maintenance of vascular barrier integrity. [72]

As illustrated in Figure 8, in endothelial cells, the binding of HDL to SR-BI may precede S1P receptor stimulation by S1P present in HDL. [73] After binding of S1P to S1P1 or S1P3 receptors, activation AMPK and AKT influences multiple effector molecules. It stimulates FAK, inactivates the proapoptotic protein BAD, inhibits caspases 9 and 3, the transcription factor NF-κB and the expression of adhesive molecules E-selectin and vascular cell adhesion molecule 1 (VCAM-1), and activates the endothelial nitric oxide synthase (eNOS) and the generation of NO. [74]

The activation of the mitogen activated protein kinase p38MAPK results in activation of cyclooxygenase-2 (COX-2) and in production of prostacyclin (PGI2). Further events include the **1)** upregulation of transforming growth factor β (TGFβ), which via the transcription factors Smad 2 and 3, suppresses the production of proinflammatory molecules (matrix metalloproteinases such as MMP9, as well as phospholipase A2,PLA2); **2)** the Inhibition of small G-protein Rac, which suppresses the activity of NADPH oxidase and the generation of reactive oxygen species; **3)** the inhibition of Toll-like receptor 2 (TLR2), which in turn reduces NF-κB activation and production of proinflammatory cytokines. [75]

All these effects account for well-known properties of HDL in vascular biology such as the maintenance of the endothelial barrier, and its anti-inflammatory, antiapoptotic, anti-adhesive, and vasodilatory properties. [72]

In other cell types, such as in cardiomyocytes, the activation of protein kinase src and transcription factor signal transducer and activator of transcription 3 (STAT3) via S1P2 is shown to protect against cardiomyocyte apoptosis. In smooth muscle cells,

activation of the small G-protein RhoA via S1P2 is followed by inhibition of the small G-protein Rac1, which regulates cell migration. [76]

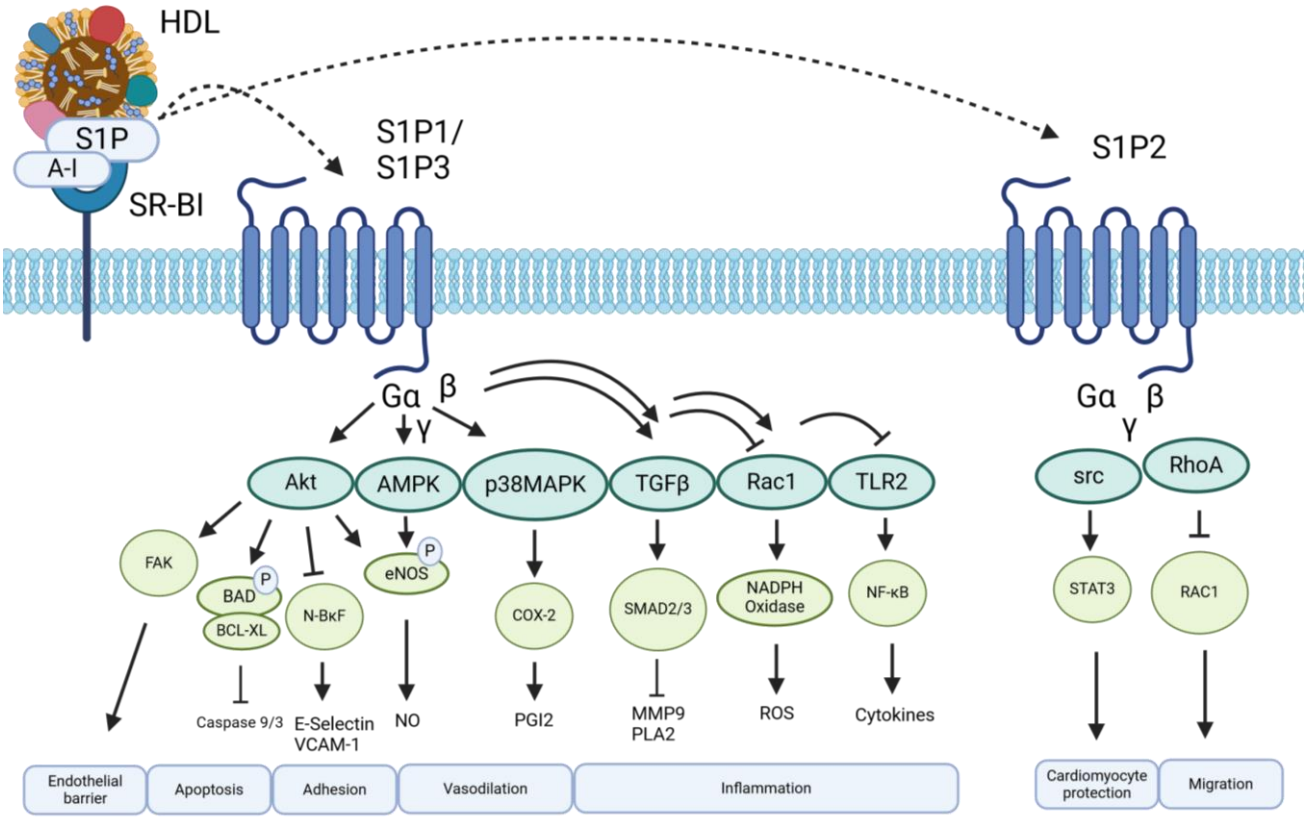

Figure 8: S1P signaling after binding of HDL to SR-BI. S1P binds and activates S1P1, S1P2 and S1P3 receptors, resulting in various biological functions. [75] Illustrated with BioRender.

Little is known about the link between cholesterol homeostasis and MEK-ERK5 pathway. RNA sequencing analyses of ERK5 knockdown show downregulation of cholesterol related genes like LDLR, SREBF and HMGCS1. Lipidomics of ERK5 knockdown revealed reduced diacylglycerol levels. [77] Previous findings postulated LDLR regulation by ERK5. Downregulation of ERK5 leads to less LDLR expression and an impaired LDL uptake. Whereas ERK overexpression leads to an increase in LDLR expression and higher LDL uptake. [78]

2.6 The endothelial lipase G (LIPG)

2.6.1 Protein structure of LIPG

The endothelial lipase G (LIPG), encoded by the gene *LIPG* and discovered in endothelial cells, is a 55 kDa protein, that is secreted into the extracellular space as a 68 kDa protein after maturation. By binding to heparin-sulfate proteoglycans (HSPGs)

it remains associated with the cell surface. Maturation involves glycosylation on different sites, which are responsible for protein secretion, enzyme activity and substrate specificity. Furthermore, LIPG was shown to oligomerize into a homodimer, which is active in a head-to-tail conformation. [79] Different studies identified a N-terminal 40 kDa fragment and a C-terminal 28 kDa fragment, which are cleavage residues of proprotein convertases (pPCs) and could have particular physiologic roles. [80] LIPG, lipoprotein lipase (LPL) and hepatic lipase (HL) are part of a lipase sub family, that exhibit triglyceride and phospholipase activity towards lipoproteins. [81] Each has a clearly defined N- and C-terminal structural domain, joined by a hinge region. After alignment of LIPG with HL and LPL sequences, it was shown that LIPG is a serine esterase with a catalytic triad (Ser 169, Asp 193, His 274) in the N-terminal domain. This region is responsible for phospholipase and triglyceride activity. Hydrophobic regions for protein and lipid interactions were detected (163–172 and 272–281). LPL and HL possess lid regions that are important for substrate specificity. The lid region for LIPG showed differences to the others, indicating different substrate specificities. LIPG displayed positively charged clusters, responsible for HSPGs binding. Furthermore, glycosylation sites were predicted to modulate the heparin binding properties. [81], [82] In Figure 9 a crystal structure of human LPL is shown to illustrate a lipase structure.

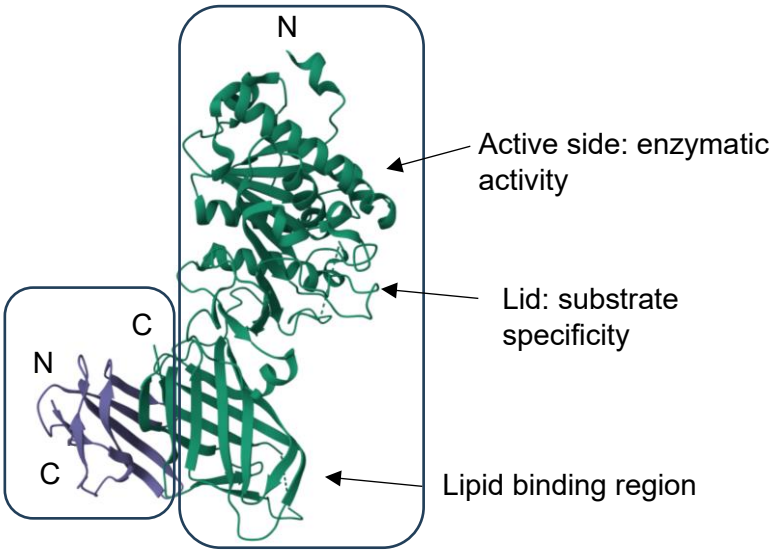

Figure 9: Crystal structure of lipoprotein lipase (LPL: 6OAU). Graphic illustration of the lipid binding region, the lid region and the active side. [83] Image accessed from Protein Data Bank and further illustrated with BioRender.

2.6.2 Functional role of LIPG in cholesterol homeostasis

LIPG functions in the plasma compartment and alters lipoprotein levels using its enzymatic and non-enzymatic functions. For the enzymatic function, LIPG is able to hydrolyze triglycerides (TAG) and phospholipids, whereby the phospholipase activity predominates. LIPG hydrolyzes phospholipids preferably in HDL and to a much lesser extent in LDL, specifically phosphatidylcholine (PC), into free fatty acids (FA) and lyso-phosphatidylcholine (LPC). The cell is then able to take up LPC and free FAs. [84]

The non-enzymatic bridging function refers to LIPG as a linking protein between lipoproteins and HSPGs on the cell surface. Due to both actions of LIPG on HDL, (i) modification of HDL-particle composition *via* its phospholipase activity, and (ii) HDL-binding to the cell surface enhanced by LIPG independently of its catalytic function, LIPG could influence HDL-actions on cells by different ways. LIPG is able to promote bilateral cholesterol transport between HDL and cells *via* SR-BI. [85] LIPG is also able to facilitate hepatic HDL holo-particle uptake *via* SR-BI in hepatic cells. [86] This means that HDL can be internalized by SR-BI and taken up by endosomal vesicles, although this event is not very frequent. After that, HDL particles have been shown to be secreted out of the cell in a process called retro-endocytosis. [87] In the liver, SR-BI mainly takes up HDL-derived cholesterol esters by forming a hydrophobic tunnel. [88] Interestingly, efficient cholesterol ester uptake *via* SR-BI in liver cells has been shown

to require initial LIPG-hydrolysis of HDL, contributing to HDL catabolism. [86], [89] In peripheral (non-hepatic) cells, SR-BI also enables efflux of free cholesterol ester out of cells into HDL. Furthermore, the expression of SR-BI re-distributes cholesterol within the plasma membrane, increasing cholesterol availability to the extracellular space. [88] The most notable physiological role of SR-BI is the clearance of body cholesterol through RCT (see chapter 2.4.1). As already mentioned, HDL is a key player in RCT, in which it promotes the efflux of excess cholesterol from peripheral tissue and returns it to the liver for biliary excretion. [90] Lipid-depleted HDL dissociates from SR-BI and re-enters circulation. [88] According to this, HDL functions as a cholesterol acceptor in peripheral tissues but a cholesterol donor in liver hepatocytes, and SR-BI enables both processes. Importantly, LIPG-catalyzed modification of HDL was shown to diminish the ability of HDL to mediate SR-BI dependent cholesterol efflux. [91] For this reason, high expression of LIPG has been believed to have a negative impact on RCT. However, *in vivo* studies in mice, show that overexpression of LIPG in the liver does not compromise overall RCT. [92] In macrophages, LIPG was shown to promote cholesterol efflux via ApoA1-ABCA1-dependent mechanism, since cholesterol efflux by this route was decreased after LIPG suppression but increased after LIPG overexpression. [93]

In addition to the several above-mentioned reports regarding the influence of LIPG on cholesterol exchange between cells and HDL particles, also HDL-signaling properties (see chapter 2.5.3) appear to be influenced by LIPG, since LIPG knockdown abrogated phosphorylation events and vascular-biological effects triggered by S1P [94]. Altogether, LIPG seems to be able to influence different steps of RCT, from cholesterol efflux in peripheral cells to selective cholesterol ester uptake in the liver, as well as HDL-signaling properties, and a deeper understanding of these actions is required. Finally, LIPG was shown to have higher lipolysis activity towards HDL compared to LDL. [84] However, LDL is still shown to be a relevant substrate for LIPG. In contrast to HDL, LIPG is more efficient in bridging LDL to HSPGs on the cell surface, which is facilitating LDL uptake by LDLR.

2.6.3 The importance of LIPG in breast cancer

Lipid and cholesterol metabolism play an important role in biological processes. They contribute to cell membrane structure and their biological functions. Lipids and cholesterol also function as signaling molecules and take part in energy metabolism and storage. These metabolic pathways are regulated according to the cellular

demands to maintain homeostasis for sustaining cell viability and function. [95] Breast cancer cells are rapidly proliferating cells, that show altered lipid metabolism to meet the increased demand of nutrient uptake. Lipid *de novo* synthesis, extracellular uptake and oxidation pathways are highly activated. [96] Lipids and cholesterol are circulating through the blood stream building the core components of lipoproteins (e.g. LDL, HDL) which are the exogenous source of lipids and cholesterol. For the lipids and cholesterol to enter the cell, the lipoproteins need to be hydrolyzed. As mentioned, LIPG is a lipase that catabolyzes lipoproteins and provides free fatty acids for cellular uptake. LIPG also bridges lipoproteins to its respective cellular receptors for selective cholesterol ester uptake, but also for cholesterol efflux. [93], [97] High expression of LIPG in breast cancer has been reported in several studies. [1], [98] These studies have proven a role for LIPG in breast cancer progression by different mechanisms. Slebe *et. al.* demonstrated the relevance of LIPG in metastasis formation and tumor growth by supplying the cells with exogenous lipids *via* its lipolytic function. [98] Lo *et. al.* reported that LIPG supports different metastatic features of TNBC cell lines by both its catalytic and non-catalytic functions. [99] Furthermore, they uncovered that LIPG's oncogenic mechanism relies on activation of the DTX3L-ISG15 pathway, an emerging pathway in cancer. [100] Cadenas *et. al.* showed a correlation between high LIPG expression and shorter metastasis free survival rate in breast cancer patients. This publication also highlighted the contribution of LIPG expression to survival under oxidative stress condition. The cellular lipid requirement of cells under oxidative stress is met by enhanced fatty acid uptake from hydrolysis of HDL and increased lipid droplet formation when ROS level inhibit *de novo* fatty acid synthesis. [1]

None of these studies have addressed the question of how LIPG could influence tumor cell cholesterol homeostasis in breast cancer. Given the impact of LIPG expression and catalytic activity on HDL and the consequences for different steps of the reverse cholesterol transport (see chapter 2.6.2), it is conceivable that LIPG expression in breast cancer cells influences either their cholesterol levels or their ability to regulate their cholesterol exchange with lipoproteins. Therefore, understanding the role of LIPG in the regulation of tumor cell cholesterol levels was one of the goals of this thesis.

2.6.4 Possible function of LIPG in breast cancer *via* regulation of cholesterol homeostasis

The importance of cholesterol metabolism in breast cancer has been investigated by several groups. The increase in cholesterol demand by rapidly proliferating breast cancer cells is met by upregulation of cholesterol uptake, increasing *de novo* cholesterol synthesis and altering cholesterol efflux. [101] Cholesterol is incorporated in the cell membrane and plays an important role in metastasis formation and signaling regulation leading to metastasis. Potentially, cholesterol localizes in lipid rafts and contributes to integrin- and focal adhesion complex-signaling resulting in enhanced adhesion and migration, relevant processes in metastasis. [102] LIPG could potentially supply cholesterol esters to breast cancer cells by bridging LDL to its receptor (LDLR) for subsequent endocytosis. Additionally, bridging HDL to the SR-BI receptor and enhancing SR-BI-mediated selective cholesterol ester uptake, as observed in the liver, could also be possible. [103] Based on the relevance of cholesterol for tumor cell proliferation, by this means LIPG could support tumor growth. At the same time, LIPG could also be involved in promoting cholesterol efflux in breast cancer cells in a similar way as observed in macrophages. [93] This could help breast cancer cells fine-tune their cholesterol levels, avoiding cholesterol toxicity and supporting survival. Finally, it is conceivable that LIPG´s catalytic activity on HDL could influence HDL-mediated signaling in breast cancer. This would have an impact in metastasis-related processes such as cell adhesion and migration.

The potential contribution of LIPG in cholesterol homeostasis in breast cancer cells may provide a mechanistic explanation for the association of LIPG expression with metastasis progression and tumor growth observed in previous studies. [98], [1]

3. Objective

LIPG expression is associated with shorter metastasis free survival rate and with tumor progression in breast cancer. [1], [98] The release of free fatty acids from HDL by the catalytic activity of LIPG and their uptake by tumor cells was shown to contribute to tumor survival. [1] Importantly, modification of serum lipoproteins, mainly HDL, by LIPG is known to influence their function in body cholesterol homeostasis. However, it has not been investigated yet if LIPG expression in tumors influences tumor cell cholesterol homeostasis and whether by this means it promotes tumor cell metastasis. The strong overexpression of LIPG observed in a subset of breast tumors and cell lines could represent an advantage to deal with their increased cholesterol content. LIPG can exert various functions on lipoproteins (summarized in Figure 10). LIPG can use its enzymatic activity towards phosphatidylcholine in HDL to release free fatty acids (FAs) and lysophosphatidylcholine (LPC), thereby supplying cells and promoting proliferation and survival. *Via* its non-catalytic function LIPG can bridge HDL and LDL to their respective receptors and facilitate either LDL uptake via LDLR endocytosis or cholesterol exchange with HDL via the HDL receptor SR-BI. Although not illustrated, selective cholesterol ester uptake from HDL could be potentially possible as well. LIPG can also support excess cholesterol efflux *via* ABCA1 and ABCG1 via ApoA1 or mature HDL as acceptors respectively to ensure optimal cholesterol homeostasis. Thus, overexpression of LIPG by tumor cells may affect all these functions.

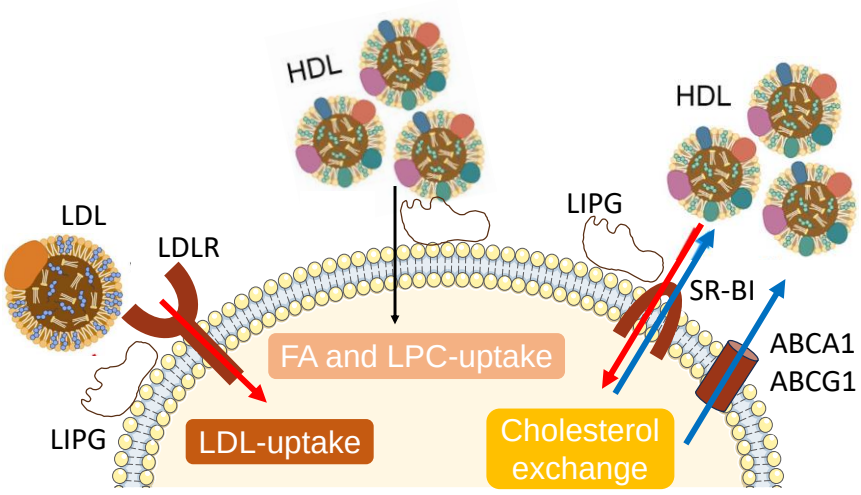

Figure 10: Illustration of extracellular fatty acid and cholesterol supply by LIPG (EL). LIPG either cleaves LPC into PC and free FAs. Or LIPG bridges LDL and HDL to its receptors on the cell surface, enabling internalization of the lipoproteins and specific cholesterol ester uptake. Excess cholesterol in the cell is transported out of the cell *via* ABCA1, ABCG1 and SR-BI. Illustrated with BioRender.

The aim of this thesis was to investigate the mechanisms by which LIPG contributes to breast cancer metastasis. In view of its multiple actions on lipoproteins, which are involved in the maintenance of systemic cholesterol homeostasis, one hypothesis was that LIPG contributes to the regulation of cholesterol levels within breast cancer cells using lipoproteins for cholesterol exchange, and that by these mechanism, metastasis-relevant processes, which are cholesterol-dependent, such as cell adhesion or migration, can be facilitated or become more efficient. In the first part of the study, the relevance of LIPG in metastasis formation was studied by silencing LIPG in high-LIPG-expressing breast cancer cell lines and investigating the consequences in cell adhesion and migration and in the expression of adhesion molecules. Second, the importance of cholesterol in cell adhesion was investigated in breast cancer cells by interventions that affect their cholesterol levels, such as cholesterol addition or withdrawal. Third, to assess the influence of LIPG on cholesterol exchange with lipoproteins in breast cancer cells, intracellular cholesterol levels were quantified after silencing LIPG and subsequent incubation with HDL and LDL. Additionally, gene expression changes in cholesterol homeostasis related genes (SR-BI, LDLR, ABCA1, ABCG1) were monitored after silencing LIPG. Finally, the influence of LIPG on HDL-mediated signaling progression was studied, since pathways known to be activated by HDL may also support metastasis. To this aim, LIPG depleted cells were treated with HDL and changes in the HDL signaling cascade were analyzed by looking into protein expression and phosphorylation.

4. Material

4.1 Cell Lines

Table 4: List of used cell lines.

Cell line	Name	Supplier
MDA-MB-468	Mammary breast cancer line, triple negative subtype	ATCC:HTB-132
HCC1954	Mammary breast cancer line, HER2 positive subtype	ATCC:HTB-2338
HCC1954Luc	Stable transferred cell line with luciferase plasmid, HER2 positive subtype	Generated by Annika Glotzbach
HUVEC	Human Umbilical Vein Endothelial Cells	Immunology department
OVCAR4	Ovarian cancer line, high-grade serous subtype	ATCC:HTB-76
OVCAR4Luc	Stable transferred cell line with luciferase plasmid, high-grade serous subtype	Generated by Zhwan Mahmoud

4.2 Cell Culture Media

Table 5: List of used culture media for cell cultivation and treatment.

Components	Supplier
Dulbeccos Modified Eagle Medium (DMEM) 4.5 g/L Glucose	PAN-Biotech Cat# P04-03550
Roswell Park Memorial Institute 1640 (RPMI1640)	PAN-Biotech Cat# P04-18500
Ham's F-12K (Kaighn's) Medium	Life Technologies

	Cat# 21127022
Fetal bovine serum GOOD (FBS GOOD)	PAN-Biotech Cat# P40-37500
Endothelial cell growth supplement with heparin (ECGS /H)	Promocell Cat# E0031
Sodium Pyruvate	Sigma-Aldrich Cat# S8636
Penicillin-Streptomycin	PAN-Biotech Cat# P06-07100
Gibco serum	Gibco, Life Technologies Cat# 10270106
Methyl-β-Cyclodextrin	Sigma-Aldrich Chemie GmbH
Cholesterol solubilized (complexed with cyclodextrin)	Sigma-Aldrich Chemie GmbH
Geneticin™ (G418)	Life Technologies Cat# 10131035

4.3 Formulations for Media

Table 6: List of media recipies.

Cell line	**Composition**
MDA-MB-468	500 mL DMEM 4.5 g/L Glucose 10% GOOD FBS 1% Penicillin-Streptomycin
HCC1954	500 mL RPMI1640 10% GOOD FBS 1% Sodium pyruvate
HCC1954luc	500 mL RPMI1640 10% GOOD FBS 1% Sodium pyruvate 2 mL G418
OVCAR4	500 mL RPMI1640

	10% Gibco FBS
OVCAR4Luc	500 mL RPMI1640 10% Gibco FBS 2 mL G418
HUVEC	500 mL Ham's F-12K 10% FBS 1% Penicillin-Streptomycin 0.5% ECGS /H

4.4 Agents for Cell Treatment

Table 7: List of agents for cell treatment and coating.

Substances		**Concentration**
Trypsin Inhibitor	Dissolved in DEPC-water (stock: 50 mg/mL)	0,5 mg/mL in cell suspension
Fibronectin	Stock: 1 mg/mL	20 µg/mL in DEPC-water
Vitronectin	Stock: 1 mg/mL	20 µg/mL in DEPC-water
Collagen I	Stock: 1 mg/mL	20 µg/mL in DEPC-water
Laminin	Stock: 1 mg/mL	20 µg/mL in DEPC-water

4.5 Primers and Probes

Table 8: List of primers and probes.

Probes	**Supplier**
ABCA1	Life Technologies, Hs00184500_m1
ABCG1	Life Technologies, Hs00245154_m1
ITGAV	Life Technologies, Hs00233808_m1
HMGCR	Life Technologies, Hs00168352_m1
LDLR	Life Technologies, Hs01092525_m1
LIPG	Life Technologies, Hs00195812_m1
SCARB1	Life Technologies, Hs00969821_m1
LRP1	Life Technologies, Hs00233856_m1
LPL	Life Technologies, Hs00173425_m1
PCSK6	Life Technologies, Hs01060079_m1

SOAT1	Life Technologies, Hs00162077_m1
UBC	Life Technologies, Hs00824723_m1

4.6 siRNA/DNA for Transfection and Culture Medium

Table 9: List of siRNA for knockdown, DNA for overexpression and used transfection reagents.

siRNA/DNA/media	**Supplier**
LIPG B	Invitrogen, Life technologies Cat# s17962
LIPG D	Invitrogen, Life technologies Cat# s113929
LIPG F	Invitrogen, Life technologies Cat# s190265
ITGAV1	Invitrogen, Life technologies Cat# s7569
ITGAV2	Invitrogen, Life technologies Cat# s7568
SCARB1	Invitrogen, Life technologies Cat# s2649 oder s2648?
LDLR	Invitrogen, Life technologies Cat# s7
LRP1	Invitrogen, Life technologies Cat# s8279
LRP1	Invitrogen, Life technologies Cat# s8278
MedGC	Invitrogen, Life technologies Cat# 12935300
Ambion Neg 2	Invitrogen, Life technologies Cat# 4390846
Opti-MEM	Gibco, Life Technologies
Lipofectamine 2000	Invitrogen, Life Technologies Cat# 13778150
pCMV/ hygro-negative control vector	Hölzl Diagnostika Handels GmbH

pCMV-LIPG-Flag vector	Hölzl Diagnostika Handels GmbH
X-tremeGene HP DNA transfection reagent	Sigma-Aldrich Cat# 6366244001

4.7 Antibodies

Table 10: List of Antibodies.

Antibody	**Supplier**	**Dilution**
Beta-Actin	Sigma-Aldrich, A5216	1:5000
ITGAV	Abcam, ab208012	1:1000
SR-BI	Abcam, ab217318	1:1000
pFAK (Y397)	Cell Signaling Technology, 3283S	1:1000
FAK	Cell Signaling Technology, 3285S	1:1000
pERK1/2 (Thr202/Tyr204)	Cell Signaling Technology, 3283S	1:1000
ERK1/2	Cell Signaling Technology, 3285S	1:1000
pAKT (Ser473)	Cell Signaling Technology, 4051S	1:1000
AKT	Cell Signaling Technology, 2920S	1:1000
pERK5 (T218/Y220)	Cell Signaling Technology, 3371S	1:1000
ERK5	Cell Signaling Technology, 3372S	1:1000
ABCG1	Invitrogen, MA5-35185	1:1000
HMGCR	Invitrogen, MA5-35242	1:1000
LIPG N-terminal (from rabbit)	Abcam plc, Cambridge Cat# Ab24447	1:500
Calnexin (from mouse)	BD #04977 Cat# 610523	1:1000

Anti-rabbit-HRP (from goat)	Cell Signaling Technology Cat# 25	1:1000
Anti-mouse-HRP (from goat)	Cell Signaling Technology Cat# 31	1:3000

4.8 Chemical Reagents

Table 11: List of chemical reagents.

Chemical	**Supplier**
Acrylamide (30%)	AppliChem GmbH
Ammonium peroxodisulfate (APS)	Invitrogen Life Technologies GmbH
Anode buffer concentrate A	Carl Roth GmbH&Co. KG
Bromphenol blue	Carl Roth GmbH&Co. KG
Bovine serum albumin (BSA)	Sigma-Aldrich Chemie GmbH
Cathode buffer concentrate	Carl Roth GmbH&Co. KG
DEPC treated water	Invitrogen Life Technologies GmbH
Dithioerythritol (DTE)	GERBU, Biotechnik GmbH
Dimethyl sulfoxide (DMSO)	Sigma-Aldrich Chemie GmbH
Ethanol	Fisher Scientific GmbH
Fibronectin	Sigma-Aldrich Chemie GmbH
Formaldehyde	AppliChem GmbH
Glycerol	Carl Roth GmbH&Co. KG
Glycine	Carl Roth GmbH&Co. KG
Hydrochloric acid (HCl)	VWR International GmbH
Isofluran	Sigma
Isopropanol	J.T. Baker
Luciferin	Promega
Methanol	Sigma-Aldrich Chemie GmbH
Methyl-beta-Cyclodextrin	Sigma-Aldrich Chemie GmbH
Nonidet P-40 substitute	F. Hoffmann-La Roche AG
Paraformaldehyde 4%	Carl Roth GmbH&Co. KG
Sodium chloride (NaCl)	VWR International GmbH
Sodium dodecyl sulfate (SDS)	SERVA Electrophoresis GmbH

Sodium hydroxide	Carl Roth GmbH&Co. KG
Stripping buffer	Thermo Fisher Scientific GmbH
Tetraethylen diamine (TEMED)	Carl Roth GmbH&Co. KG
Trypsin 0.05% / EDTA	PAN-Biotech GmbH
Tris	Carl Roth GmbH&Co. KG
Triton X-100	Carl Roth GmbH&Co. KG
Soybean Trypsin Inhibitor	Sigma-Aldrich Chemie GmbH
Tween20	Fisher Scientific GmbH

4.9 Buffer Solutions

Table 12: List of buffer solutions.

Buffer	**Composition**
Anode Buffer	100 mL buffer concentrate 200 mL Methanol 700 mL ddH2O
APS	10% (w/v) APS in ddH2O
Blocking buffer for Western Blotting	5% BSA in TBS-T
Cathode Buffer	100 mL buffer concentrate 200 mL Methanol 700 mL ddH2O
Enhanced chemiluminescence	2.5 mL 250 mM Luminol 0.55 mL 90 mM p-CA Fill up with 0.1 mM Tris to 250 mL
Loading buffer (5x)	2.25 mL 1M Tris-HCL pH 6.8 5 mL glycerol 0.5 g SDS 5 mg bromophenol blue 2.5 mL 1 M DTT
Precipitation buffer (proteins)	4 M ammonium sulfate in H2O
RIPA lysis buffer recipe	50 mM Tris-Cl (pH 7.5) 150 mM NaCl 1% Nonidet P-40 (NP-40)

	0.5% Sodium deoxycholate 0.5% SDS
Running buffer (10x)	30.3 g Tris 144 g glycerol 10 g SDS adjust to a volume of 1 L with ddH2O pH should be 8.3
Separation buffer	3 M Tris in H2O pH 8.8 with HCl
Stripping buffer	pH 2.2 15 g glycin 1 g SDS 10 mL Tween 20 Adjust to a volume of 1 L with ddH2O
TBS (10x)	pH 7.4 12 g Tris 53 g NaCl adjust to a volume of 1 L with ddH2O
TBS-T	100 mL TBS (10x) 500 µL Tween 20 adjust to a volume of 1 L with ddH2O

4.10 Kits and Size Standards

Table 13: List of Kits and Size Standards.

Kits/ size standards	**Supplier**
BCA protein assay kit	Thermo Fisher Scientific Inc. (Pierce Protein Research Products)
cDNA kit	Thermo Fisher Scientific Inc. (Applied Biosciences)
CellTiter-Blue cell viability assay	Promega Corporation
Cholesterol Assay Kit	Abcam
Triglyceride Assay Kit	Abcam
Magic marker	Invitrogen Life Technologies GmbH

TaqMan master mix	Thermo Fisher Scientific Inc. (applied Biosciences)
Western lightning Plus-enhanced	Chemiluminescence substrate PerkinElmer
Precision plus protein dual color standard	Bio-Rad Laboratories
QIAshredder	Qiagen GmbH
Qiagen RNeasy mini kit	Qiagen GmbH

4.11 Disposable Consumables

Table 14: List of disposable consumables.

Consumables	**Name**	**Supplier**
96-well plate	TC-Plate 96-well, Standard F TC-Plate 96-well, Black, clear bottom	Sarstedt AG&Co., Nürnbrecht
6-well plate	TC-plate 6 well, Standard, F	Sarstedt AG&Co.
24-well plate	TC-plate 24 well, Standard, F	Sarstedt AG&Co.
12-well plate	TC-plate 12 well, Standard, F	Sarstedt AG&Co.
Cell culture flasks	TC-flask T25, T75, T175, Standard	Sarstedt AG&Co.
Cell scraper	For scraping cell lysates	Sarstedt AG&Co.
Cover slips	Imaging dish for microscopy	Menzel
Microscopy slides	Imaging dish for microscopy	Thermo Fisher Scientific Inc. (Pierce Protein Research Products)
Sterile pipettes	Serological pipettes with cotton plug	Sarstedt AG&Co.

PDVF-Membran	Membrane for Western blotting	Immobilon PVDF Membran PerkinElmer, Inc.
Reaction tubes (0.5-5 mL)	Eppendorf tubes	Eppendorf AG
Single wells	35 mm diameter, with glass bottom	MaTek Corporation

4.12 Laboratory Equipment

Table 15: Laboratory equipment.

Equipment	**Name**	**Manufacturer**
Blot imager	Vilber Fusion Fx7	Vilber Lourmat
Blot chamber	fast blot B44	Biometra GmbH
CARS		
Cell Counting Device	Casy cell Counter Innovatis	F. Hoffmann-La Roche AG
Centrifuges	centrifuge megafuge 10R centrifuge MiniSpin plus	Thermo Fisher Scientific Inc. (Pierce Protein Research Products) Eppendorf
Electrophoresis chamber		Bio-Rad Laboratories
Microscopes	confocal microscope (LSM) FV1000 Olympus Optical microscope eclipse TS 100 Nikon	Olympus Nikon
NanoDrop	NanoDrop ND-1000	Thermo Fisher Scientific Inc.
Thermo-cycler	qRT-PCR system ABI 7500	Thermo Fisher Scientific Inc. (applied Biosciences)
pH meter	CG842	Schott
Plate reader	Infinite M200 SpectraFluor Plus	Tecan

Power supplies	For SDS-PAGE and Western blot	Biometra GmbH
RAMAN	Imaging	Oxford Instruments WITec alpha300R
Sterile hood		Hereaus
Sonicating device		Thermo Fisher Scientific Inc. (Pierce Protein Research Products)
Thermo cycler	Tgradient	Biometra GmbH
Transfer chamber	B34 Protein Blotter	Biometra GmbH
UV/ Vis spectrometer	V-530	Jasco
Water bath		Labortechnik

5. Cellular Approaches

5.1 Cell-based methods

5.1.1 Cell Cultivation

The adherent breast cancer cell lines MDA-MB-468 and HCC1954Luc, used for all experiments, were grown in monolayer in T175 flasks at 37°C and 5% CO_2. They were cultivated in RPMI1640 or DMEM (4.5 g/L Glucose) medium with different supplements (Table 5). The DMEM (4.5g/L Glucose) for MDA-MB-468 was supplemented with 10% FBS Good. FBS Good is a standardized serum, which provides growth factors. For HCC1954Luc, RPMI1640 was used, which includes 10% Gibco FBS, 1% sodium pyruvate and 2 mL Geneticin (G418). Geneticin is necessary for selecting cells, which stably express luciferase. OVCAR4Luc cells were cultivated in RPMI1640 with 10% FBS and 2 mL G418 at 37°C and 5% CO2. Human umbilical vein endothelial cells (HUVEC) were cultivated in Ham's F-12K medium with 10% FBS, 0.5% endothelial cell growth supplement with heparin (ECGS/H) and 1% penicillin streptomycin, which is an antibiotic. HUVEC cells were incubated at 37°C and 5% CO_2. After the cells reached 80-90% confluency, they were washed with phosphate buffered solution (PBS) and incubated with Trypsin/EDTA (Ethylenediaminetetraacetic acid) at 37°C and 5% CO_2 for 5 min. Trypsin is cleaving focal adhesions like integrins to detach the cells from the culture flask. EDTA is a chelating agent, that binds divalent cations and interferes with integrin activity. The cell suspension is then taken up with 8 mL of fresh medium to stop trypsin activity. For additional cultivation the cells were added to a new T175 flask, in the needed dilution, with 25 mL medium.

5.1.2 Cell Counting

Before counting the cells, the cell suspension was centrifuged for 5 min at 800 rpm at RT and the cell pellet was resuspended in 20 mL media. This step is necessary to discard cell debris and dead cells. 100 µL of the cell suspension were given into 1 mL CASY Tonic in a CASY Cup. Then, the cells were counted using the CASY Cell Counter (F. Hoffmann-La Roche AG) according to the manufacturer's protocol. CASY measures the conductivity between two electrodes separated by a defined pore. Cells are suspended in CASYton, a defined buffer solution. During measurement, cells passing through the pore generate an electrical pulse. The intensity of the signal directly correlates with the volume of the cell. Hence CASY detects the volume of each cell passing through the pore.

5.1.3 Extraction of Proteins, RNA, Triglycerides, and Cholesterol

After defined cell treatments in 6-well plates, the cells were washed and harvested. For extraction of the cell surface associated LIPG, the medium was discarded, cells were washed with PBS and incubated with 500 µL medium, containing 10 U/mL Heparin. Heparin is a glycosaminoglycan located at the cell membrane that can bind several extracellular components. The cells were treated over night at 37°C and 5% CO_2. The heparin-bound protein fraction was centrifuged for 10min at 10,000 rpm and 4°C to separate proteins from cell fractions and dead cells. After centrifugation the heparin-bound proteins are located in the supernatant and the cell remains are found in the pellet. Afterwards, the supernatant was transferred to a new reaction tube treated with 4M NH_2SO_4 overnight at 4°C and subsequently centrifuged at 4°C for 1 h to precipitate the protein. The obtained cell pellet was resuspended in 16 µL RIPA buffer and 4 µL loading buffer for immunoblotting.

For extraction of the intracellular protein fraction, the attached cells were treated with 150 µL RIPA and scraped using a cell scraper. Afterwards, the cell suspension was sonicated in a reaction tube. Then, the obtained cell lysate was centrifuged at 4°C for 30 min and the supernatant containing the solubilized proteins was transferred into a new reaction tube. For long time storage, the samples were initially shock frozen and placed at -80°C.

To obtain ribonucleic acid (RNA), the cells were washed with PBS. 700 µL RLT buffer was added to each well and the cells were scraped and collected in a reaction tube. For long time storage, the samples were shock frozen and placed at -80°C.

For gaining TAG, the cells were washed with PBS and treated with 150 µL 5% NP40/ddH2O. The cells were scraped, sonicated and collected in a reaction tube. For long time storage, the samples were shock frozen and placed at -80°C.

To collect cells for cholesterol quantification, the cells were trypsinized with 200 µL trypsin/EDTA for 5 min at 37°C and 5% CO_2. The cell suspension was collected in 800 µL media. Afterwards the cell suspension was counted, using the CASY Cell Counter (F. Hoffmann-La Roche AG). 500.000 cells per sample were centrifuged for 5 min at 10.000 rpm. The cell pellet was shock frozen and stored at -80°C for later cholesterol extraction.

5.1.4 Transient Knockdown *via* siRNA

SiRNAs are synthetic RNA duplexes consisting of two multimer oligonucleotides annealed together to form short/small interfering RNAs (siRNAS) which are designed to recognize specific target mRNA molecules. To obtain better results these traditional duplexes are often chemically modified. The siRNAs can be commercially obtained from different companies. SiRNA operates through a post-transcriptional mechanism known as RNA interference (RNAi). After being incorporated into the RNA-induced silencing complex (RISC), the siRNA guides the complex to its complementary mRNA target based on sequence homology. Once bound, the Argonaute protein within the RISC complex cleaves the mRNA, marking it for degradation. This prevents the mRNA from being translated into a polypeptide chain, effectively silencing gene expression. [104] For performing a transient knockdown (KD) of target genes, the small interfering RNA (siRNA) technology was used. For efficient delivery of siRNAs to the cells a liposome-based transfection method with Lipofectamine was employed. This required 500 µL Optimem, 1.5 µL siRNA and 5 µL Lipofectamine (Invitrogen) for a 6-well plate. The transfection mixture had to be pre-incubated for 20 min at RT. Subsequently, the transfection mixture was given to a well and thoroughly distributed. $4 \cdot 10^5$ cells were plated on the transfection mixture and incubated for 72 h at 37°C and 5% CO_2.

5.1.5 Luciferase transfection and single cell cloning

To generate Luciferase expressing cells, the cell line OVCAR4 was transfected with the firefly-luciferase plasmid (*luc*) pGL4.51[luc2/CMV/Neo] (Promega) as well as with the pCMV6 [Neo] empty vector control.

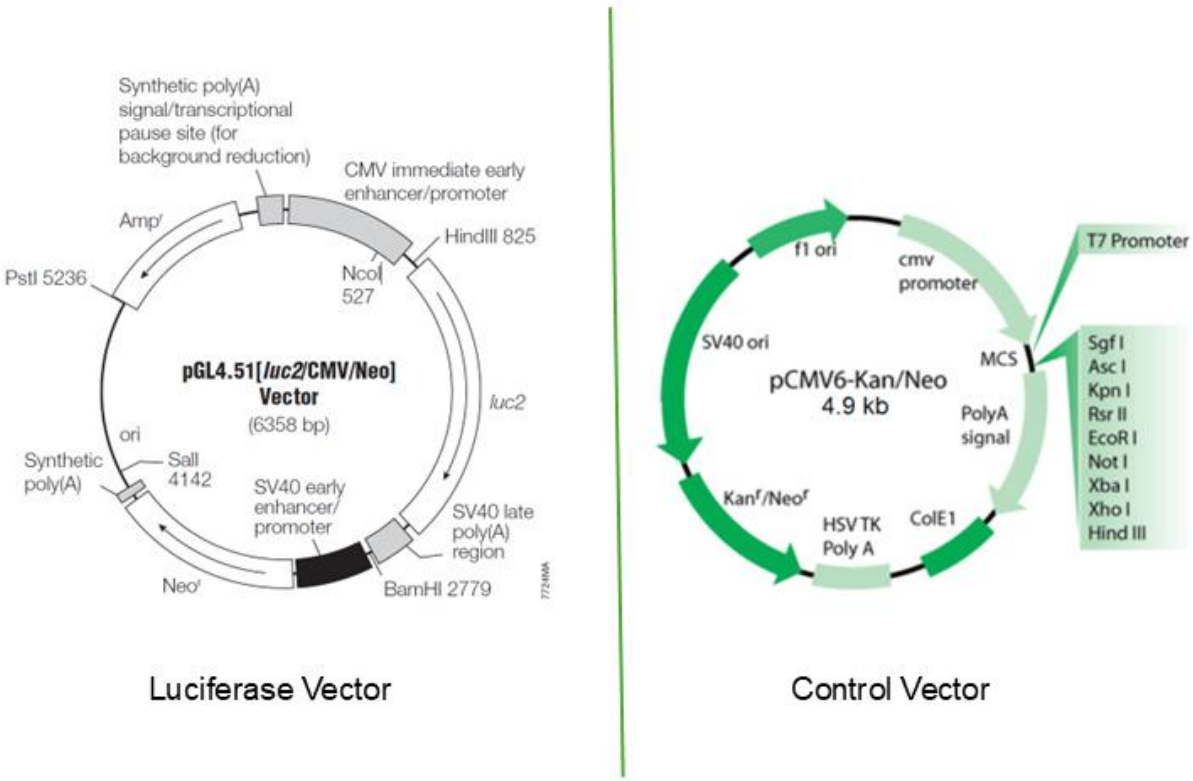

Figure 11: Plasmids used for luciferase transfection and control transfection. Images accessed from homepage of the manufacturers. [105], [106]

The cells were cultivated in a 24-well plate till they reached 70% confluency. For transfection the Lipofectamine 3000 Transfection Kit (Invitrogen) was used according to the manufacturer's instructions. In the first reaction tube 0.5 µL Lipofectamine 3000 was added to 25 µL Optimem. In the second reaction tube 500 ng DNA and 1 µL P3000 reagent were added to 25 µL Optimem. The contents of both tubes were combined and incubated at RT for 15 min. Then, 50 µL were added to each well for 7 h at 37°C and 5% CO_2. After 7 h the media was substituted with fresh media, containing G418 at a pre-determined concentration using an antibiotic kill-curve. G418 is an antibiotic used for selecting cells transfecting the luciferase expressing plasmid. The luciferase-expressing plasmid contains a G418 antibiotic resistance gene, which allows cells to survive when exposed to G418. Cells that fail to incorporate the plasmid, and therefore lack both the antibiotic resistance gene and the luciferase gene, are unable to survive under G418 treatment and die as a result.

After expansion of the cells, the selective growth of the luciferase expressing cells was confirmed by a luciferase assay. The ONE-Glo™ Luciferase Assay System (Promega) was used to determine luciferase expression in transfected cells with pGL4.51. This

assay is based on 5´-fluoroluciferin, which is oxidized by luciferase and emits luminescence. 100 µL Glo reagent was given to attached cells in a black 96-well plate. The cells were incubated for 3 min in the dark at room temperature (RT). In the end the luminescence signal was detected using a plate reader.

Next, single cell cloning of the luciferase positive cells was performed. For this approach 100 cells were seeded in a 15 cm culture dish. The cell growth was observed until single colonies were visible. Single colonies were manually picked by using a 100 µl pipette tip and transferring the single colony to a 96-well plate for further cultivation. Positive OVCAR4Luc clones were frozen and stored in liquid nitrogen.

5.2 Biochemical Techniques

5.2.1 Real-Time Quantitative Polymerase Chain Reaction (RT-PCR)

RNA was isolated using the Qiagen RNeasy Mini Kit by first lysing the cells and homogenizing the sample. The lysate was then mixed with ethanol to promote RNA binding to the silica membrane of the spin column. The column was washed multiple times to remove contaminants, and finally, RNA was eluted in RNase-free water. The RNA concentration was measured using the NanoDrop2000 (Thermo Fisher). The absorbance reading at 260 nm is used to calculate the concentration based on the Beer-Lambert law, where an absorbance of 1 corresponds to approximately 40 µg/mL of RNA. The purity of the sample is assessed by calculating the ratios of absorbance at 260 nm to 280 nm (for protein contamination) and 260 nm to 230 nm (for contaminants like phenol or other organic compounds). When samples do not fulfill quality criteria, indicated by abnormal 260/280 or 260/230 ratios, it suggests the presence of contaminants. Such contaminated samples may not perform well in downstream applications, like qPCR or sequencing, as these contaminants can inhibit enzymatic reactions or cause inaccurate results.

Following cDNA synthesis program and Master Mix were used to synthesize copy-DNA (cDNA).

Table 16: cDNA-program.

Step	Temperature	Time
Incubation	25°C	10 min
Reverse Transcription	37°C	120 min
Inactivation	85°C	5 min
	4°C	∞

Table 17: cDNA-Master-Mix.

Component	Amount
10x RT-PCR buffer	2 µL
25x dNTP	0.8 µL
10x RT-random primer	2 µL
Reverse transcriptase	1 µL
H_2O	4.2 µL

In RT-PCR, TaqMan chemistry is employed, which consists of specific forward and reverse PCR primers along with TaqMan probes. A TaqMan probe is an oligonucleotide that contains a 5' reporter dye and a 3' quencher. Fluorescence Resonance Energy Transfer (FRET) detects the proximity between the quencher and the reporter. During polymerization, the Taq polymerase's 5' to 3' exonuclease activity cleaves the probe, separating the quencher from the reporter, leading to an increase in fluorescence. As the reaction progresses, fluorescence intensity increases with each cycle, corresponding to the amount of amplified target. Fluorescence is measured automatically after each cycle, and the ΔΔCT method is used to calculate relative mRNA expression levels. The ΔΔCT method is a technique used in qPCR to determine the relative expression of a target gene. It normalizes the target gene's expression to a reference (housekeeping) gene, then compares it across different conditions (e.g., treated vs. control). The result is expressed as a fold change using the formula 2−ΔΔCT2^ {-\Delta \Delta CT}2−ΔΔCT, representing the relative expression difference between the samples. [107]

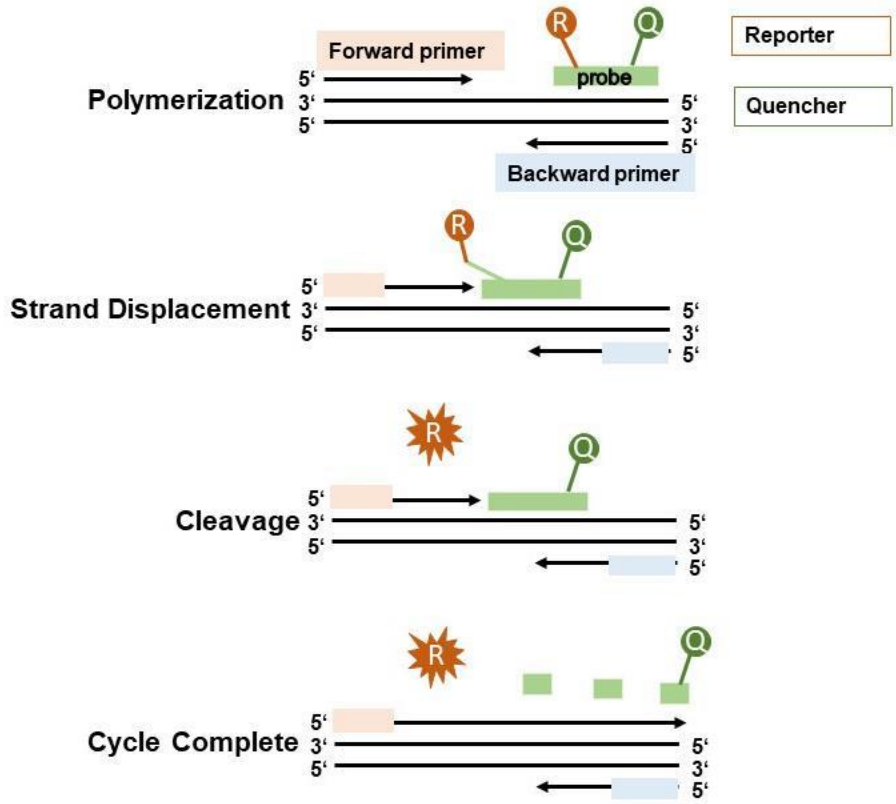

Figure 12: RT-PCR cycle adapted from life technologies.com. [107] Illustrated with PowerPoint.

To analyze the relative mRNA expression, a real-time PCR (RT-PCR) was performed. The following PCR program and Master Mix were used.

Table 18: RT-PCR program.

Step	**Temperature**	**Time**
Heating up	50°C	2 min
Enzyme activation	95°C	101 min
Denaturation	95°C	15 sec
Annealing and Elongation	60°C	1 min
Repetition of Denaturation, Annealing and Elongation		40 times

Table 19: RT-PCR Master-Mix.

Component	**Amount**
cDNA	5 µL
TaqMan Master Mix	12.5 µL
Primer Mix	1.25 µL
H_2O	6.25 µL

5.2.2 Western blotting

The Bicinchoninic Acid (BCA) protein quantification kit (Pierce) was used to quantify protein concentrations. The BCA Assay determines protein concentration by reducing copper ions (Cu^{2+}) to copper ions (Cu^{1+}) in the presence of proteins, followed by the formation of a purple-colored complex when Cu^{1+} reacts with bicinchoninic acid. The intensity of the color is proportional to the protein concentration and can be measured at 562 nm using a spectrophotometer. This method is sensitive and compatible with various substances, making it widely used for protein quantification. A standard curve was generated by pipetting different bovine serum albumin (BSA) concentrations into a 96-well plate. 5 µL of each sample, were diluted 1:5 with 20 µL ddH_2O. Then, 196 µL of reagent A and 4 µL of reagent B were given into each well. After 30 min incubation at 37°C in the dark, the absorption was measured at 562 nm in a plate reader (Tecan Infinite M200). The BSA standard curve was used to calculate the concentration.

In the next step, a sodium dodecyl sulfate polyacrylamide gel electrophoresis (SDS-PAGE) was used to separate the protein mixture according to weight and size. First, a SDS-Gel was prepared according to Table 20.

Table 20: SDS-Gel components for a 10% gel.

	Separation buffer (40 mL)	Stacking buffer (16 mL)
ddH_2O	16 mL	14.5 mL
1,5 M Tris (pH 8,8)	10 mL	-
1 M Tris (pH 6,8)	-	2.5 mL
10% SDS	0.4 mL	0.2 mL
30% Acrylamid	13.2 mL	3 mL
10% Ammoniumpersulfat	0.4 mL	0.3 mL
Tetramethylethylendiamin (TEMED)	0.16 mL	0.15 mL

A defined concentration of protein (25 µg) was mixed with loading buffer in a ratio of 1:5. The samples were heated at 95°C for 5 min in a heating block to denature the protein and then loaded onto the gel. To assign the molecular weight, Protein Markers were loaded onto the gel as well. The device ran at 15 mA per gel, till the proteins ran through the stacking gel into the separation gel. The protein separation took place at 30 mA per gel for approximately 1 h. For transferring the proteins from the SDS-PAGE to a membrane for western blotting, the semi-dry method was chosen. Hereby, 3 blotting papers, the membrane, the gel with separated proteins and a further blotting paper were stacked onto the blotting device. Each compartment was soaked in blotting buffer beforehand. Then, the blotting took place at 230 mA for 30 min. After the Western blot the membrane was blocked for 1 h at RT in 5% BSA or 5% Milk. For detection of specific proteins the membrane was incubated with primary antibodies overnight at 4°C in the respective blocking buffer, in a specified concentration (Table 10). After several washing steps, the secondary antibody was incubated at RT in the appropriate blocking buffer and dilution. The secondary antibodies used are labeled with horse radish peroxidase (HRP). To visualize the protein bands luminol is oxidized by HRP enzyme into chemiluminescent light. Luminol is part of the enhanced chemiluminescence (ECL, Bio-Rad) reagent, which is catalyzed with 5% H_2O_2. The detection of chemiluminescence was at the wavelength 428 nm, using the Fusion Fx7 imager.

For further protein detection the membrane was stripped once with mild stripping buffer. A loading control is crucial in immunoblotting (Western blotting) as it ensures

comparable load amounts of protein in each lane for all samples. This is essential for the accurate interpretation of protein expression levels. Loading controls typically involve detecting a protein that is consistently expressed across all samples, such as Actin, Tubulin, or GAPDH.

5.2.3 Cholesterol Measurement

To extract intracellular cholesterol, the frozen cell pellets were resuspended in the extraction reagent chloroform:isopropanol:NP40 (7:11:0.1). After sonicating the samples, the suspensions were centrifuged at 10.000 rpm for 5 min. The supernatant was transferred into a new reaction tube, which evaporated at 55°C under liquid nitrogen supply for 2 h. The extracted cholesterol was taken up in assay buffer and sonicated again. To determine the cholesterol concentration, the Cholesterol-Cholesteryl Assay (Abcam) was performed according to the manufacturer's protocol. The Abcam cholesterol assay is designed for the sensitive and accurate quantification of cholesterol in biological samples. It measures both free cholesterol and total cholesterol, allowing the differentiation between the two by first enzymatically converting cholesterol esters into free cholesterol. The reaction results in a colorimetric or fluorometric signal, which is proportional to the cholesterol concentration and can be measured using a spectrophotometer or fluorometer. This assay is commonly used in research to assess cholesterol levels in cells, tissues, and plasma, contributing to studies on metabolism, cardiovascular disease, and lipid regulation. In the fluorometric cholesterol assay, a fluorescent signal is generated through an enzymatic reaction where cholesterol esters are first hydrolyzed into free cholesterol, which is then oxidized by cholesterol oxidase, producing hydrogen peroxide. The hydrogen peroxide reacts with a fluorogenic substrate in the presence of peroxidase, forming a fluorescent product. This fluorescence is proportional to the cholesterol concentration and is measured using a fluorometer, providing a highly sensitive method for cholesterol. The fluorescence intensity is measured at an excitation value of 535 nm and an emission value of 587 nm in a plate reader (Tecan Infinite M200). The final concentration is calculated by a cholesterol standard curve.

5.2.4 Triglyceride Assay

The cell extracts collected in NP40 were sonicated and heated at 95°C to extract all the lipids. After centrifugation at 10.000 rpm for 5 min, the supernatant was transferred into a reaction tube with 15 µL ddH_2O. A volume of 25 µl from each sample was used

for triglyceride measurement using the Triglyceride Assay Kit (Abcam). TAG detection is based on cleaving TAGs into free fatty acids and glycerol. Glycerol is oxidized and reacts with a probe, which creates a fluorescent signal (Ex/Em = 535/587nm). The fluorescent signal was detected in the plate reader (Tecan Infinite M200). Triglyceride levels in cells were normalized to total protein concentration, allowing results to be expressed per unit of protein. The final concentration was calculated using a TAG standard.

5.2.5 Adhesion Assay

Cell adhesion on extracellular matrix components was analyzed in 96-well plates. Before performing the adhesion assay, 5 wells per condition were coated with 50 µL fibronectin (20 µg/mL working solution) over night. The excess fibronectin solution was discarded, and the wells were dried under sterile conditions for 20 min. Then, the wells were treated with 1% BSA in 1x PBS overnight.

On the day of the experiment, the cells were trypsinized and collected in medium with 1% FBS and Trypsin Inhibitor (500 µg/mL) for 20 min. After centrifugation for 5 min at 800 rpm, the cell pellet was resuspended in fresh medium with 1% fetal bovine serum (FBS). Then, the cells were rotated for 1-2 h at 37°C and 5% CO_2. $5 \cdot 10^4$ cells per condition were seeded in a well and allowed to attach for 15 or 30 min at 37°C and 5% CO_2. Afterwards, the unattached cells were removed, and the attached cells were fixed and stained for 20 min with 1% crystal violet 10% EtOH/ddH2O. After washing, plates were dried and images were taken. To quantify the attached cells, the cells were destained first with 0,2% TritonX-100. Then, the absorbance was measured at 570 nm, using a plate reader (Tecan Infinite M200).

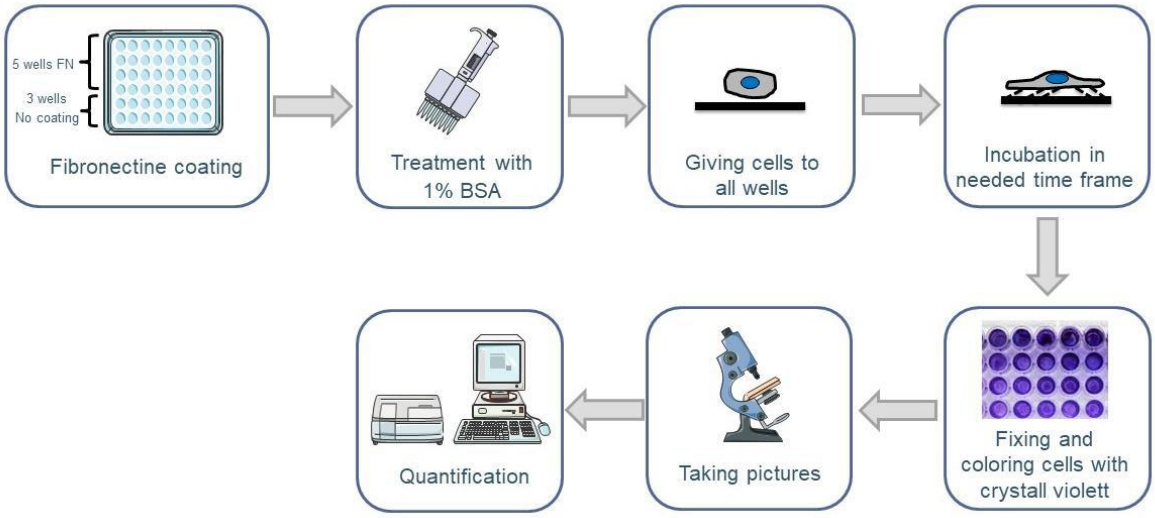

Figure 13: Adhesion Assay procedure. Illustrated with PowerPoint and Servier Medical Arts.

5.2.6 Migration Assay

To assess cell migration, $5 \cdot 10^5$ treated cells were seeded into an insert in a 12-well plate in media without FBS. This insert possesses a permeable membrane and allows the cells to migrate along a gradient. The necessary gradient is created using 500 µL media with 10% FBS in the well. Therefore, the cells can migrate from a 0% FBS condition to a 10% FBS condition for 24 h at 37°C and 5% CO_2. On the next day, the inserts were discarded and the migrated cells on the well, were fixed and stained for 20 min with crystal violet in methanol. Cells were imaged by using the Keyence microscope. For quantification the color intensity was assessed with ImageJ. The color intensity was normalized to the cell count of each condition.

5.2.7 Cell-titer Blue Assay (CTB-Assay)

The CTB Assay is a fluorometric method to detect cell viability. The assay is based on the cell ability to convert the dye resazurin to the fluorescent resorufin. Only viable cells are able to convert the dye, since dead cells lose their metabolic capabilities.

The CTB Assay was performed on cells seeded in a 6-well plate. All medium was discarded, and the cells were washed with PBS. Then, 400 µL media without FBS and 80 µL CTB reagent were given to each well. The plate was incubated at 37°C and 5% CO_2, until the blue color of the CTB reagent turned pink. Afterwards, 100 µL of each condition were pipetted into a black 96-well plate in triplicates. The fluorescence was measured using a plate (Tecan Infinite M200) reader at 540 nm excitation and 590 nm emission.

5.2.8 Cholesterol manipulation using Cholesterol and methyl-β-Cyclodextrin

The cells were seeded in a 6-well plate and incubated at 37°C and 5% CO_2 till they reached 80-90% confluency. Then, the cells were washed and media without FBS was added. To increase the cholesterol content of the cells, soluble cholesterol (cholesterol:cyclodextrin complex, Sigma) was added in a concentration range from 100 µL/mL till 800 µL/mL for 2 h . For withdrawing cholesterol, the cells were treated for 2 h with 1 mM, 2.5 mM and 5 mM methyl-β-cyclodextrin (Sigma).

Methyl-β-Cyclodextrin is a macrocyclic ring of glucose. It has a hydrophobic interior and a hydrophilic exterior, which enables the complexation of hydrophobic compounds like cholesterol. In our experiment Methyl-β-cyclodextrin is used to deplete cholesterol from the cell membrane and disrupt the cholesterol homeostasis.

5.3.9 Cell-cell adhesion to HUVEC cells

HUVEC were cultivated in Ham's F-12K medium with 10% FBS, 0.5% endothelial cell growth supplement with heparin (ECGS/H) and 1% penicillin streptomycin. HUVEC cells were incubated at 37°C and 5% CO_2. For the cell-cell adhesion experiment, $5 \cdot 10^5$ HUCEC cells were plated in a 96-well plate overnight at 37°C and 5% CO_2. MDA-MB-468 cells were stained with 2 µg/mL Hoechst (Life Technologies) in medium for 20 min at RT in the dark. The cells were centrifuged and the supernatant was discarded. Afterwards, the cells were washed with medium once to remove the remaining unbound staining. $5 \cdot 10^5$ MDA-MB-468 in medium were plated on top of the HUVEC cells for 15 min or 30 min at 37°C and 5% CO_2. After the incubation time the medium was discarded and the plates were washed three times with PBS. The cells were fixed with 4% PFA and images were taken with the Keyence microscope. Hoechst binds to cellular DNA and is visible at 460 nm, which was detectable in the *blue* channel. Cell nuclei of attached cells were manually counted with ImageJ. Unspecific attached cells to the well plate were subtracted as background control.

5.3 Imaging

5.3.1 RAMAN spectroscopy

Raman spectroscopy is a label free technique based on the light scattering phenomena. This method is commonly used to identify compounds with their unique fingerprint. After the sample is illuminated, the laser beam interacts with the bonds present in the sample molecules. As a result, the bonds may bend, stretch, or twist,

causing an energy shift compared to the incident laser beam. This change in energy provides the spectral signature of the compound revealing its chemical composition. [108] The Raman Imaging Microscope WITec alpha300R (Oxford Instruments) was used to collect the spectra. The Zeiss LD EC Epiplan-Neofluar Dic 50x magnification objective was used to pre-select the imaging area. A large-scale image scan was performed within an area of 10x10 µm. The integration time amounted to 10 sec and the excitation wavelength of the laser was 532 nm. After experiments the Raman data was further processed which includes background subtraction and normalization, was performed by Muzaffar Panhwar.

6. Results

6.1. The role of LIPG breast cancer

High LIPG expression is associated with a shorter metastasis free survival rate in breast cancer patients, but its contribution metastasis formation requires in-depth mechanistic insights. [1] Investigations of initial metastasis processes *in vitro* indicated that loss of LIPG in triple negative breast cancer (TNBC) cell lines slows down adhesion, migration and spheroid formation processes. Moreover, loss of LIPG also showed less tumor growth in xenograft studies *in vivo*. [98], [99] However, the exact mechanisms are not clarified yet. The goal of this thesis was to investigate whether LIPG contributes to the metastatic process by regulating tumor cells cholesterol levels.

To this aim, LIPG was silenced in two breast cancer cell lines. MDA-MB-468 is a cell line belonging to the TNBC subtype, which is associated with a high risk of recurrence and metastasis. [109] HCC1954 is a breast cancer cell line of the HER2+ subtype with no expression of estrogen and progesterone receptor. HER2+ breast cancer is characterized by a high mortality rate and poor prognostic outcomes without treatment. [110] Previous work has shown that both cell lines display high LIPG expression. [1] Therefore, they were suitable for silencing LIPG. Most experiments were performed in MDA-MB-468 cells and key experiments were validated in the second cell line, HCC1954. This cell line is suitable for *in vivo* studies and was stably transfected with a luciferase expressing plasmid, which allows *in vivo* imaging studies. It is therefore referred to as HCC1954Luc.

In the first part of this chapter, experimental evidence is provided for a role of LIPG in metastasis-related processes *in vitro*, such as cell adhesion to extracellular matrix, cell-cell adhesion and cell migration. Second, the importance of cholesterol in cell adhesion is studied by interventions that alter cellular cholesterol levels. Subsequently, it is demonstrated that LIPG influences cellular cholesterol levels via interactions with lipoproteins. Lastly, LIPG-regulated effects of lipoproteins on gene expression and intracellular signaling pathways are characterized.

6.1.1 LIPG silencing influences cellular metastatic processes in breast cancer cell lines

6.1.1.1 Silencing LIPG in breast cancer cells with siRNA results in loss of LIPG mRNA and protein expression

In preliminary experiments, LIPG knockdown conditions were implemented and adhesion processes in MDA-MB-468 cells were analyzed. [111] To investigate the influence of LIPG on further metastasis-related processes, LIPG knockdown was performed in MDA-MB-468 and HCC1954Luc with three different siRNA oligos (B, D, F). First, the knockdown of LIPG was confirmed in MDA-MB-468 (Fig. 14) and HCC1954Luc (Fig. 15) on mRNA and protein by qPCR and Western blot respectively. Furthermore, the effect of the knockdown on cell viability was analyzed. Figure 14B shows that LIPG knockdown in MDA-MB-468 cells did not result in significant loss of cell viability in the knockdown conditions LIPG B, D, F compared to the control conditions full media (FM), Lipofectamine (Lipo) and scrambled si-RNA (si-scr). The LIPG mRNA expression (Fig 14C) was strongly decreased in all knockdown conditions compared to the control condition. The highest decrease was achieved with siRNA oligo B. All three si-RNA conditions displayed no LIPG protein bands compared to the control conditions in the Western blots (Fig. 14D). The strongly decreased LIPG mRNA and protein expression suggested a successful knockdown.

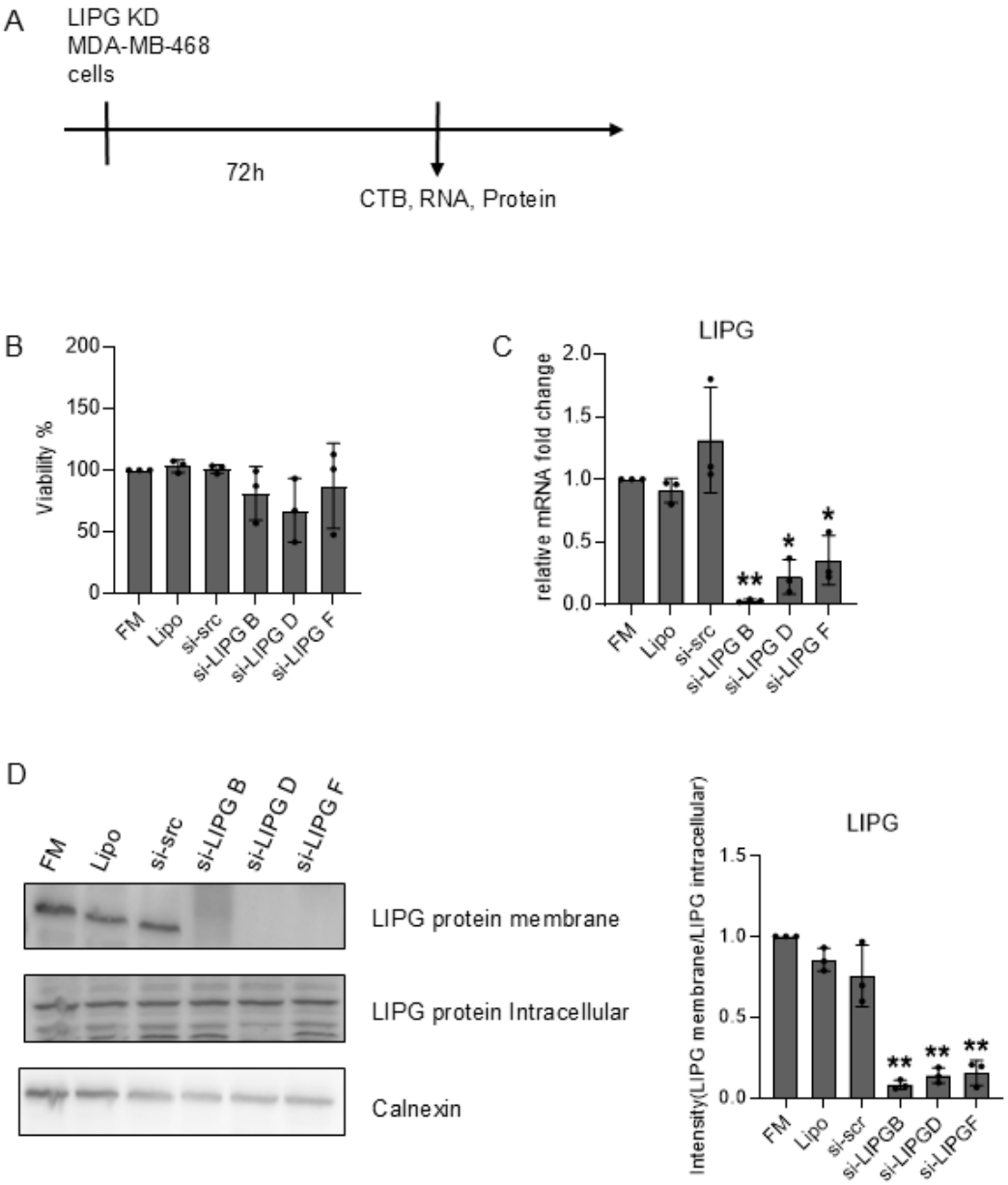

Figure 14: Confirmation of LIPG knockdown in MDA-MB-468 cells with analysis of mRNA expression, protein expression and cell viability. Cell viability (A) of all si-RNA were accessed using CTB assay and fluorescent measurement at 540 nm. LIPG knockdown was analyzed on mRNA level (B) with quantitative RT-PCR and the use of UBC as an endogenous control. Immunoblotting of LIPG protein expression was investigated (C) in cell lysates with calnexin as a loading control. The results represent the mean ± SD (n=3). *p < 0.05; **p < 0.01; Student's t test, unpaired, two sided. These results were first documented in the master thesis of Zhwan Mahmoud. [111]

In HCC1954Luc cells, the oligos si-LIPG B and si-LIPG D, but not si-LIPG F, significantly reduced cell viability (Fig. 15B). The LIPG mRNA (Fig. 15C) and protein (Fig. 15D) expression was strongly decreased in all knockdown conditions compared

to the control condition also in this cell line. Therefore, the LIPG knockdown was also successful in HCC1954Luc cells.

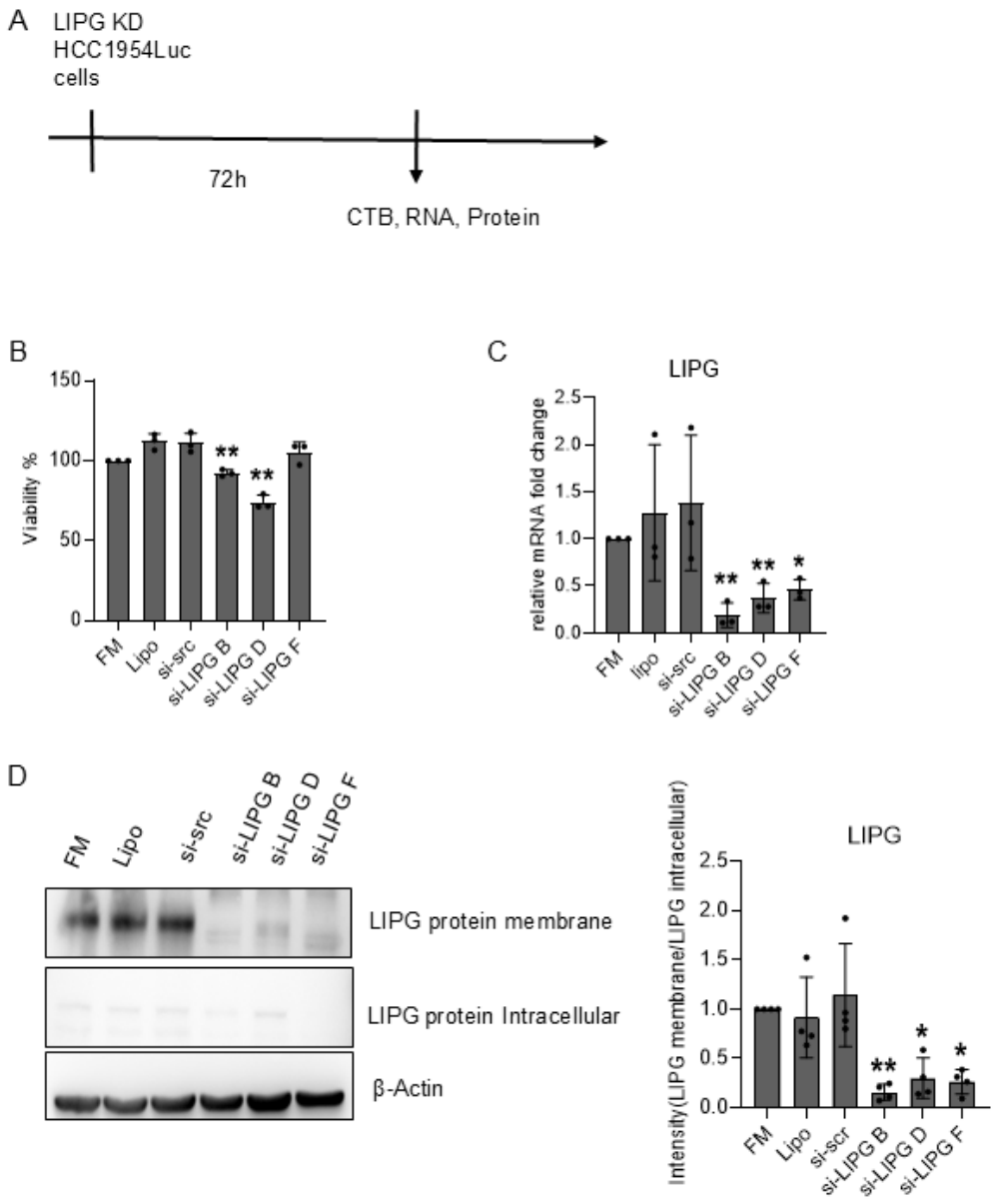

Figure 15: Confirmation of LIPG knockdown HCC1954Luc cells with analysis of mRNA expression, protein expression and cell viability. Cell viability (A) of all si-RNA were accessed using CTB assay and fluorescent measurement at 540 nm. LIPG knockdown was analyzed on mRNA level (B) with quantitative RT-PCR and the use of UBC as an endogenous control. Immunoblotting of LIPG protein expression was investigated (C) in cell lysates with calnexin as a loading control. The results represent mean ± SD (n=3). *p < 0.05; **p < 0.01; Student's t test, unpaired, two sided.

Having demonstrated that the LIPG knockdown is successful, the next step was to investigate the consequences of loss of LIPG on metastasis-related processes, such as cell adhesion and migration.

6.1.1.2 LIPG KD results in a transiently slowed down adhesion to the extracellular matrix

Cell adhesion to the extracellular matrix (ECM) is a cellular event necessary for the metastasis of tumor cells. The ECM consists of many components, which become recognized and bound by cellular integrin heterodimers. Ligands of the ECM are fibronectin, vitronectin, laminin and collagen. [112] To investigate whether LIPG influences cell adhesion to the extracellular matrix, the kinetic of cell adhesion to cell culture plates previously coated with different ECM components was monitored after LIPG knockdown in MDA-MB-468 and HCC1954Luc cells. In Figure 16B and 17B the adhesion kinetics of LIPG KD cells to fibronectin were compared to control cells. In the cell adhesion assay to fibronectin, both cell lines MDA-MB-468 and HCC1954Luc, showed a significant decrease in cell adhesion after 15 min attachment time in all knockdown conditions. After 30 min, no significant difference in cell adhesion was detected, suggesting that the ability to attach was not completely impaired but only transiently decreased.

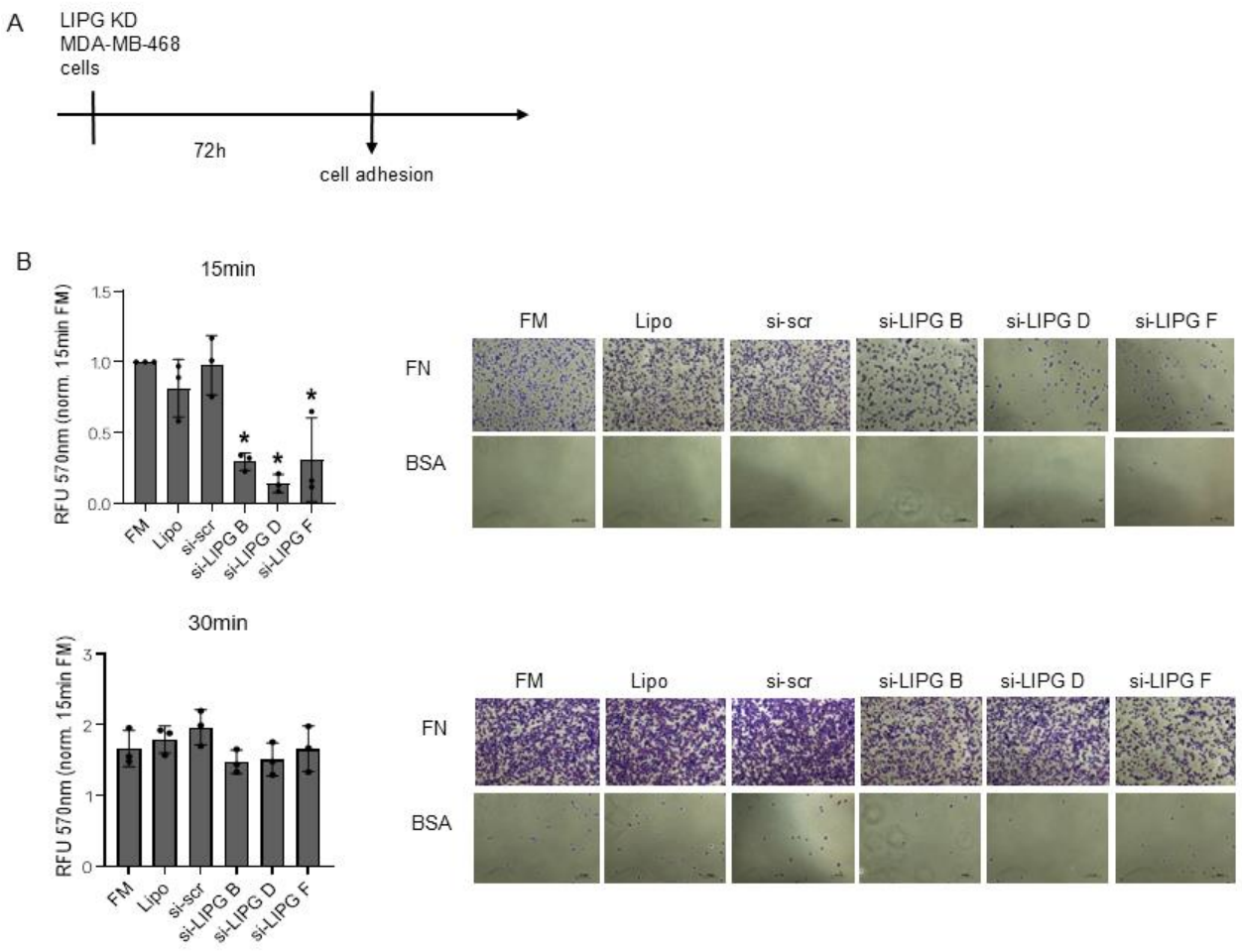

Figure 16: Cell adhesion after LIPG KD in MDA-MB-468 cells. The cell adhesion to a fibronectin matrix or to BSA as control was assessed after 15 min and 30 min in media containing 1% FBS (A). Background absorption from BSA controls was subtracted from the fibronectin-coated wells, and the final absorbance was measured at 570 nm (B). The results represent the mean ± SD (n=3). *p < 0.05; Student's t test, unpaired, two sided. These results were first documented in the master thesis of Zhwan Mahmoud. [111]

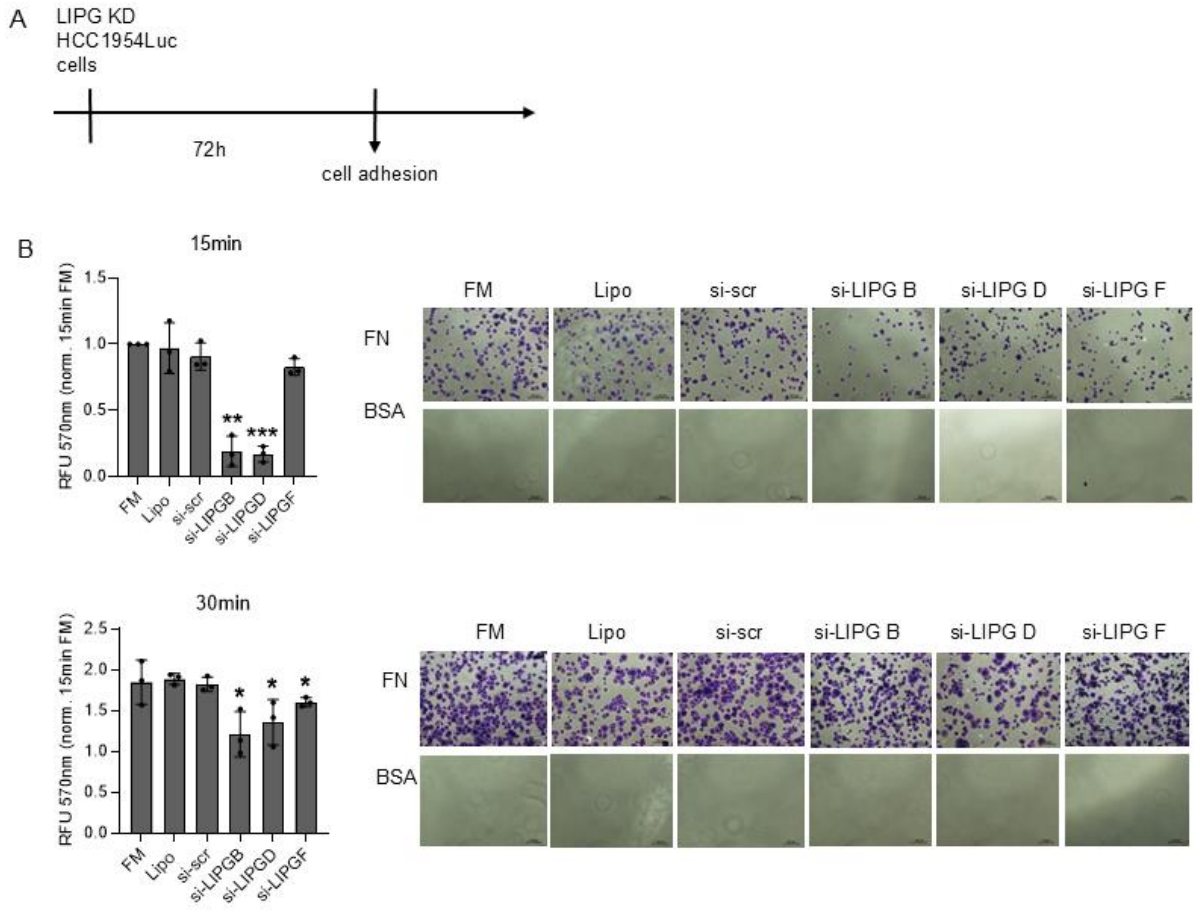

Figure 17: Cell adhesion after LIPG KD in HCC1954Luc cells (A). Adhesion was assessed after 15 min and 30 min in media containing 1% FBS. Background absorption from BSA controls was subtracted from the fibronectin-coated wells, and the final absorbance was measured at 570 nm (B). The results represent the mean ± SD (n=3). *p < 0.05; **p<0.01; ***p<0.001. Student's t test, unpaired, two sided.

Cell adhesion to other components of the extracellular matrix (laminin, collagen and vitronectin) was investigated in MDA-MB-468 cells as well (Fig. 18A). LIPG KD in MDA-MB-468 cells showed a significant decrease in cell attachment on laminin for si-LIPG B and F after 15 min. After 30 min the decrease in cell adhesion was significant only with the si-LIPG B (Fig. 18B). Cell adhesion on collagen was significantly decreased after 15 min incubation time for all si-RNA oligos si-LIPG B, D and F. After 30 min the decrease in cell adhesion was not significant (Fig. 18C). On vitronectin coating, cell adhesion of LIPG KD MDA-MB468 cells was significantly decreased after 15 min and 30 min with all siRNA oligos si-LIPG B, D and F compared to the control conditions (Fig. 18D). These results show a significant contribution of LIPG to the kinetics of cell adhesion, independent of the ECM protein component after 15 min. After 30 min, only adhesion to vitronectin was significantly decreased after LIPG KD. Therefore, in

general, the effect on adhesion was transiently slowed down. This suggests that LIPG is not an essential component but affects only the kinetics of the attachment process.

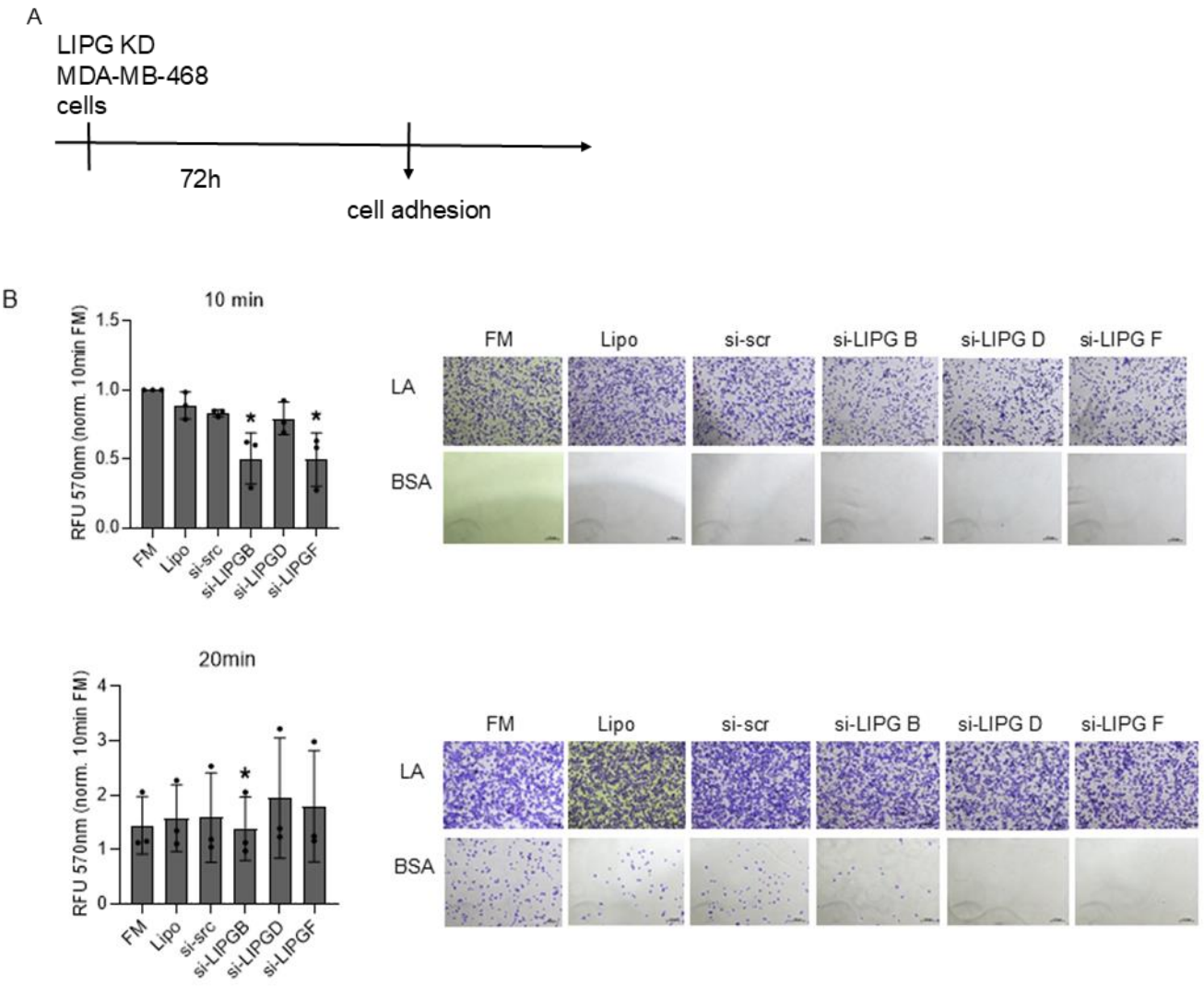

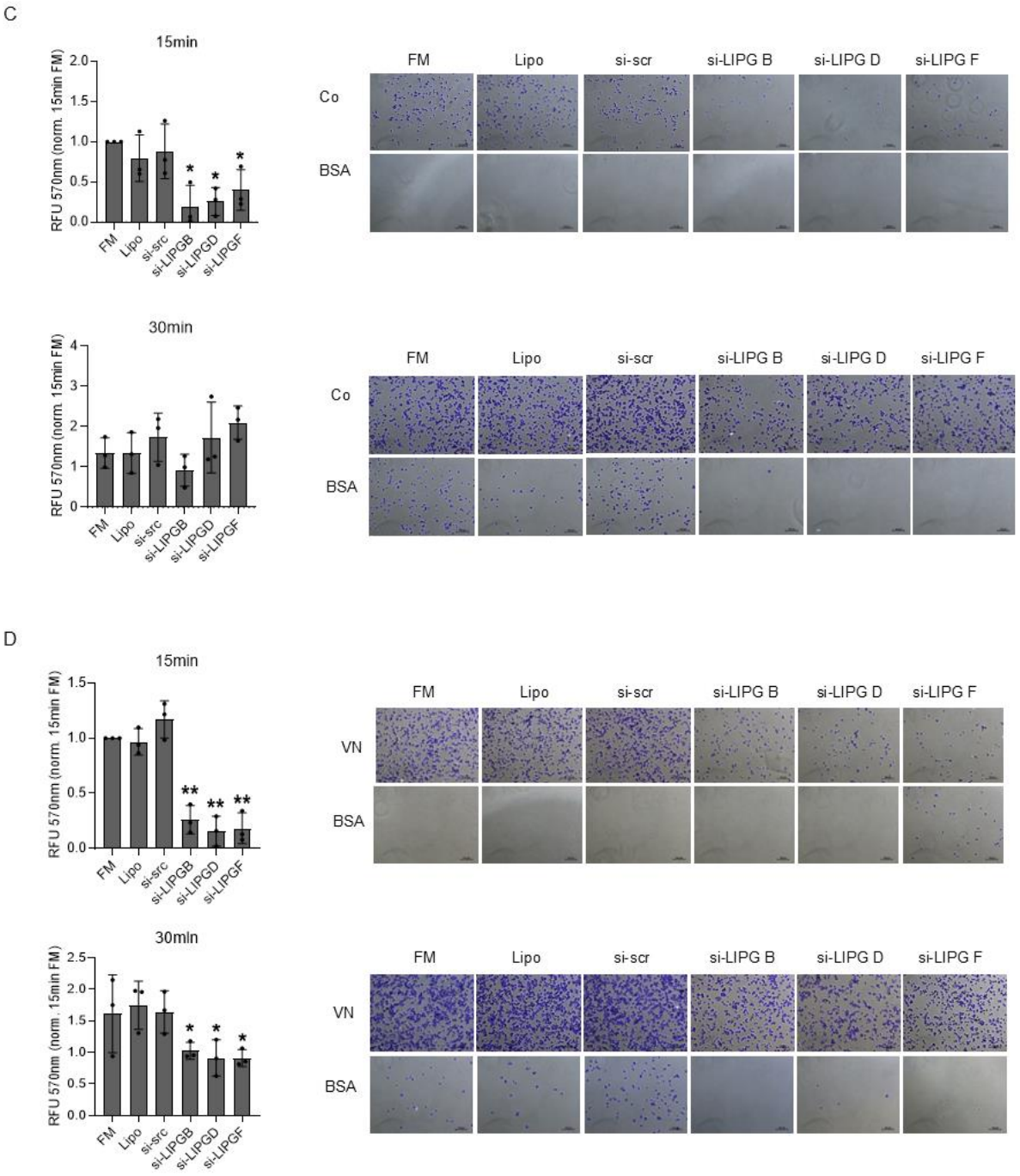

Figure 18: Decrease in adhesion of LIPG KD in MDA-MB-468 cells on vitronectin, laminin or collagen. (A) Illustration of experimental design. Adhesion after 15min and 30min in media with 1% FBS on laminin (B), collagen (C) or vitronectin (D). BSA control was subtracted from the ECM protein coated wells and absorption was measured at 570 nm. The results represent the mean ± SD (n=3). *p<0.05; **p<0.01; Student's t test, unpaired, two sided.

6.1.1.3 LIPG knockdown results in a transiently slowed down cell adhesion to endothelial cells

Cell adhesion to vascular endothelial cells is also an important step during the metastatic process. To investigate a possible contribution of LIPG to this process, the cell adhesion kinetic of MDA-MB-468 cells to a monolayer of human umbilical vascular cells (HUVEC) cells was monitored. The MDA-MB-468 cells were previously labeled with Hoechst to distinguish them from HUVEC cells and the fluorescence signal quantified after fixation and washing. (Fig. 19A).

As seen in Figure 19B, the knockdown of LIPG resulted in a significant decrease in cell-cell adhesion after 15 min with all siRNA oligos tested. 30 min after attachment, the decrease was no longer seen, indicating transiently slowed down cell-cell adhesion kinetic, as also observed in the experiments of cell adhesion to the ECM.

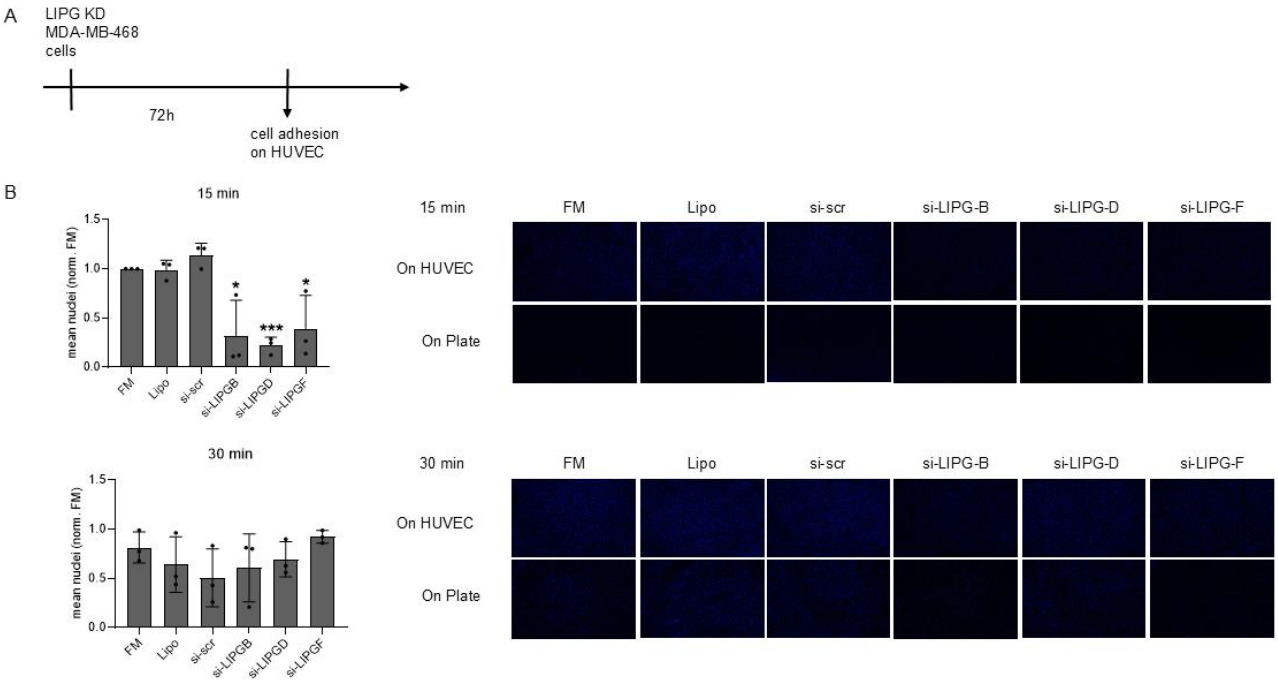

Figure 19: Decrease in cell adhesion of LIPG silenced MDA-MB-468 to a monolayer of HUVEC cells (A) Illustration of experimental design. (B) Adhesion of Hoechst-labeled MDA-MB-468 cells after 15 min and 30 min in media with 1% FBS. The fluorescence of the attached cells was imaged using Keyence Microscope. The images were quantified with ImageJ and the background fluorescence (on plate) was subtracted. The results represent mean ± SD (n=3).

6.1.1.4 LIPG knockdown results in significantly reduced cell migration

Increased cell migration is an acquired property of transformed epithelial cells that invade the extracellular matrix. To investigate a possible contribution of LIPG to this

process, the migration of MDA-MB-468 cells in a transwell assay was monitored. (Fig 20A). As seen in Figure 20B, the knockdown of LIPG resulted in a significant decrease in cell migration with all siRNA oligos tested.

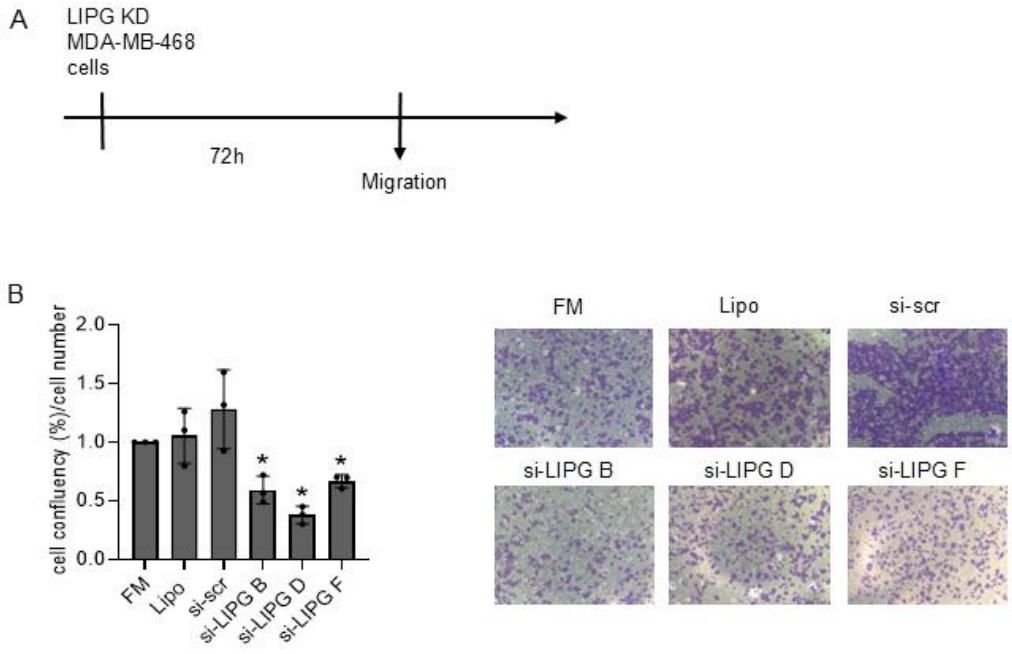

Figure 20: Decrease in cell migration of LIPG-silenced MDA-MB-468. (A) Illustration of experimental design. (B) Cell migration of MDA-MB468 cells in a transwell assay. After fixation and staining of migrated cells, the absorption was measured at 570 nm. The results represent mean ± SD (n=3).

6.1.1.5 LIPG knockdown results in decreased expression of ITGAV and FAK in breast cancer cells

The decreased cell adhesion and migration after silencing LIPG suggests that the integrin signaling in LIPG KD cells may be affected. Integrins are cell surface adhesion receptors that mediate interactions between ECM and cells and are essential for cell adhesion and migration. Integrin expression has been associated with tumor invasion, metastasis and sustained proliferative signaling. Relevant for these processes are crosstalks with EGFR-signaling, IGF-signaling and intracellular recruitment of protein kinases like FAK or SRC. [113] Integrin αV (ITGAV) is overexpressed in patients with metastatic disease and is correlated with poor survival. ITGAV is an α subunit and can dimerize with five different β subunits. The resulting heterodimers can recognize a variety of ECM ligands, including fibronectin and vitronectin. [112]

FAK is a nonreceptor tyrosine kinase that regulates Integrin signaling and is responsible for cell proliferation, survival and migration. Activation of FAK is regulating downstream signaling pathways like PI3K, AKT and MEK signaling. FAK downregulation leads to less invasion and metastasis formation. Whereas FAK overexpression shows higher metastasis and invasive carcinomas. [114] Since integrin and FAK are the predominant regulators of such cellular processes relevant to the metastasis cascade, these proteins were analyzed after LIPG KD in MDA-MB-468 by Western blot (Fig. 21). The impact of LIPG silencing on ITGAV and FAK expression in MDA-MB-468 is presented in Figure 21B-C. LIPG KD for 72 h in MDA-MB-468 led to a slightly reduced protein expression of ITGAV and FAK in the LIPG KD conditions compared to the si-scr control conditions. Producing more replicates could add significance to the seen findings. However, the phosphorylation of FAK (pFAK) was significantly lowered in all LIPG knockdown conditions, demonstrated affected FAK signaling in the absence of LIPG. This observation could possibly explain the decreased migration and slowed down adhesion processes. The transient decrease of adhesion may be due to the formation of other integrin heterodimers, rescuing the adhesion process.

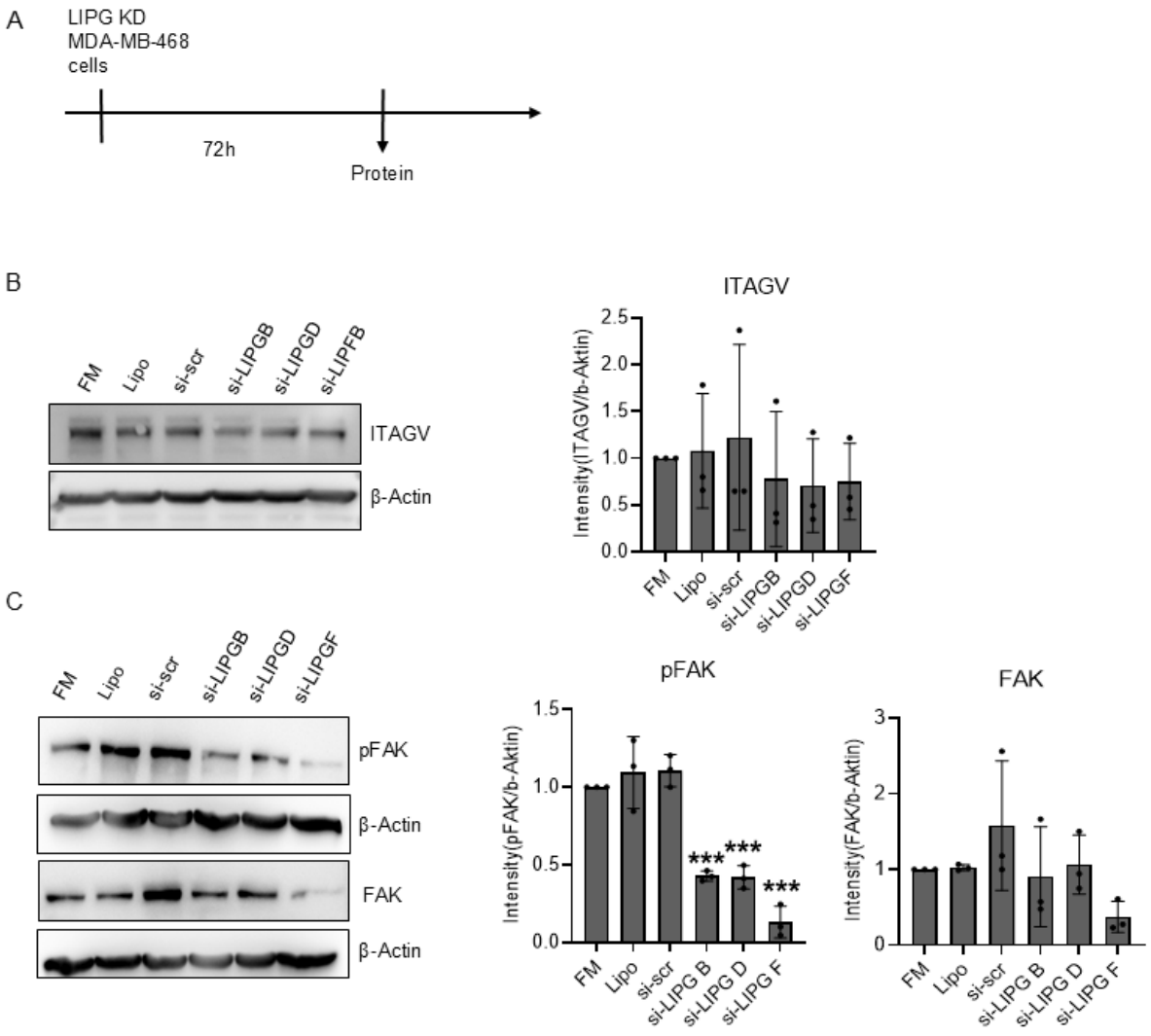

Figure 21: Expression of ITGAV, FAK and pFAK after LIPG KD in MDA-MB-468 cells. (A) Illustration of experimental design. MDA-MB-468 cells were cultivated for 72 h and cell lysates were collected and immunoblotted for ITGAV (B) FAK and pFAK (C) with β-Actin as the loading control. The results represent the mean ± SD (n=3-4). **p<0.01. Student's t test, unpaired, two sided.

Integrin Vα and FAK expression was analyzed after LIPG KD in HCC1954Luc by Immunoblotting as well (Fig. 22). In HCC1954Luc cells, ITAGV expression was also slightly but not significantly reduced after LIPG knockdown compared to the control condition si-scr (Fig. 22B). FAK phosphorylation was also slightly lowered after knockdown with the oligos si-LIPGB and si-LIPG F, but these findings were not significant (Fig. 22C). Interestingly, FAK expression was significantly reduced only in si-LIPG B, indicating impaired FAK signaling only with this siRNA oligo. Unfortunately, the results with the other siRNA oligos were too variable (Fig. 22C).

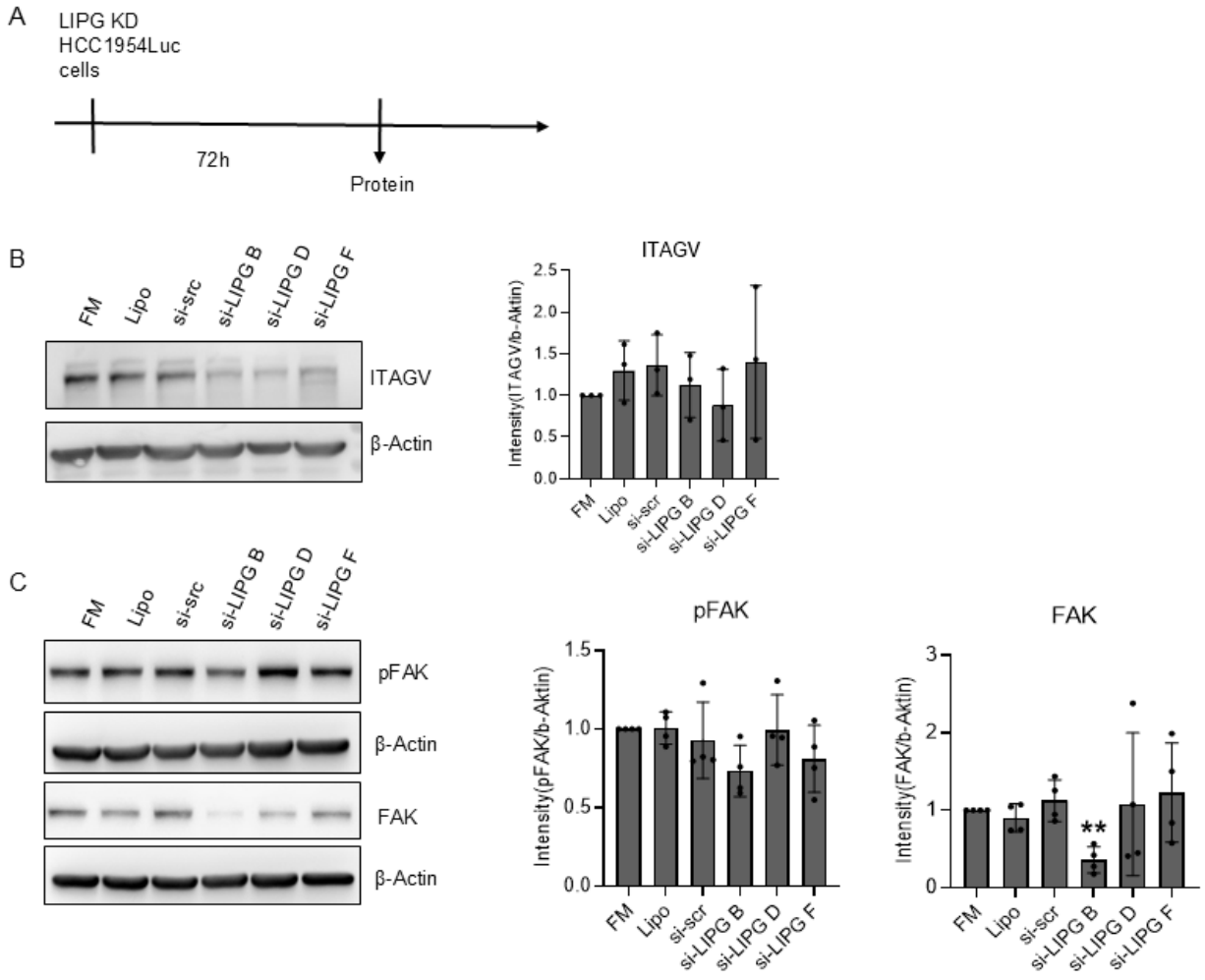

Figure 22: Expression of ITGAV, FAK and pFAK after LIPG KD in HCC1954Luc cells. (A) Illustration of experimental design. MDA-MB-468 cells were cultivated for 72 h and cell lysates were collected and immunoblotted for ITGAV (B) FAK and pFAK (C) with β-Actin as the loading control. The results represent the mean ± SD (n=3-4). **p<0.01. Student's t test, unpaired, two sided.

6.1.1.6 Silencing ITGAV impairs cell adhesion to specific extracellular matrix components

Integrins are crucial receptors for cell adhesion and initiating intracellular cellular signaling. There are 24 possible Integrin heterodimers with distinct cellular functions. Some are responsible for adhesion to the ECM like ITAGV and some are responsible for survival and proliferation. [115] Downregulation of one subunit may have an impact on cell viability and adhesion but other Integrin heterodimers may compensate. A knockdown of ITGAV was performed with two siRNA oligos (siITGAV1 and siITAGV2) for comparing its effects on adhesion to those of LIPG. The ITAGV knockdown was also analyzed on cell viability, mRNA expression and protein expression. The knockdown of ITAGV in MDA-MB-468 cells led to a reduced cell viability (Fig. 23B).

Protein (Fig. 23C) and mRNA expression (Fig. 23D) of ITGAV was significantly decreased, which confirmed a successful knockdown. In the cell adhesion assay to fibronectin (Fig. 23E), ITGAV KD showed a significant decrease in cell adhesion after 15 min. After 30 min cell adhesion in the ITGAV KD conditions ITGAV1 and ITGAV2 was still significantly decreased. Due to the downregulation of ITGAV, heterodimerization of its product Integrin αV with various β subunits is likely impaired. This may result in less integrin activation and affected connection to the ECM, causing loss of cell viability and less cell attachment. The phenotypic loss of cell adhesion of ITAGV KD was much more severe and not just transiently slowed down compared to LIPG KD. This showed that, in contrast to ITGAV, LIPG is not an essential adhesion molecule but suggested a role for LIPG as an adhesion facilitator, which seemed necessary for initial attachment processes.

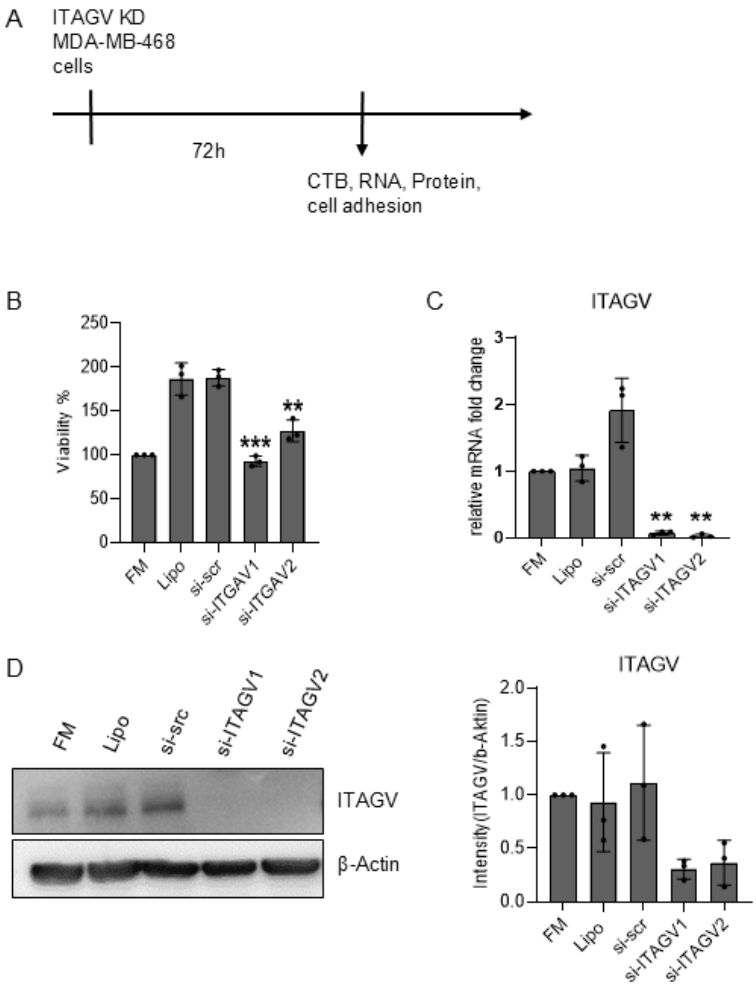

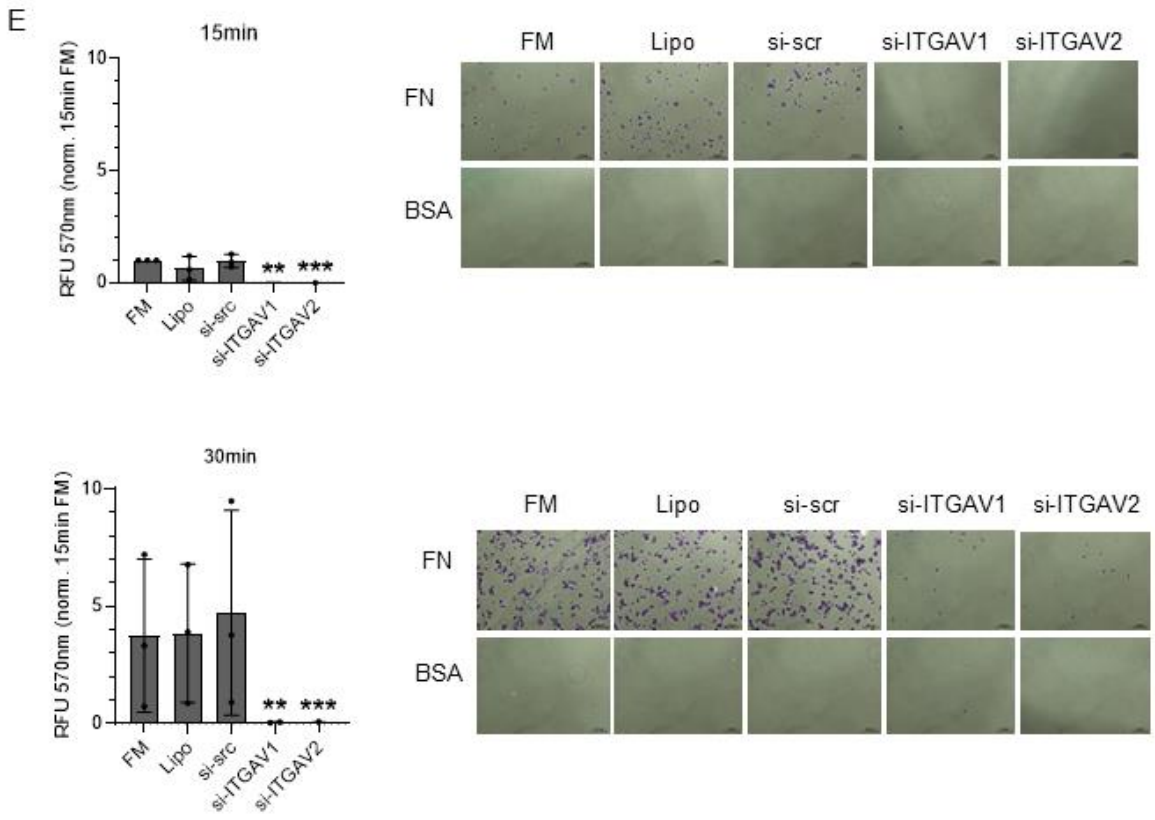

Figure 23: Confirmation of ITGAV knockdown in MDA-MB-468 cells with analysis of mRNA expression, protein expression and cell viability detection. (A) Illustration of experimental design. Cell viability (B) of all si-RNA were accessed using CTB assay and fluorescent measurement at 540 nm. The results represent mean ± SD (n=3) of technical replicates. ITGAV knockdown was analyzed on mRNA level (C) with quantitative RT-PCR and the use of UBC as an endogenous control. Immunoblotting of LIPG protein expression was performed (D) in cell lysates with β-Actin as a loading control. Adhesion of MDA-MB-468 cells was assessed after 15 min and 30 min in media with 1% FBS (E). BSA control was subtracted from the fibronectin coated wells and absorption was measured at 570 nm. The results represent the mean ± SD (n=3). **p<0.01; ***p<0.001. Student's t test, unpaired, two sided.

The knockdown of ITAGV in HCC1954Luc cells also led to a reduced cell viability (Fig. 24B). The knockdown of ITGAV was also successful in this cell line, as demonstrated by mRNA and protein expression of ITGAV by qPCR (Fig. 24C) and Western blot (Fig. 24D) respectively. The results of the cell adhesion assay to fibronectin after the ITGAV knockdown with the HCC1954Luc cells were comparable to the results obtained in MDA-MB468 cells. The ITGAV KD led to a significantly decreased cell adhesion after 15 min which remained significantly lower after 30 min (Fig. 24E), demonstrating the importance of ITGAV in this process.

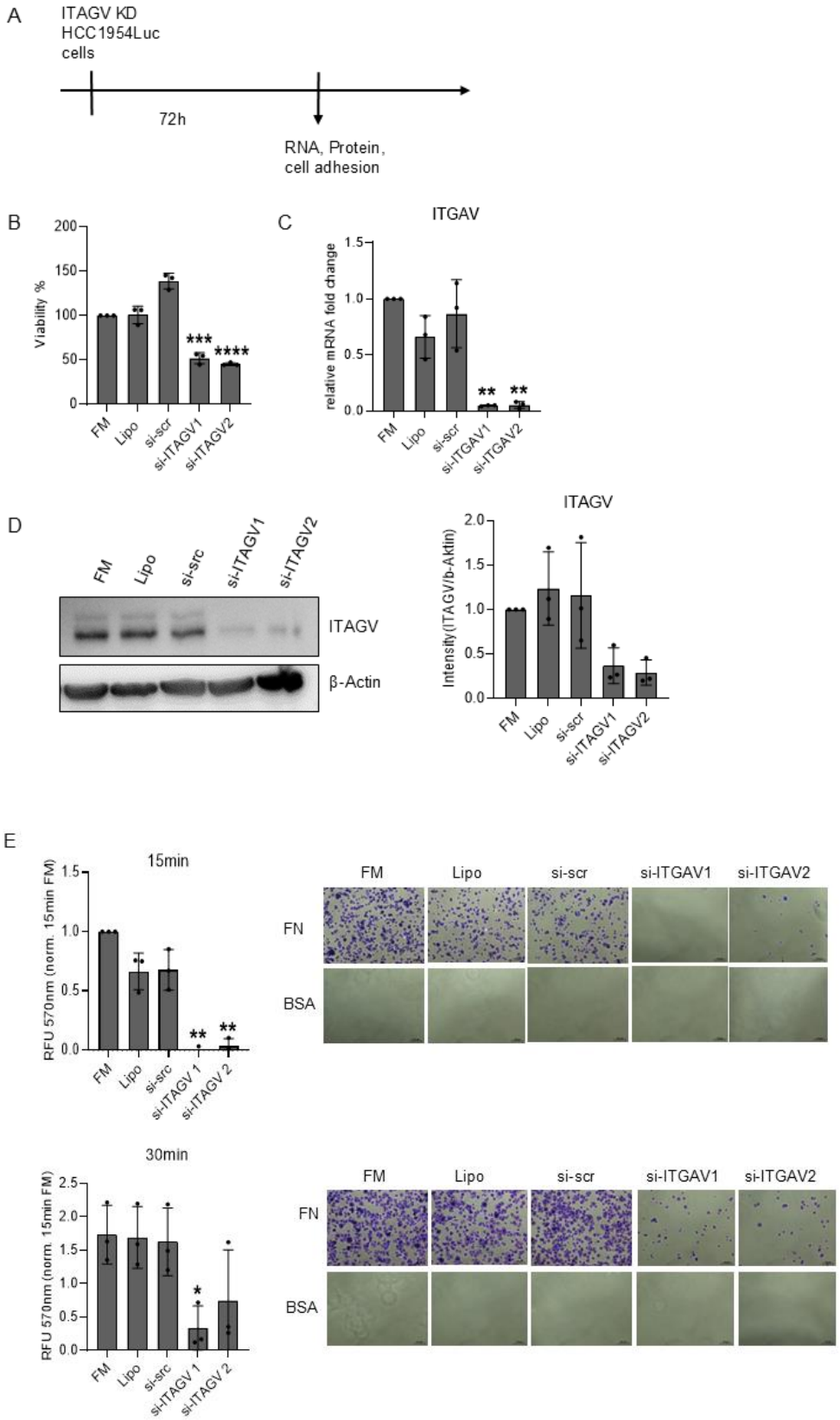
A
ITAGV KD
HCC1954Luc
cells
72h
RNA, Protein,
cell adhesion
B
Viability %
200
150
100
50
0
***
****
FM
Lipo
si-scr
si-ITAGV1
si-ITAGV2
C
ITAGV
relative mRNA fold change
1.5
1.0
0.5
0.0
**
**
FM
Lipo
si-scr
si-ITGAV1
si-ITGAV2
D
FM
Lipo
si-src
si-ITAGV1
si-ITAGV2
ITAGV
β-Actin
ITAGV
Intensity(ITAGV/b-Aktin)
2.0
1.5
1.0
0.5
0.0
FM
Lipo
si-scr
si-ITAGV1
si-ITAGV2
E
15min
RFU 570nm (norm. 15min FM)
1.5
1.0
0.5
0.0
**
**
FM
Lipo
si-src
si-ITAGV 1
si-ITAGV 2
FM
Lipo
si-scr
si-ITGAV1
si-ITGAV2
FN
BSA
30min
RFU 570nm (norm. 15min FM)
2.5
2.0
1.5
1.0
0.5
0.0
*
FM
Lipo
si-src
si-ITAGV 1
si-ITAGV 2
FM
Lipo
si-scr
si-ITGAV1
si-ITGAV2
FN
BSA

Figure 24: Confirmation of ITGAV knockdown in HCC1954Luc cells with analysis of mRNA expression, protein expression and cell viability detection. (A) Illustration of experimental design. Cell viability (B) of all si-RNA were accessed using CTB assay and fluorescent measurement at 540 nm. The results represent mean ± SD (n=3) of technical replicates. ITGAV knockdown was analyzed on mRNA level (C) with quantitative RT-PCR and the use of UBC as an endogenous control. Immunoblotting of LIPG protein expression (D) in cell lysates with β-Actin as a loading control. Adhesion of HCC1954Luc cells was assessed after 15 min and 30 min in media with 1% FBS (E). BSA control was subtracted from the fibronectin coated wells and absorption was measured at 570 nm. The results represent the mean ± SD (n=3). *p<0.05; **p<0.01; ***p<0.001; ****p<0.0001 Student's t test, unpaired, two sided.

ITGAV is an α Integrin subunit, which mainly recognizes fibronectin and vitronectin after dimerization with a β subunit. Since ITAGV KD led to less adhesion on fibronectin, the question arises, whether adhesion to other extracellular matrix proteins is also affected. The adhesion process of MDA-MB-468 after ITAGV knockdown was monitored on a laminin, a collagen and a vitronectin matrix (Fig. 25). ITAGV KD in MDA-MB-468 resulted in significantly decreased cell adhesion on laminin coating after 15 min and 30 min (Fig. 25B). On collagen, the ITAGV KD did not decrease adhesion compared to the control conditions (Fig. 25C), indicating that attachment to collagen is not dependent on ITGAV. On a vitronectin matrix, neither the 15 min nor 30 min time points showed significant changes in cell adhesion after ITAGV KD (Fig. 25D). However, a slight decrease was visible, which could be significant with more replicates. Thus, all in all, ITAGV seemed to be relevant for specific adhesion on fibronectin and laminin coating, but not for adhesion on vitronectin and collagen.

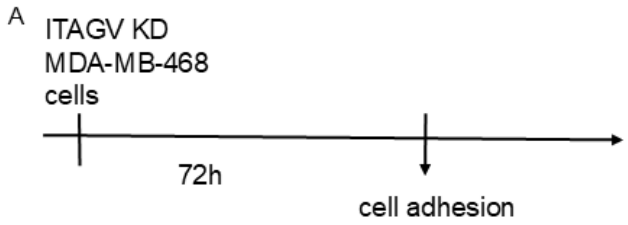

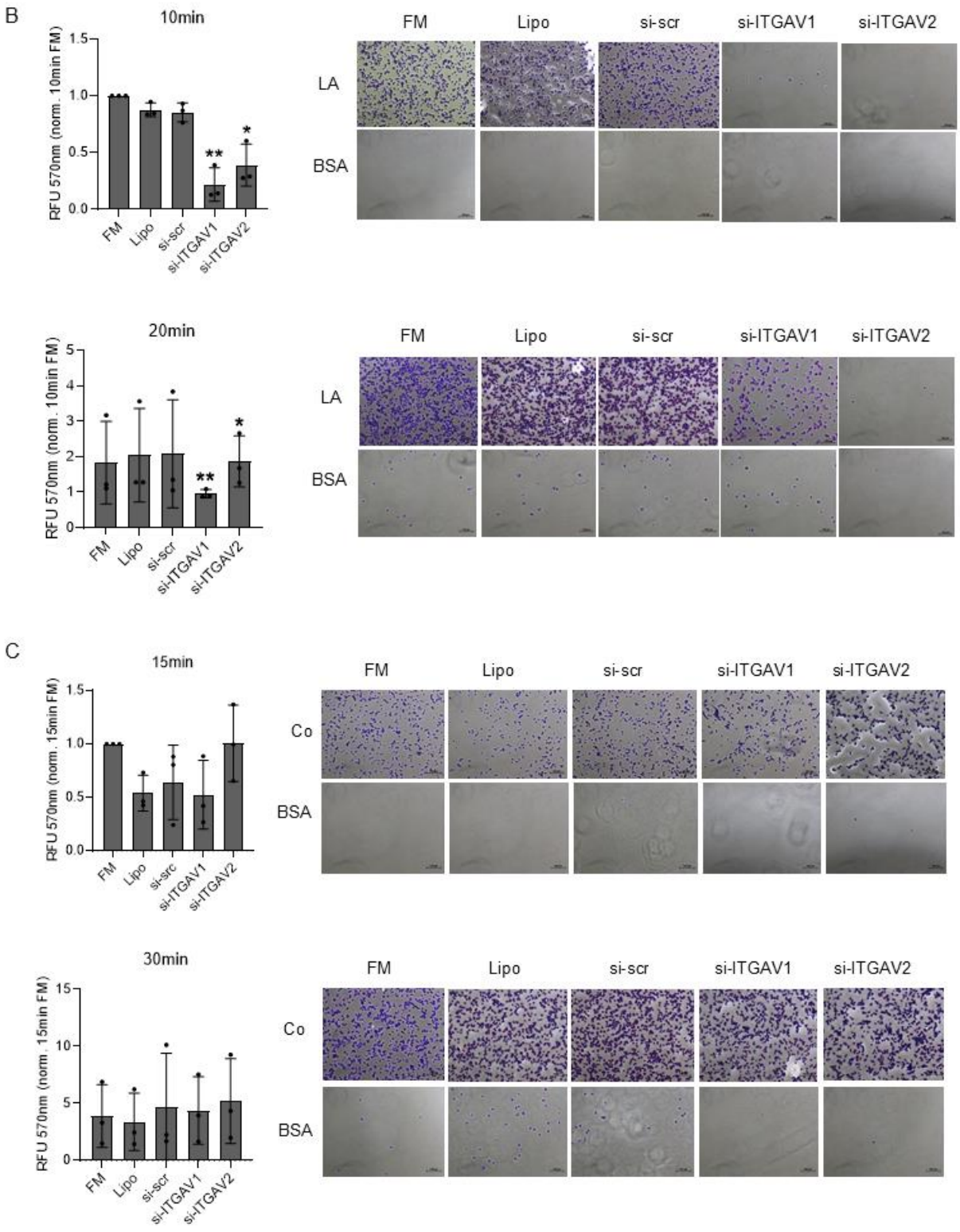
B
10min
RFU 570nm (norm. 10min FM)
FM
Lipo
si-scr
si-ITGAV1
si-ITGAV2
LA
BSA
20min
C
15min
RFU 570nm (norm. 15min FM)
si-src
Co
30min

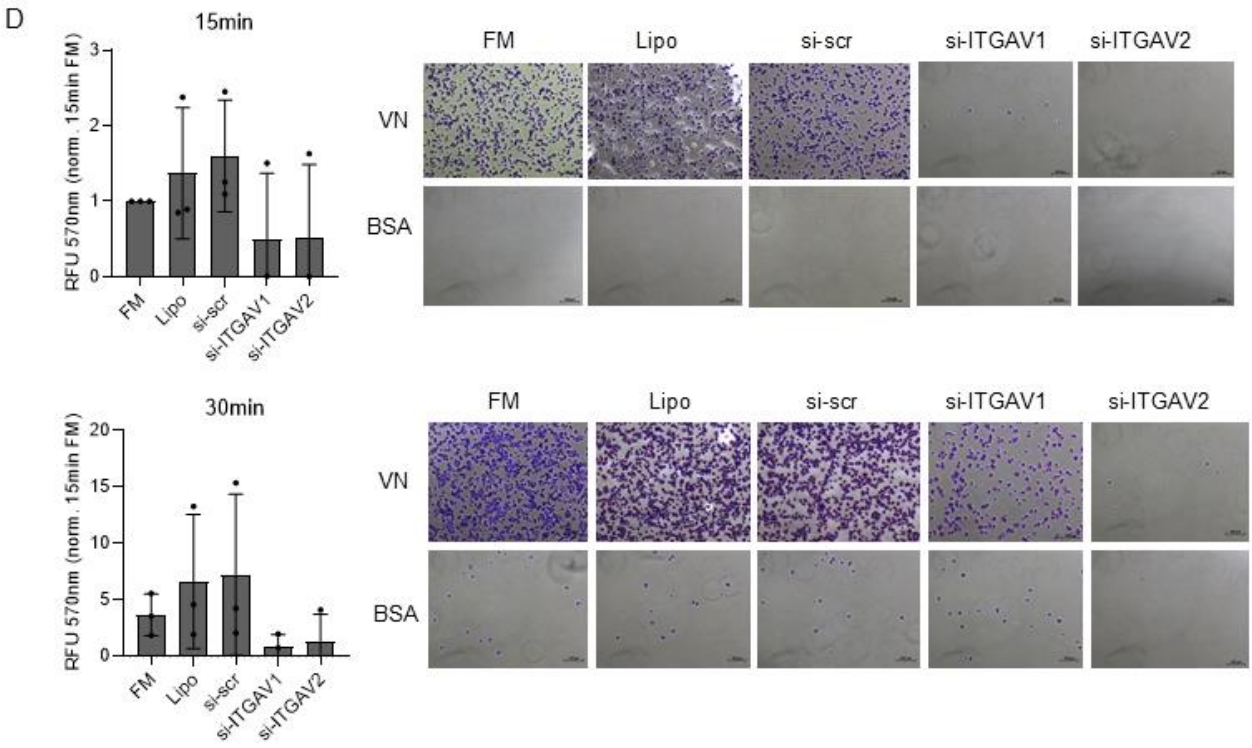

Figure 25: Cell adhesion after ITAGV KD in MDA-MB-468 cells on vitronectin, laminin or collagen. (A) Illustration of experimental design. Adhesion after 15 min and 30 min in media with 1% FBS on laminin (B), collagen (C) or vitronectin (D). BSA control was subtracted from the ECM protein coated wells and absorption was measured at 570 nm. The results represent the mean ± SD (n=3). *p<0.05; **p<0.01; Student's t test, unpaired, two sided

6.1.2 The role of cholesterol in cell survival and adhesion

LIPG was shown to impact cell adhesion to the extracellular matrix and to vascular endothelial cells, as well as migration. All cellular processes relevant to metastasis formation, since silencing LIPG led to a slowed down cell adhesion and migration *in vitro*. These effects might be mediated by reduced ITAGV and FAK protein expression in LIPG KD conditions (Fig. 21 and Fig. 22). Loss of ITAGV and FAK protein expression may in turn lead to reduced Integrin signaling and less expression of relevant downstream transcription factors relevant for metastasis. [118] Additionally, LIPG might also impact adhesion processes or influence integrin expression *via* changes in intracellular cholesterol accumulation or distribution. It is reported that LIPG has a multitude of functions on the metabolism and uptake of lipoproteins in different contexts. [97] But whether these functions affect cellular cholesterol homeostasis in cancer cells and whether such potential LIPG-mediated cholesterol changes can regulate cell adhesion and migration processes has not been investigated so far.

Therefore, the next goal was to clarify the role of cholesterol on metastasis-related processes in MDA-MB-468 cells.

6.1.2.1 Cholesterol addition and -depletion influence cell viability in a time-dependent manner

Changes in intracellular cholesterol content and cholesterol distribution are known to influence membrane stiffness in lipid rafts, leading to alterations in cell morphology and adhesion processes. Cholesterol depletion leads to higher cell stiffness, due to lack of interactions between the plasma membrane and actin cytoskeleton. [119] In triple negative breast cancer (TNBC) cell lines cholesterol depletion has been shown to reduce migration. [87, 88] However, other studies have reported that lower cholesterol levels promote breast cancer cell migration by increasing membrane fluidity and deformability. [86, 89] This requires clarification. Therefore, the next step was to investigate the influence of cholesterol in cell adhesion in the breast cancer cell lines used in the present study. Cholesterol interventions (cholesterol addition and withdrawal) are likely to influence cell viability and therefore require determination of the optimal concentration and incubation time, which was done in MDA-MB-468 cells (Fig. 26).

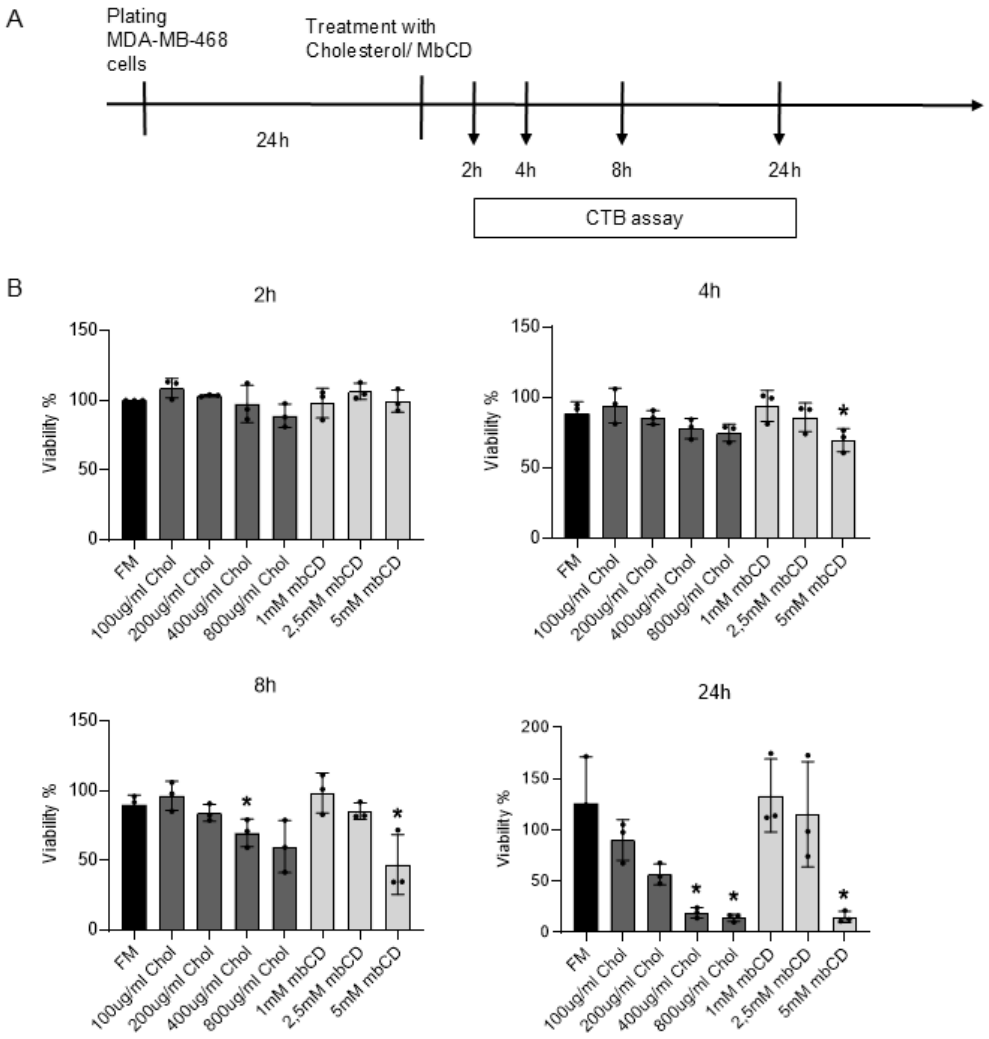

Figure 26: Cell viability assessment after cholesterol manipulation in MDA-MB-468 cells. (A) Illustration of experimental design. (B) Cholesterol addition was performed in concentrations of 100 µg/mL, 200 µg/mL, 400 µg/mL and 800 µg/mL cholesterol (water-soluble) for 2 h, 4 h, 8 h and 24 h in media without FBS. Cholesterol depletion occurred in concentrations of 1 mM, 2.5 mM and 5 mM methyl-β-Cyclodextrin for 2 h, 4 h, 8 h and 24 h in media without FBS. Cell viability was accessed using CTB assay and fluorescent measurement at 540 nm. The results represent the mean ± SD (n=3). *p<0.05. Student's t test, unpaired, two sided.

As shown in Figure 26B, two hours after incubation with cholesterol or methyl-β-cyclodextrin in time dependency, the cell viability was not compromised. After 4 h incubation with 5 mM methyl-β-cyclodextrin the cell viability was slightly affected. Incubation with 400 µg/mL cholesterol or 5 mM methyl-β-cyclodextrin for 8 h also decreased viability of MDA-MB-468 cells significantly. 24 h incubation with 400 µg/mL and 800 µg/mL cholesterol or 5mM methyl-β-cyclodextrin further decreased cell viability below 30 %.

6.1.2.2 Cholesterol addition and -depletion lead to decreased cell attachment to fibronectin

For investigating the effects of cholesterol interventions on cell adhesion, the condition that did not compromise cell viability, the 2 h time point was chosen (Fig. 27). The accumulation of cholesterol within the cells, and in addition, also their triglyceride content was first quantified to confirm the success of the treatment (Fig. 27A).

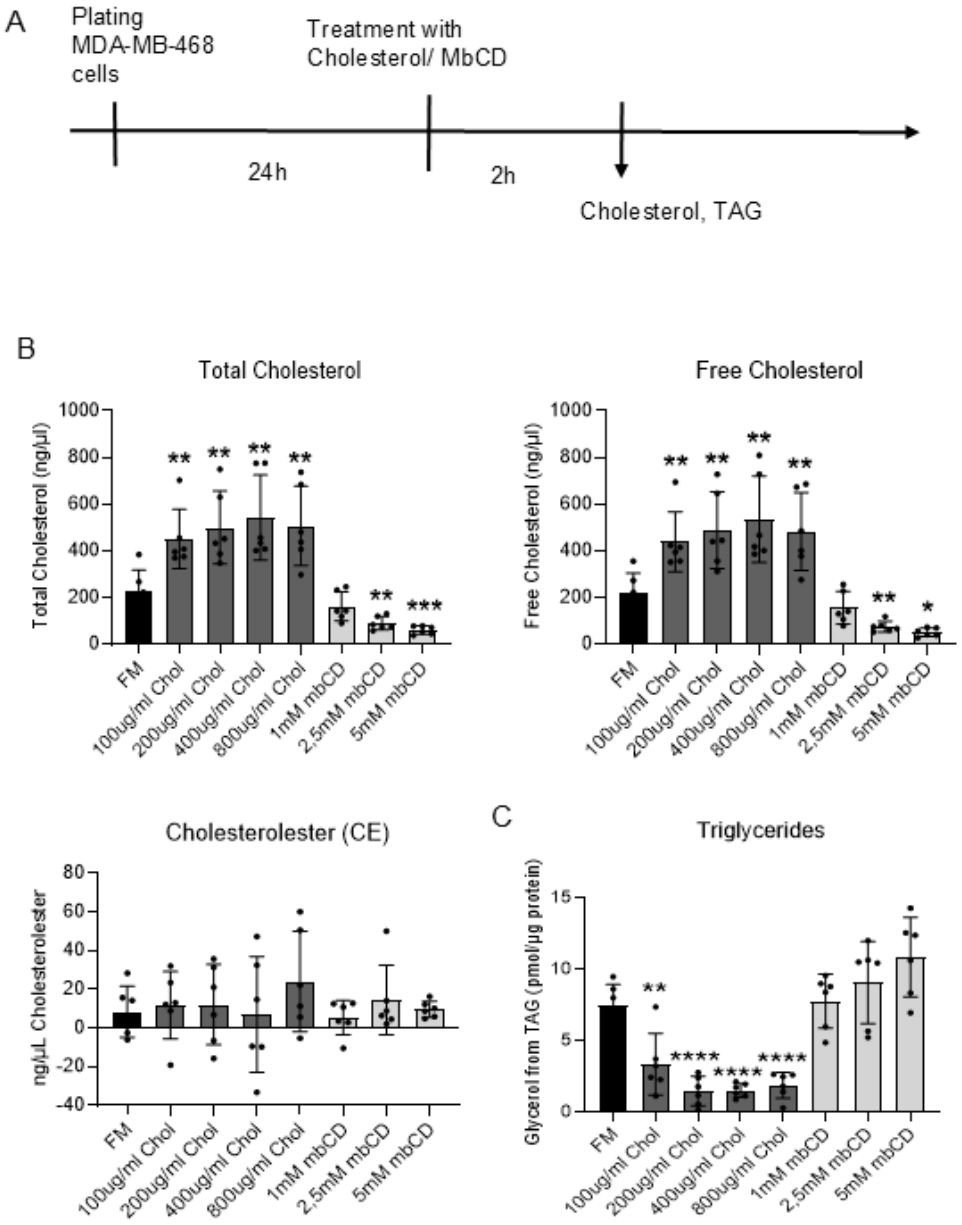

Figure 27: Intracellular cholesterol and triglyceride measurement after cholesterol manipulation in MDA-MB-468 cells. (A) Illustration of experimental design. (B) Cholesterol addition was performed in concentrations of 100 µg/mL, 200 µg/mL, 400 µg/mL and 800 µg/mL cholesterol (water-soluble) for 2 h in media without FBS. Cholesterol depletion occurred in concentrations of 1 mM, 2.5 mM and 5 mM methyl-β-Cyclodextrin for 2 h in media without FBS. Cholesterol content (A) was measured using Abcam Quantification Kit and fluorescence detection at 590 nm. Triglycerides content (B) was measured using Abcam Quantification Kit and fluorescence detection at 590 nm. The results represent the mean ± SD (n=6). *p<0.05; **p<0.01; ***p>0.001; ****p<0.0001. Student's t test, unpaired, two sided.

As expected, cholesterol treatment of MDA-MB-468 lead to a significant increase of intracellular total and free cholesterol, whereas treatment with methyl-β-cyclodextrin significantly decreased intracellular total and free cholesterol level (Fig. 27B). The levels of esterified cholesterol and cholesterol esters (CE) showed high variability and no significant alteration (Fig. 27B). The cellular triglyceride level decreased after cholesterol treatment and increased with methyl-β-cyclodextrin level (Fig. 27C). The triglyceride content behaved inversely to the cholesterol content upon cholesterol manipulation. This observation implied a tightly regulated triglyceride and cholesterol homeostasis, which were influencing each other. After having confirmed that the cholesterol manipulation was successful, an adhesion assay was performed to investigate if cholesterol regulates cell adhesion to fibronectin. Figure 28 shows cell adhesion kinetics of MDA-MB-468 after cholesterol manipulation for 2h.

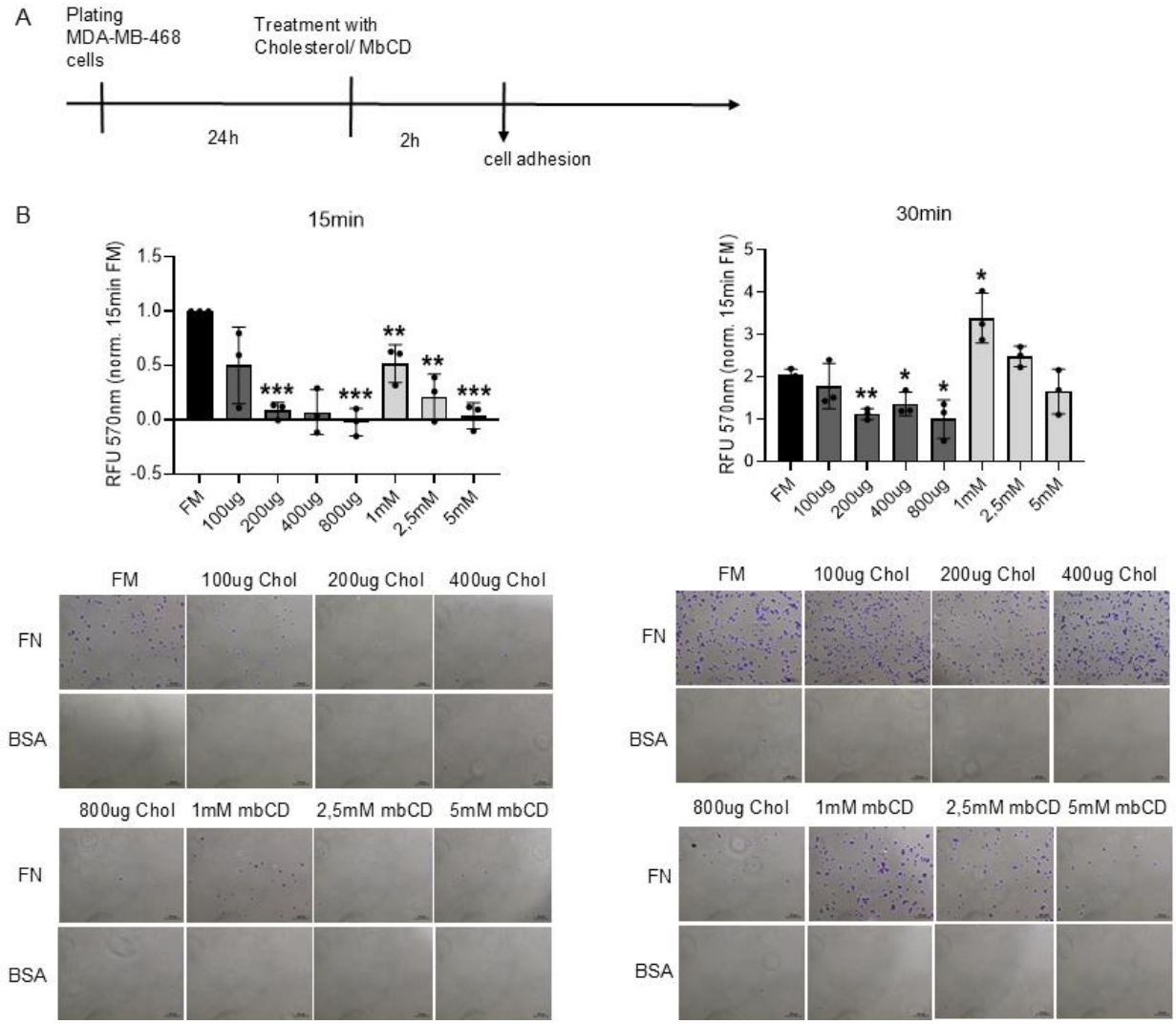

Figure 28: Cell adhesion on fibronectin after cholesterol manipulation in MDA-MB-468 cells. (A) Illustration of experimental design. (B) Cholesterol addition was performed in concentrations of 100 µg/mL, 200 µg/mL, 400 µg/mL and 800 µg/mL cholesterol (water-soluble) for 2 h in media without FBS. Cholesterol depletion occurred in concentrations of 1 mM, 2.5 mM and 5 mM methyl-β-cyclodextrin for 2 h in media without FBS. Adhesion was assessed after 15 min and 30 min in media with 1% FBS. BSA control was subtracted from the fibronectin coated wells and absorption was measured at 570 nm. The results represent the mean ± SD (n=3). *p<0.05; **p<0.01; ***p<0.001. Student's t test, unpaired, two sided.

As shown in Figure 28B, adhesion of MDA-MB-468 showed a significant decrease after 15 min incubation time in almost all treatment conditions with cholesterol or methyl-β-cyclodextrin. After 30 min, the cells previously treated with 200 µg/mL, 400 µg/mL and 800 µg/mL cholesterol treatment still showed less attachment compared to the FM control. Cholesterol depletion with 1 mM methyl-β-cyclodextrin increased adhesion instead. These experiments supported the previous studies that alterations of cellular cholesterol affect cell adhesion. [119, 120, 121] In the present study, it became clear that

both interventions can retard cell adhesion kinetic, but cholesterol addition appears to affect it more severely.

6.1.2.3 Cellular cholesterol manipulation results in transcriptional changes of cholesterol metabolism-related genes

Manipulating cholesterol level in MDA-MB-468 cells might also impact genes related to cholesterol metabolism. As previously mentioned (see chapter 2.4), key genes regulating cholesterol levels are LDLR and SCARB1 for extracellular cholesterol uptake; HMGCR, which is the rate limiting step for *de novo* cholesterol synthesis and ACAT, which regulates cholesterol esterification. In addition, ABCA1, ABCG1 and SCARB1, which are responsible for cholesterol efflux. Most of these genes respond to changes in cellular cholesterol [32], and this was investigated in MDA-MB-468 breast cancer cells. In addition to the mentioned genes, also expression of LIPG was investigated. Figure 29 demonstrates changes in cholesterol related genes after cholesterol manipulation.

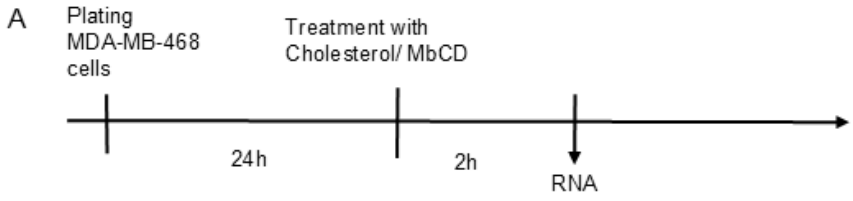

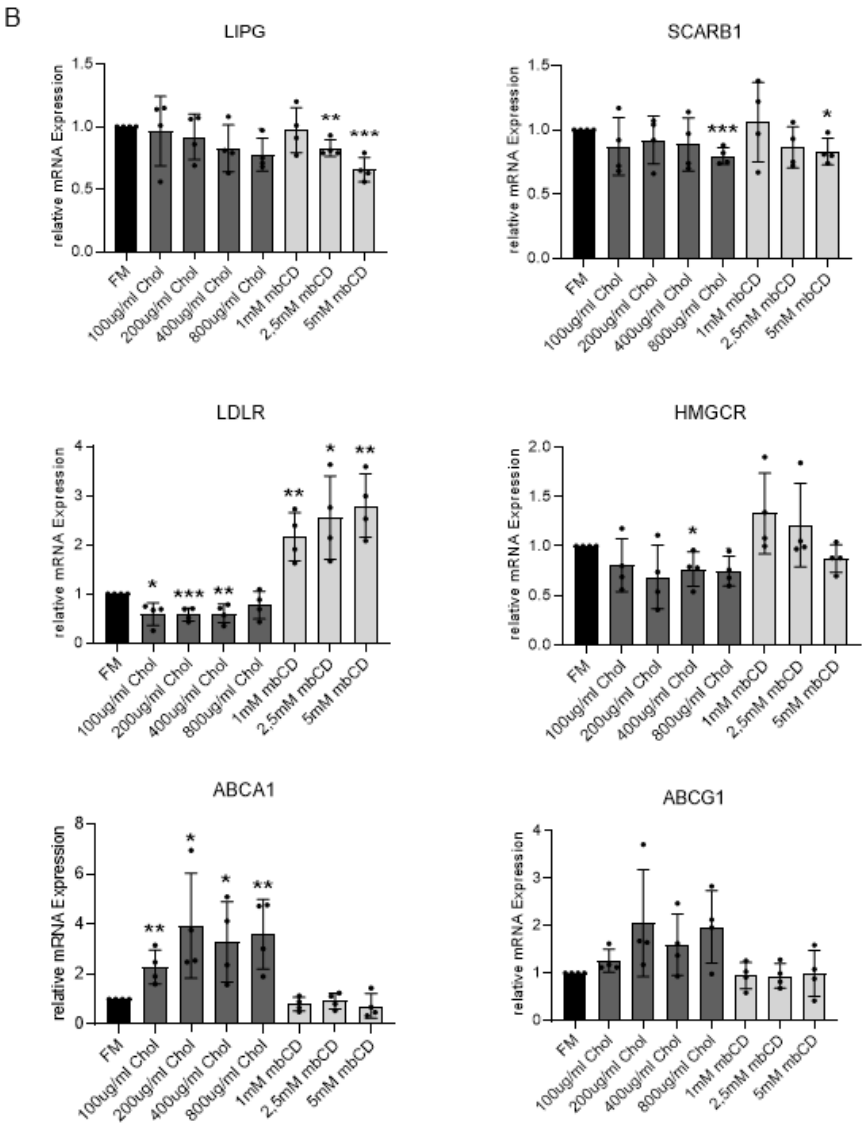

Figure 29: Changes of relative mRNA expression of cholesterol related genes after cholesterol manipulation in MDA-MB-468 cells. (A) Illustration of experimental design. (B) Cholesterol addition was performed in concentrations of 100 µg/mL, 200 µg/mL, 400 µg/mL and 800 µg/mL cholesterol (water-soluble) for 2 h in media without FBS. Cholesterol depletion occurred in concentrations of 1 mM, 2.5 mM and 5 mM methyl-β-cyclodextrin for 2 h in media without FBS. Relative mRNA expression was assessed by quantitative RT-PCR and the use of UBC as an endogenous control. The results represent the mean ± SD (n=4). *p<0.05; **p<0.01; ***p<0.001. Student's t test, unpaired, two sided.

As shown in Fig. 29B, the most prominent changes in gene expression were visible for LDLR and ABCA1. LDLR mRNA expression was significantly downregulated after cholesterol addition and significantly upregulated after cholesterol depletion. ABCA1 was significantly upregulated after cholesterol addition, but cholesterol depletion did not change its mRNA expression. Thus, cells reacted to intracellular cholesterol changes by adjusting gene expression to counteract these changes. For instance, the

cholesterol addition led to higher cellular cholesterol content and the cell reacted by decreasing cholesterol uptake through lower LDLR expression and increasing cholesterol efflux through higher ABCA1 expression. On the other hand, cholesterol depletion increased the cholesterol demand, and the cell increased extracellular cholesterol uptake by upregulating LDLR expression. Interestingly, LIPG and SCARB1 showed a similar pattern of response, with a slight downregulation both after cholesterol addition and depletion.

6.1.3 The role of LIPG in cellular cholesterol homeostasis

One of the main questions to be answered in this thesis is whether LIPG influences cholesterol levels in breast cancer cells. Based on literature reporting an important role for LIPG in lipoprotein metabolism (see chapter 2.6.2), the next step was to investigate the influence of LIPG on cholesterol exchange with lipoproteins. Even though LIPG's predominant function is in HDL metabolism, both LDL and HDL are potential substrates/binding partners of LIPG, since LIPG has been shown to interact with both HDL and LDL particles (see chapter 2.6.2). Given that both lipoprotein types play multiple roles in cholesterol trafficking - LDL being mainly responsible for cellular cholesterol uptake and HDL for cholesterol efflux followed by delivery to the liver –the next approach aimed at investigating cellular cholesterol levels in breast cancer cells after silencing LIPG at various conditions of serum or glucose withdrawal and after incubation with HDL and LDL lipoproteins. In addition to investigating changes in cholesterol, also expression of genes involved in cholesterol metabolism were analyzed after LIPG knockdown, especially such genes known to respond to cellular cholesterol alterations.

6.1.3.1 LIPG knockdown results in no changes in baseline cholesterol but altered expression of cholesterol metabolism-related genes

Cell starvation is a common procedure before treatment with different agents. Starvation synchronizes cell cycles to the same level and therefore provides similar starting points for further analysis. [122] Additionally, starvation of cells, depriving them from different medium components, could give information about the ability of cells to adapt to a limited supply. Performing starvation after silencing LIPG should also reveal whether cells lacking LIPG adapt less well. Removing FBS from the medium could potentially affect cellular cholesterol homeostasis. By depleting the serum (FBS) from the cell culture medium, lipids and lipoproteins are removed, thereby preventing

exogenous supply of lipids and cholesterol. In contrast, by removing glucose from the medium, the *de novo* synthesis of lipids and cholesterol by cells will be affected. In Figure 30, the viability of MDA-MB-468 cells was analyzed upon different conditions, serum deprivation (-FBS), glucose deprivation (-Glucose) or both (-FBS-Glucose), in time dependency. In addition to cell viability, the triglyceride content and the level of LIPG expression were analyzed (Fig. 30A).

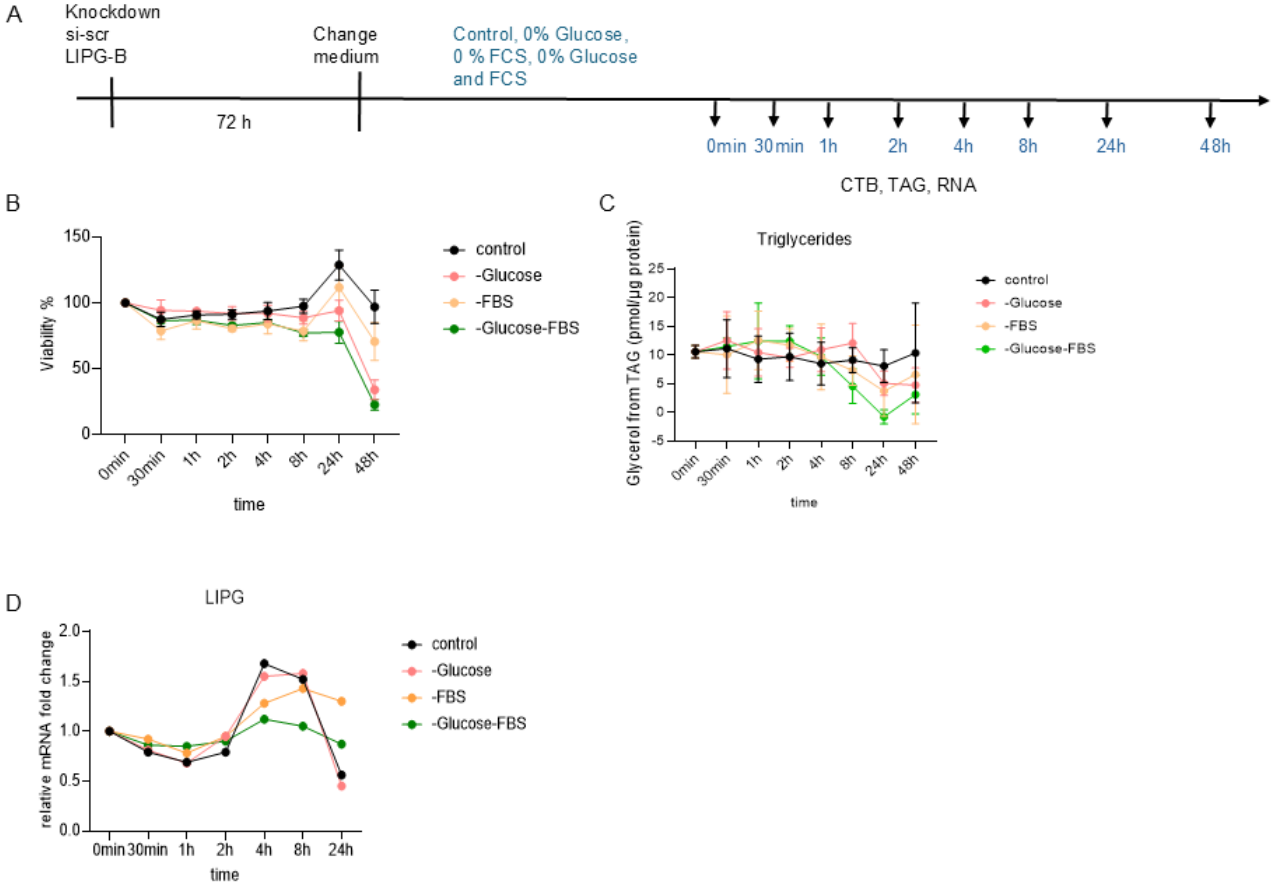

Figure 30: Viability assessment of MDA-MB-468 cells in time dependent starvation without FBS, glucose or both supplements. (A) Illustration of experimental design. MDA-MB-468 were cultivated to 90% confluency and either starved upon FBS, Glucose, both substrates or further cultivated in growth medium. Starvation and cell cultivation were monitored in time points 0 min till 24 h or 48 h. Cell viability (B) was detected using CTB and fluorescent measurement at 540 nm. Triglycerides content (C) was measured using Abcam Quantification Kit and fluorescence detection at 590 nm. Relative mRNA expression of LIPG (D) was assessed by quantitative RT-PCR and the use of UBC as an endogenous control. The results of B and C represent the mean ± SD (n=3). The results of D represent a single value (n=1).

The result of the cell viability assay (Fig. 30B) showed that deprivation of FBS or glucose from the of MDA-MB-468 cells resulted in clear changes in cell viability already after 24 h, which became more pronounced after 48 h. As expected, the control condition was the most viable, followed by the FBS deprivation condition, while the glucose deprivation condition and the combination of FBS and glucose deprivation were the most affected. Here, cell viability decreased severely after 48 h, deeming the 48 h time point as not suitable to perform further cell-based assays. The results of the triglyceride assay (Fig. 30C) showed that triglyceride levels were maintained in the control situation in all analyzed time points. After 24 h and 48 h the different starvation conditions resulted in reductions in the cellular triglyceride content. This suggests that after withdrawing glucose and serum from the medium, cells use their triglyceride reserves to survive. Regarding the expression of LIPG (Fig. 30D), it was observed that the mRNA expression increased after 4 h for every condition. This was highest in the control (FM) and serum-deprived (-FBS) conditions. Then the LIPG expression decreased till 24 h showing less LIPG mRNA expression in the control and serum-deprived condition compared to the glucose deprived and the combination starvation of FBS and glucose. This pattern of transient upregulation of LIPG is not yet understood. Given the dramatic decrease of cell viability due to deprivation of serum and glucose for 48 h, in the next experiments aimed at investigating the effect of silencing LIPG on cell viability at the described experimental conditions, only the 24 h time point was considered. Accordingly, a LIPG KD was first performed in MDA-MB-468 cells and after a medium change, si-scr and si-LIPG KD cells were further cultivated for 24 h in full medium (FM, control) or medium deprived from serum (-FBS), glucose (-Glucose) or both (-FBS-Glucose) (Fig. 31A). In addition to a cell viability assay and a triglyceride quantification, cholesterol levels were also analyzed.

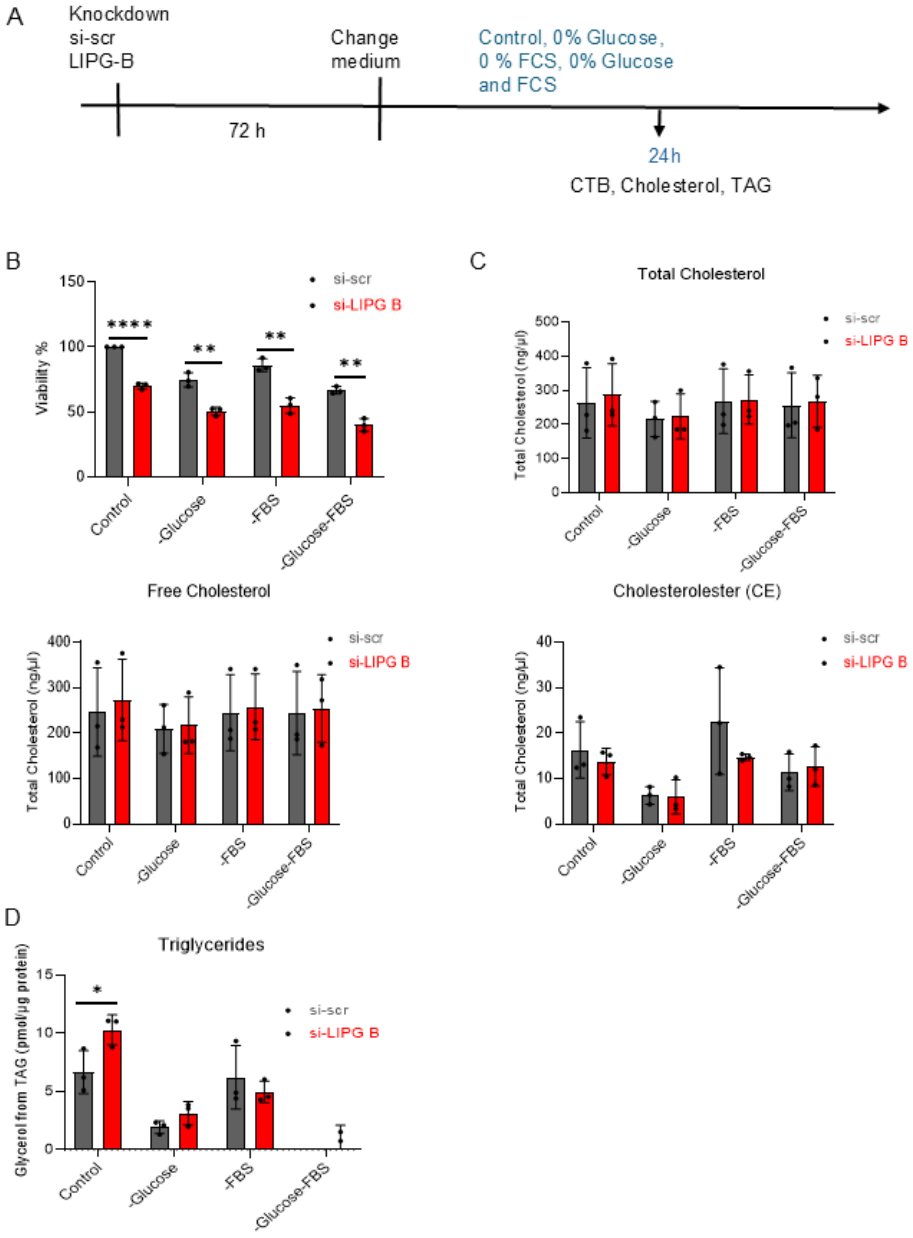

Figure 31: LIPG KD for 72 h in MDA-MB-468 cells, followed by 24 h starvation without FBS, glucose, both supplements or media change. (A) Illustration of experimental design. (B) Cell viability was detected using CTB and fluorescent measurement at 540 nm. Cholesterol content (C) was analyzed using Abcam Quantification Kit and fluorescence detection at 590 nm. Triglycerides content (D) was measured using Abcam Quantification Kit and fluorescence detection at 590 nm. The results represent the mean ± SD (n=3). *p<0.05; **p<0.01; ***p<0.001. Student's t test, unpaired, two sided.

The cell viability assay (Fig. 31B) showed that silencing LIPG lead to a general decrease in cell viability but did not render cells particularly more sensitive to any of the experimental starvation conditions, leading to more cell death. The quantification of cellular cholesterol content (Fig. 31C) showed that upon glucose starvation, serum starvation and glucose and serum starvation, the cellular total and free cholesterol

content were maintained and also showed similar levels between si-LIPG and si-scr. Cholesterol ester content was slightly higher in the si-scr control in serum-starved media compared to si-LIPG B. MDA-MB-468 cells can adapt and maintain their cholesterol content under different conditions and after LIPG knockdown. When examining changes in the triglyceride content of the cells (Fig. 31D), it was observed that the cultivation for 24 h in glucose free medium and in medium deprived of both glucose and FBS affected triglyceride levels the most. Comparing the response of si-scr and si-LIPG cells it was observed that after 24 h cultivation in regular medium the triglyceride content of LIPG KD cells was higher than that of control (si-scr) cells. Under all other conditions, the triglyceride levels were similar between control and si-LIPG KD conditions. The lack of changes in the cholesterol levels in the MDA-MB468 cells under different starvation conditions, including LIPG knockdown raised the question whether this is due to an adaptive response of cells to maintain cholesterol within a tight range. To explore such adaptive response, gene expression alterations in cholesterol-responsive genes was analyzed next. This was investigated by RT-PCR (Fig. 32A-B).

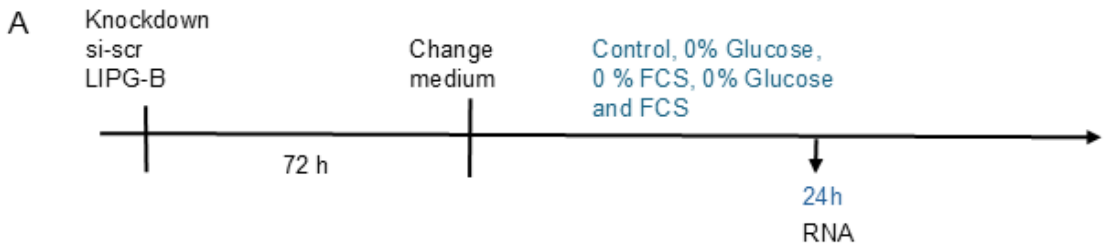

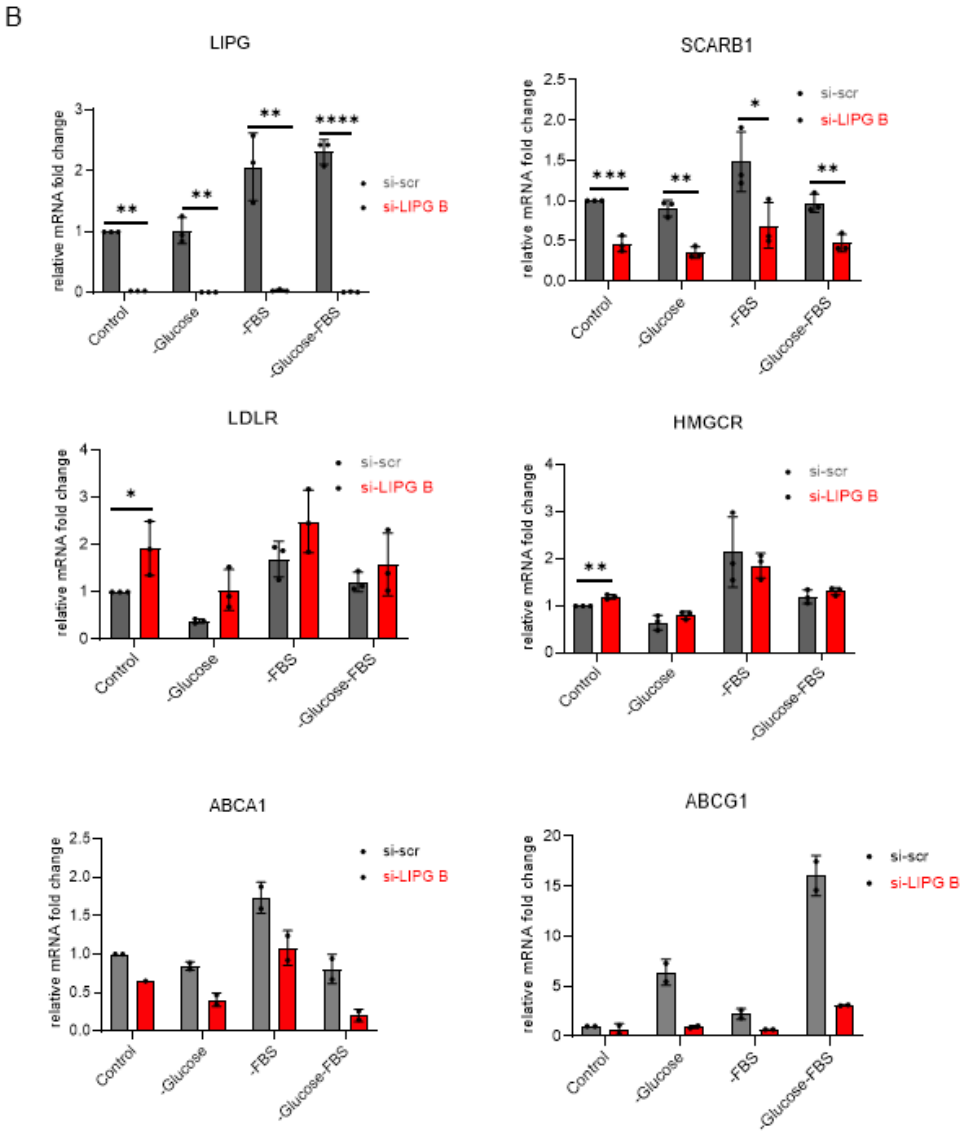

Figure 32: LIPG KD for 72 h in MDA-MB-468 cells, followed by 24 h starvation without FBS, glucose, both supplements or media change. (A) Illustration of experimental design. (B) Relative mRNA expression of LIPG, SCARB1, LDLR, HMGCR, ABCA1 and ABCG1 was assessed by quantitative RT-PCR and the use of UBC as an endogenous control. The results represent the mean ± SD (n=2-3). *p<0.05; **p<0.01; ***p<0.001; ****p<0.0001. Student's t test, unpaired, two sided.

Gene expression analysis of LIPG, SCARB1, LDLR, HMGCR, ABCA1 and ABCG1 was performed using RT-PCR (Fig. 32B). When analyzing gene expression alterations in the different starvation conditions it was observed that without FBS and without glucose and FBS, si-scr cells had higher LIPG mRNA expression, indicating that serum-deprivation may upregulate LIPG. This was abrogated in LIPG KD, as expected. In LIPG KD cells SCARB1 was significantly downregulated in all conditions compared to the si-scr conditions. This indicated a LIPG-specific effect. LDLR and HMGCR were significantly upregulated in si-LIPG KD in the control situation compared to si-scr. A

trend to higher LDLR expression in LIPG KD conditions was observed. ABCA1 and ABCG1 expressions were reduced in si-LIPG B compared to si-scr in all starvation conditions. Especially, ABCG1 remained markedly decreased in si-LIPG B cells, even when starvation conditions in the si-scr control cells increased its expression. Hereby, lack of LIPG impaired ABCG1 upregulation in response to starvation. These results altogether suggest that in response to silencing LIPG gene expression of cholesterol-metabolism genes adapt to maintain cholesterol levels. The adhesion kinetics of si-scr and si-LIPG B MDA-MB-468 cells was analyzed after the same starvation conditions of serum, glucose or serum and glucose deprivation (Fig. 33A). A cell adhesion assay on fibronectin was performed (Fig. 33B-C).

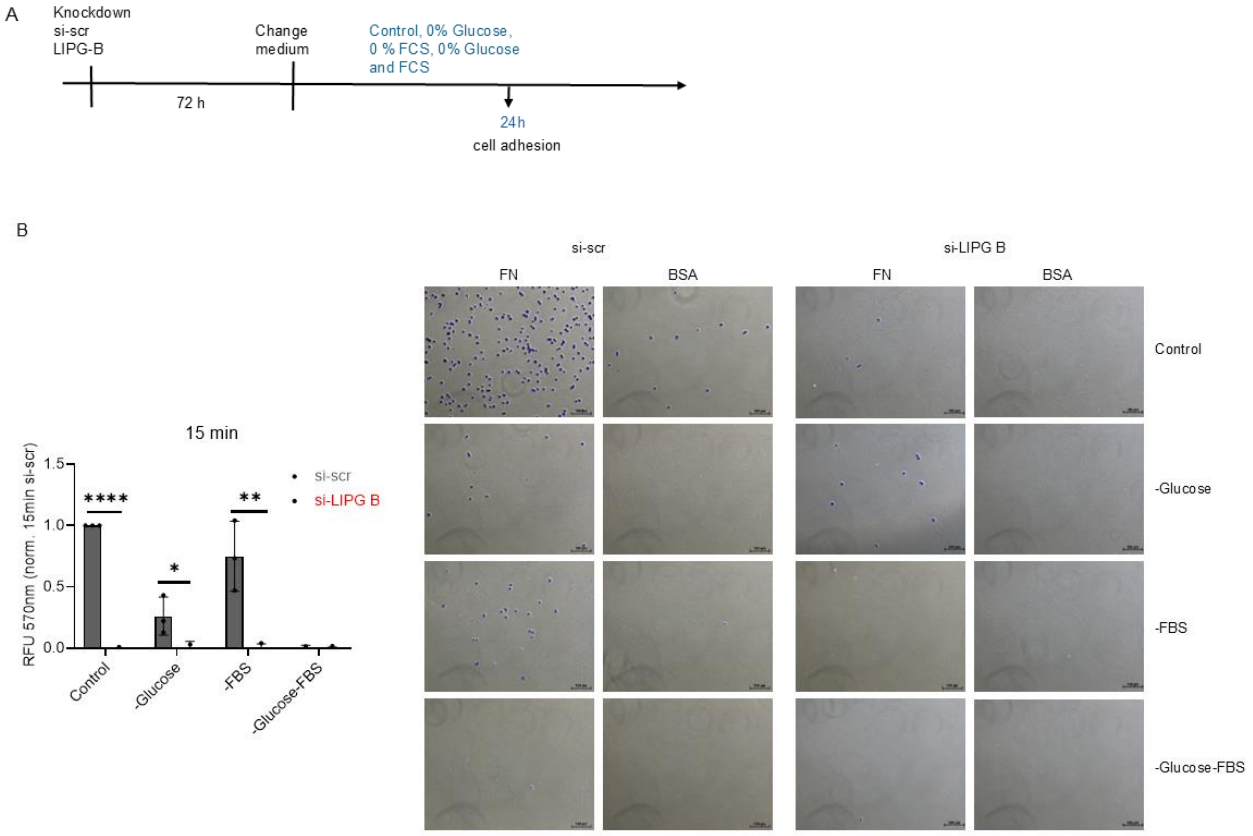

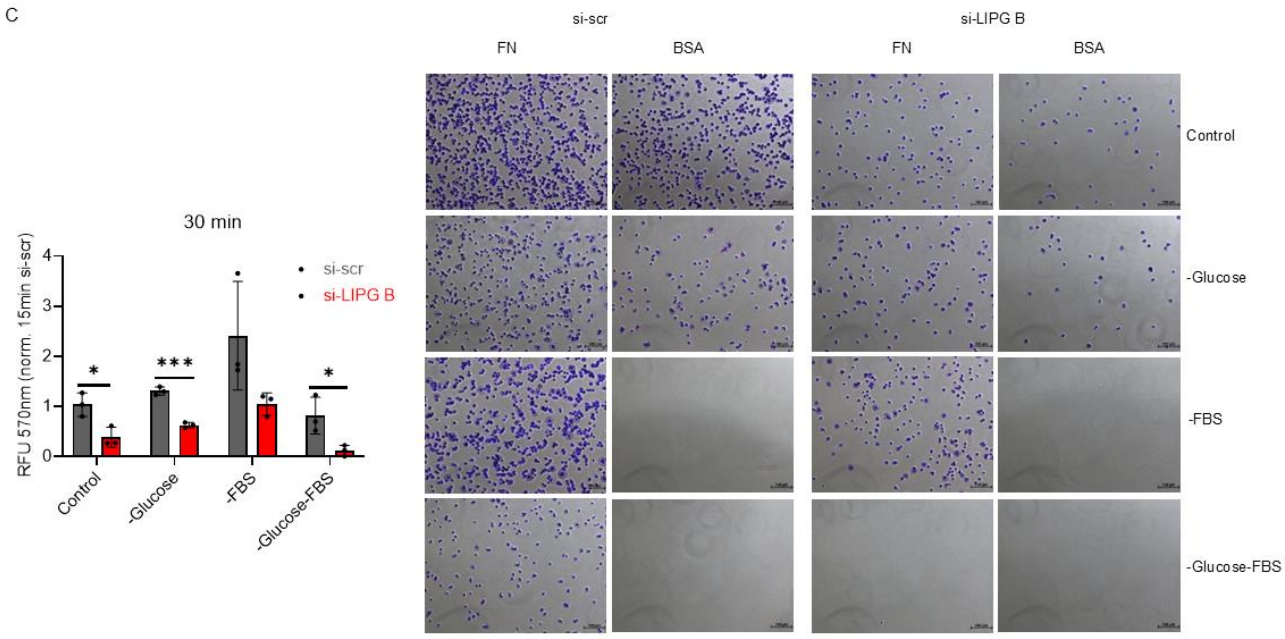

Figure 33: LIPG KD for 72 h in MDA-MB-468 cells, followed by 24 h starvation without FBS, glucose, both supplements or media change. (A) Illustration of experimental design. (B) Adhesion assay after 15 min and (C) 30 min in media with 0% FBS. BSA control was subtracted from the fibronectin coated wells and absorption was measured at 570 nm. The results represent the mean ± SD (n=3). *p<0.05; **p<0.01; **p<0.001; Student's t test, unpaired, two sided.

The results of the cell adhesion assay after 15 min attachment time (Fig. 33B) showed that in each of the starvation conditions, LIPG KD cells had a decreased adhesion capacity compared to si-scr control. In control si-scr cells, the effect of the different nutrient deprivations was also shown. Combinational FBS and glucose starvation in si-scr showed the least adhesion. After 30 min attachment time (Fig. 33C), cell adhesion had generally increased. This indicated that the starvation conditions affected the kinetics. The si-scr cells without FBS appeared to attach better compared to the other starvation conditions. The least attachment efficiency was observed without FBS and glucose. were more affected compared to the si-scr cells under each starvation condition. The apparent higher attachment after FBS deprivation may be due to the fact that less unspecific attachment to BSA is observed (see cell pictures). Therefore, subtraction of the BSA background from the fibronectin results leads to this result in the bar diagram. The results obtained from this study show that in the absence of LIPG, cholesterol levels are maintained even under glucose and FBS deprivation conditions (see Fig. 31). Although these results argue against the contribution of LIPG in the maintenance of cellular cholesterol, the gene expression changes observed after silencing LIPG (Fig. 32) reveal important alterations in cholesterol metabolism genes

that usually respond to changes in cholesterol (LDLR, HMGCR, ABCA1, ABCG1) as well as in key genes involved in cholesterol uptake and exchange with lipoproteins (SCARB1, LDLR). Moreover, this was also associated with less efficient cell adhesion of LIPG KD cells to the extracellular matrix (Fig. 33), as also seen after cholesterol manipulation (Fig. 28).

6.1.3.2. LIPG KD results in decreased protein expression of the HDL receptor SR-BI

Since LIPG knockdown was shown to lead to downregulation of SCARB1, changes in its protein product SR-BI may also occur and were investigated next (Fig. 34-35). To this aim the LIPG knockdown was performed with all three siRNA oligos and also in both cell lines, MDA-MB-468 and HCC1954Luc.

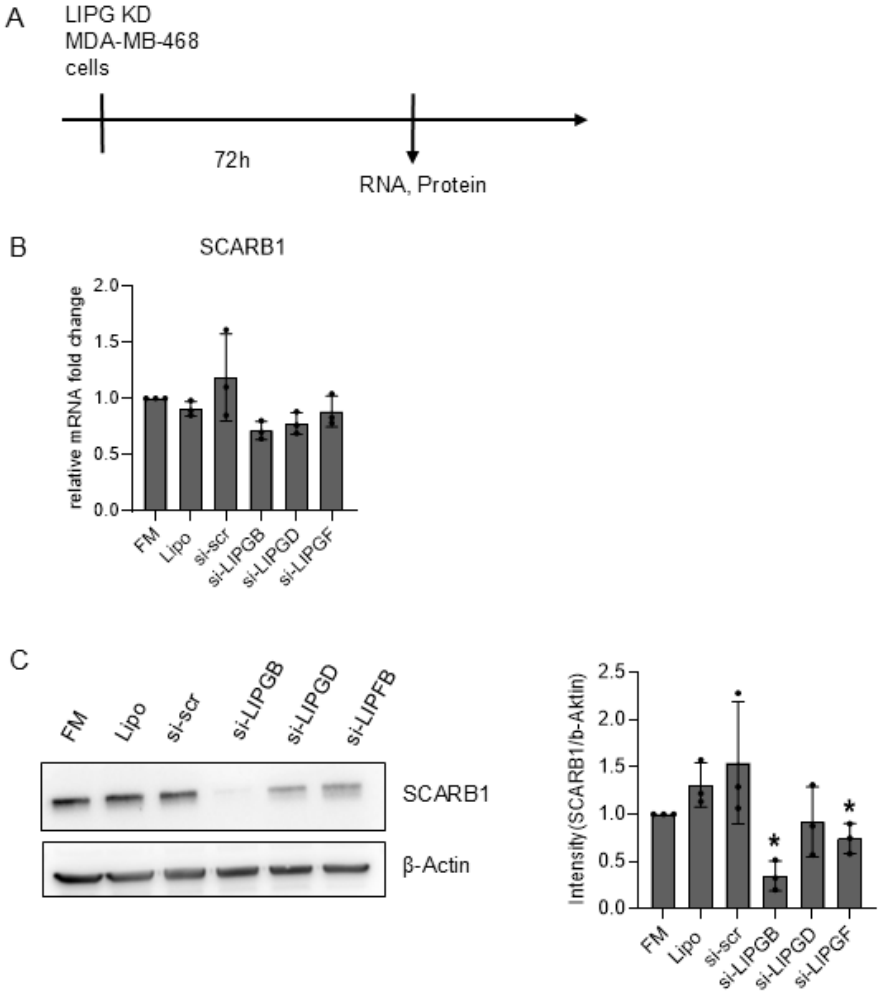

Figure 34: LIPG KD for 72 h in MDA-MB-468 cells showed downregulation of SCARB1 on protein level. (A) Illustration of experimental design. Relative mRNA expression of SCARB1 (B) was assessed by quantitative RT-PCR and the use of UBC as an endogenous control. Immunoblotting of SR-BI protein expression (C) in cell lysates with β-Actin as a loading control. The results represent mean ± SD (n=3). *p<0.05. Student's t test, unpaired, two sided.

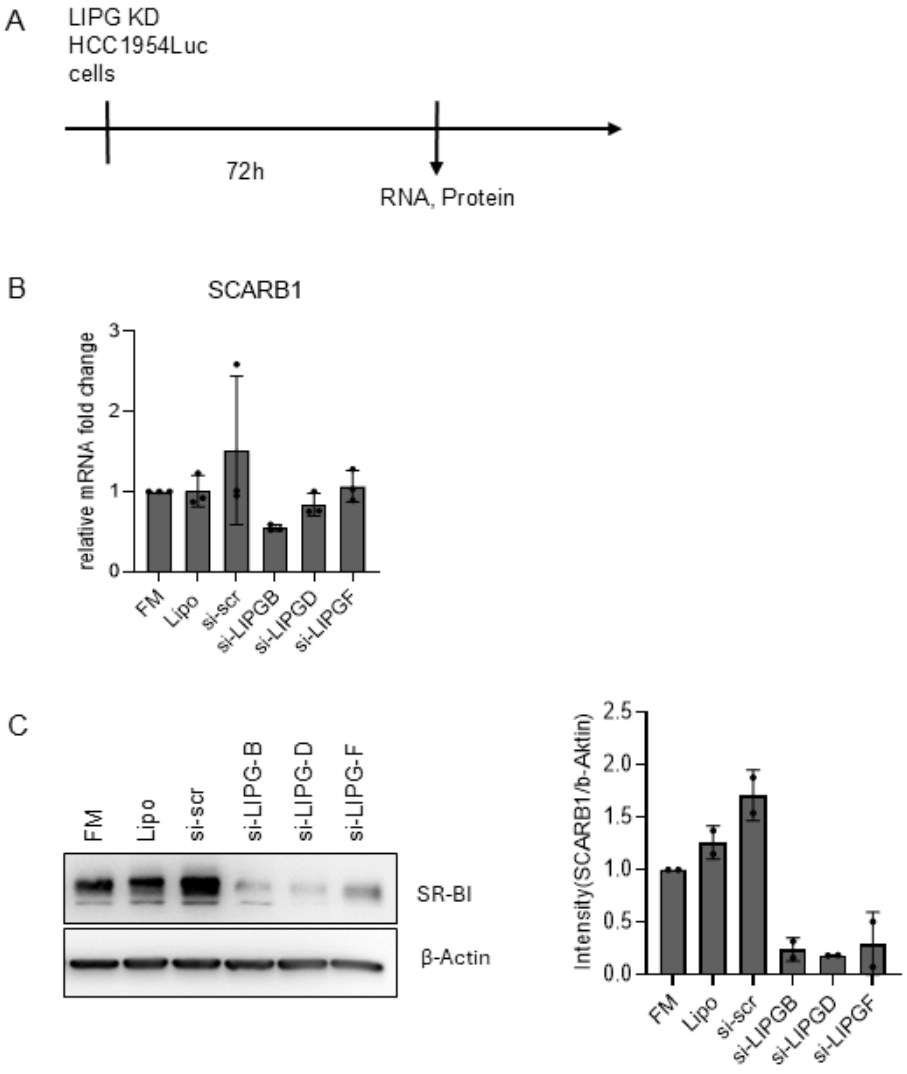

Figure 35: LIPG KD for 72 h in HCC1954Luc cells showed downregulation of SCARB1 on protein level in all oligos. (A) Illustration of experimental design. Relative mRNA expression of SCARB1 (B) was assessed by quantitative RT-PCR and the use of UBC as an endogenous control. The results represent mean ± SD (n=3). Immunoblotting of SR-BI protein expression (C) in cell lysates with β-Actin as a loading control. The results represent mean ± SD (n=2).

The LIPG knockdown for 72 h did not result in significant changes in SCARB1 mRNA expression with neither oligo, although a trend to a downregulation with oligos si-LIPG B and si-LIPG D was observed (Fig. 34-35B). This is in contrast to previous results (Fig. 32) in which further cultivation for 24h after the knockdown showed significant

decreased SCARB1 mRNA expression. However, a significant decrease of SR-BI protein expression was observed with at least two siRNA oligos in both cell lines (Fig. 34-35C). Therefore, changes in LIPG expression may influence either SCARB1 protein translation, maturation or stability. This is a novel finding that has not been reported in any publication so far. Based on this finding it would be expected that the interaction between HDL and SRBI is affected after silencing LIPG.

6.1.3.3. LIPG knockdown results in increased cholesterol accumulation in the presence of serum

Before investigating if the knockdown of LIPG influences HDL- and LDL-mediated effects on cellular cholesterol levels separately, the effect of increasing the concentration of serum (which contains a mixture of the various lipoproteins that are commonly found in blood serum, including HDL, LDL, and VLDL) in the cell culture medium was tested first. To this aim, MDA-MB468 cells were incubated with 0%, 10% and 20% FBS for 1 h, 5 h and 24 h after silencing with si-LIPG or control si-scr oligos for 72h and following a serum-starvation phase of either 1h, 5h or 24h. Intracellular levels of total, free and cholesterol esters were subsequently quantified (Fig. 36).

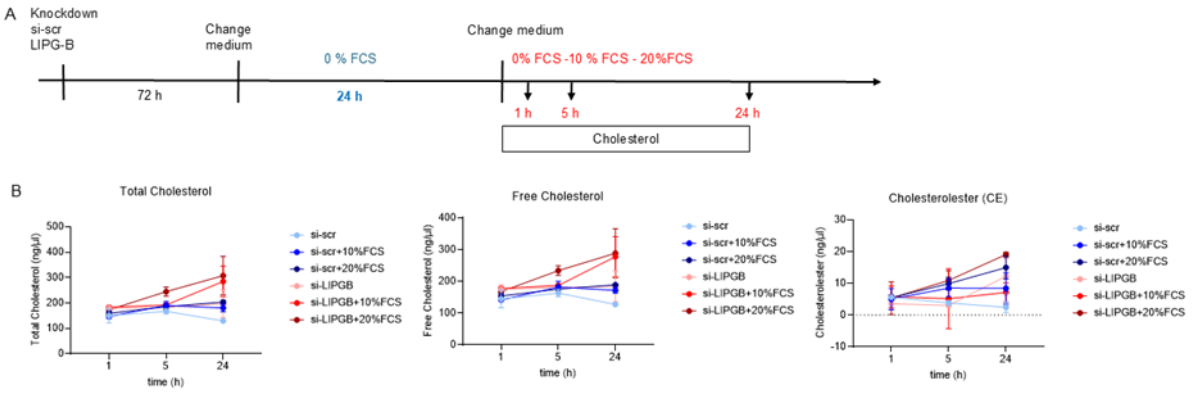

Figure 36: LIPG KD for 72 h in MDA-MB-468, followed by 24 h starvation without FBS. Starved cells were treated with 10% or 20% FBS for 1 h, 5 h or 24 h. (A) Illustration of experimental design. (B) Cholesterol content was measured using Abcam Quantification Kit and fluorescence detection at 590 nm. The results represent mean ± SD (n=2).

As shown in Figure 36B, a trend towards increased total and free cholesterol levels in LIPG deficient cells was observed during the time course of incubation with 10% and 20% FCS, and this effect was independent of the duration of the serum-starvation phase (Supplementary results). The increase in cholesterol was particularly evident in

the LIPG KD condition after 24h serum starvation followed by 5h incubation in 20 % FBS. The control si-scr cells did not increase their cholesterol levels. This suggests that under normal (LIPG-expressing) conditions, exchange of cholesterol between MDA-MB468 cells and serum lipoproteins takes place to preserve normal intracellular cholesterol levels. In LIPG-deficient MDA-MB468 cells, the cholesterol exchange with serum lipoproteins appears to be altered, leading to higher intracellular levels. Whether this is due to a diminished cholesterol efflux capabilities or higher uptake of exogenous cholesterol needs further clarification.

6.1.3.4 LIPG knockdown followed by incubation with HDL leads to a transient increase in cellular cholesterol

As already introduced, due to its catalytic activity towards phosphatidylcholine contained in HDL particles, LIPG is involved in HDL catabolism and may modify the composition and properties of HDL that influence their cholesterol exchange capacity. Additionally, it enables bridging of HDL to its receptor SR-BI. [79] which in turn enables cholesterol exchange between HDL and cells. The previous result has shown that LIPG KD results in decreased SR-BI expression (Fig. 34 and Fig. 35). For this reason, silencing LIPG in breast cancer cells may impair cholesterol exchange via HDL-SRB1 leading to altered intracellular cholesterol. To test this hypothesis, the cellular cholesterol content upon HDL treatment in MDA-MB-468 cells after silencing LIPG was analyzed (Fig. 37). To this aim, MDA-MB468 cells were incubated with different concentrations of HDL for 1 h, 5 h and 24 h after silencing with si-LIPG or control si-scr oligos for 72h and following a serum-starvation phase of either 1h, 5h or 24h. Intracellular levels of total, free and cholesterol esters were subsequently quantified. The results presented here are those generated after a 5 h starvation phase (Fig. 37A). However, similar results were shown after 1 h and 24 h starvation (Supplementary information).

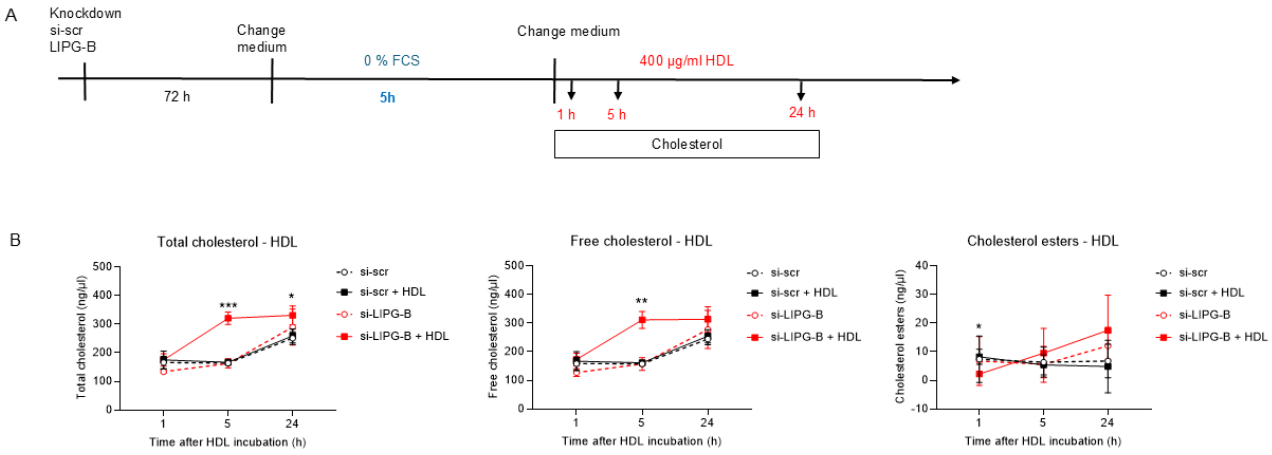

Figure 37: LIPG KD for 72 h in MDA-MB-468 cells, followed by 5 h starvation without FBS and treatment with HDL. Starved cells were treated with 400 µg/mL HDL for 1 h, 5 h or 24 h. (A) Illustration of experimental design. Cholesterol content (B) was measured using Abcam Quantification Kit and fluorescence detection at 590 nm. The results represent mean ± SD (n=3). *p<0.5; **p<0.01; ***p<0.001. Student's t test, unpaired, two sided.

As shown in Figure 37B, treatment with HDL in the control si-scr cells showed a slight increase in total and free cholesterol during the 24 h incubation period. However, in si-LIPGB KD cells, the cholesterol levels markedly increased, showing a significantly higher level after 5 h incubation. After 24 h incubation with HDL, the si-LIPGB KD cells still showed significantly higher amount of cholesterol compared to the control condition. This increase of cholesterol in LIPG-silenced cells could be due to impaired cholesterol efflux via SR-BI. On the other hand, 1h after HDL treatment the cholesterol esters in LIPG KD cells were significantly decreased compared to si-scr cells, indicating that also selective cholesterol ester uptake from HDL particles may be affected in the absence of LIPG.

6.1.3.5 LIPG knockdown followed by incubation with LDL results in increased cellular cholesterol levels

Although HDL is the preferred substrate of LIPG, LIPG is also reported to be involved in the hydrolysis of ApoB-containing lipoproteins, such as LDL, and also to increase their binding and uptake in a catalytic-independent manner via its "bridging" function. [97] LDL particles supply cells with cholesterol after binding to its receptor LDLR and internalization of LDL-LDLR complexes followed by endolysosomal degradation of LDL content. By this means, LDL uptake represents an important mechanism of acquiring exogenous cholesterol, which could be more enhanced by LIPG. To investigate whether LIPG influences this process, the intracellular cholesterol level after LDL

treatment was analyzed in si-scr and si-LIPG MDA-MB468 cells (Fig. 38). Similarly, as done for HDL, MDA-MB468 cells were incubated with different concentrations of LDL for 1 h, 5 h and 24 h after silencing with si-LIPG or control si-scr oligos for 72 h and following a serum-starvation phase of either 1 h, 5 h or 24 h. Intracellular levels of total, free and cholesterol esters were subsequently quantified. The results presented here are those generated after a 5 h starvation phase (Fig. 38A). However, similar results were shown after 1 h and 24 h starvation (Supplementary information)

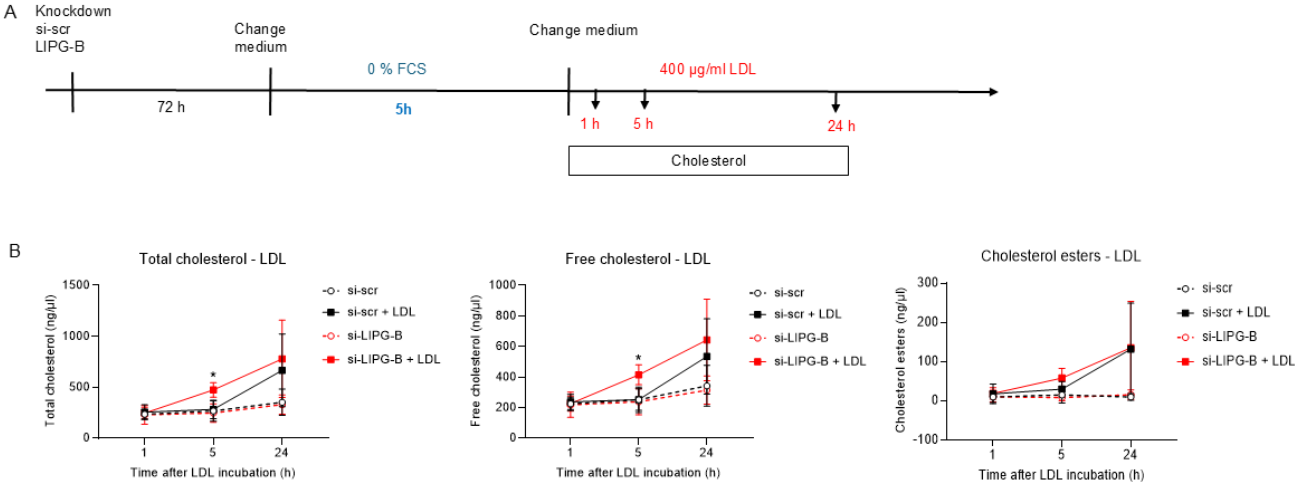

Figure 38: LIPG KD for 72 h in MDA-MB-468 cells, followed by 5 h FBS starvation and treatment with LDL. Starved cells were treated with 400 µg/mL LDL for 1 h, 5 h or 24 h. (A) Illustration of experimental design. (B) Cholesterol content was measured using Abcam Quantification Kit and fluorescence detection at 590 nm. LIPG KD for 72 h in MDA-MB-468, followed by 5 h starvation without FBS. Starved cells were treated with 400 µg/mL LDL for 1 h, 5 h or 24 h. The results represent mean ± SD (n=3). *p<0.5; Student's t test, unpaired, two sided.

As shown in Figure 38B, treatment of MDA-MB-468 cells with LDL led to a rapid accumulation of total, free cholesterol and cholesterol esters in the LIPG KD condition which was markedly higher than in the control si-scr cells 5 h after the treatment started. After 24 h treatment with LDL both LIPG KD and si-scr cells showed similarly increased total and free cholesterol levels, as well as cholesterol esters. Based on the observed upregulation of LDLR mRNA after LIPG KD, it is possible that this cholesterol increase is due to higher uptake of LDL via increased LDLR.

6.1.3.6 LIPG knockdown cells are not able to benefit from HDL-cholesterol exchange for adhesion

The observed compromised cholesterol exchange with HDL-lipoproteins might influence adhesion properties, which was investigated in a cell adhesion assay, as shown in Figure 39. To this aim, a knockdown with si-LIPG B or control si-scr oligo was performed in MDA-MB-468 cells for 72 h. After further 24 h incubation in serum-free medium, MDA-MB-468 cells were treated with 400 µg/mL HDL for 24 h. After this time, the cell adhesion assay was performed and cell adhesion on a fibronectin matrix was monitored (Fig. 39A).

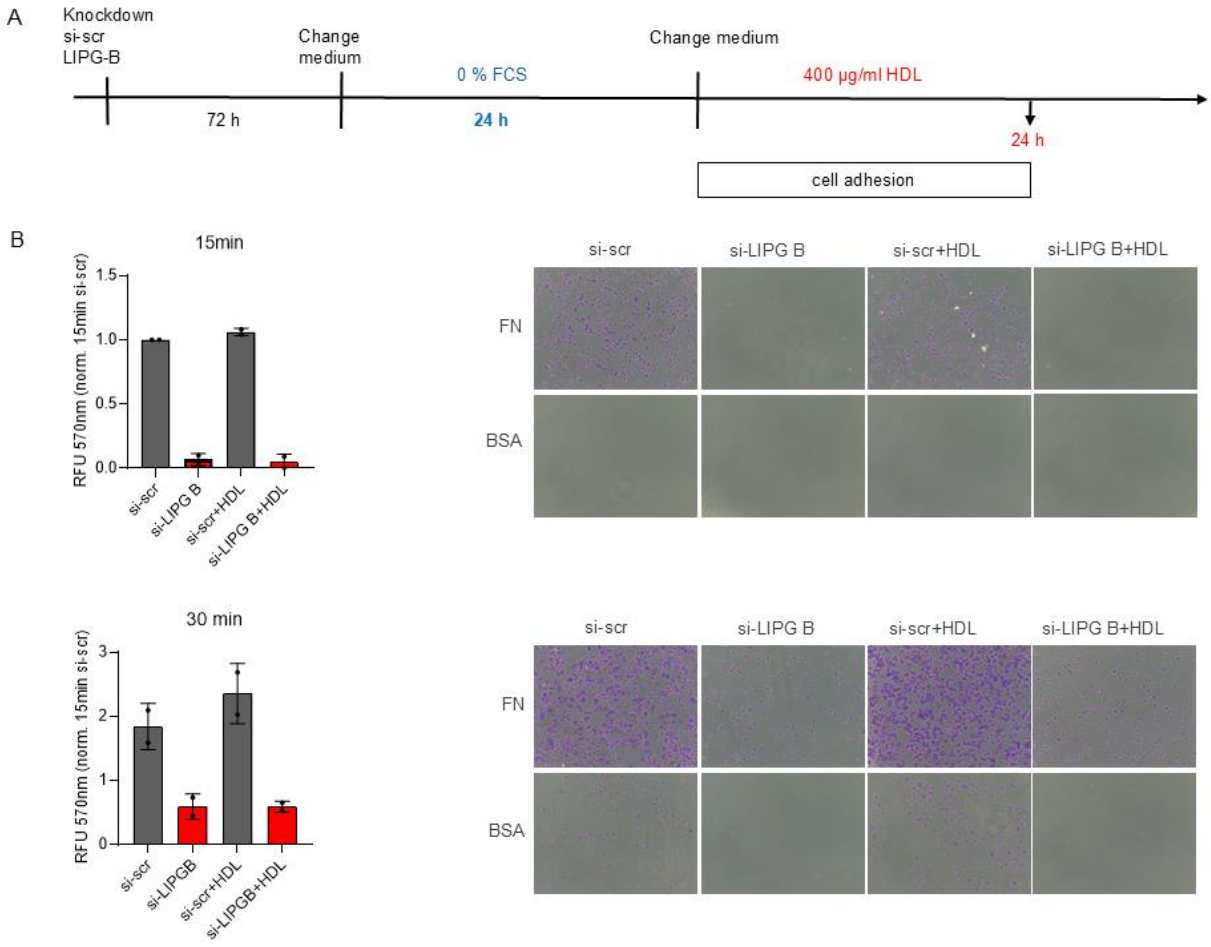

Figure 39: Adhesion assay on fibronectin after LIPG KD for 72 h in MDA-MB-468 cells, followed by 5 h starvation without FBS and treatment with 400 µg/mL HDL for 24 h. (A) Illustration of experimental design. (B) Starved Adhesion assay was performed after 2 h rotation with 400 µg/mL HDL in medium without FBS. The cells were incubated for 15 min or 30 min in medium with 0% FBS. BSA control was subtracted from the fibronectin coated wells and absorption was measured at 570 nm. The results represent mean ± SD (n=2).

As shown in Figure 39B, control si-scr cells attached much more efficiently than si-LIPG-cells, both after 15 min and 30 min attachment time. In addition, a slight effect of HDL was observed in si-scr control cells, with a trend to better attachment in the presence of HDL. However, this was not observed in LIPG KD cells. This result suggested that HDL, most likely via cholesterol exchange, favors cellular adhesion processes in the control situation. However, HDL treatment in LIPG KD cells did not rescue their loss of adhesion properties. Thus, due to loss of LIPG, cells cannot benefit from pro-adhesion effects of HDL. Although more experiments are required to test this hypothesis, it is likely that LIPG KD cells accumulate cholesterol, because they cannot use HDL to get rid of their excess cholesterol and therefore adhesion was slower, showing less cell plasticity and inert behavior.

6.1.4 Analysis of intracellular cholesterol content after HDL treatment using RAMAN-Spectroscopy

In previous data shown in Figure 37 cholesterol accumulation in si-LIPG B with HDL treatment was assessed using the Abcam Quantification Kit. The Abcam Kit was able to detect total and free cholesterol, as well as cholesterol ester. However, information about different cholesterol species was missing. Raman Spectroscopy has been proposed as a useful technique for analysis of biological materials. It allows invasive-free analysis of vibrational energy of molecules, providing quantitative knowledge of molecular composition. [123] The cellular cholesterol composition after LIPG KD needs further clarification in regard to its various species. Using Raman Spectroscopy an in-depth analysis could be provided (Fig. 40).

Table 21: List of characteristic peaks for cholesterol, cholesterol ester and Triacylglycerol, derived from *Czamara et. al.* [124]

Compound	Wavelength (nm)	Vibration
Free Cholesterol	2930	CH2 symmetric stretching
	2864	CH3 symmetric stretching
	1672	C=C stretching
	1442	CH2 scissoring mode
	1178	C-C, C-H stretching
	1130	C-C, C-H stretching
	1078	C-C, C-H stretching
	701	Cholesterol ring def.
Cholesteryl palmitate (CPA)	2937	CH2 symmetric stretching
	2861	CH3 symmetric stretching
	2845	CH2 symmetric stretching
	1668	C=C stretching
	1442	CH2 scissoring mode
	1298	C-C, C-H stretching
	1131	C-C, C-H stretching
	1066	C-C, C-H stretching
	702	Cholesterol ring def.
Cholesteryl stearate (CSA)	2885	CH2 symmetric stretching
	2852	CH3 symmetric stretching
	1671	C=C stretching
	1444	C=C stretching
	1301	C-C, C-H stretching
	1133	C-C, C-H stretching
	1066	C-C, C-H stretching
	702	Cholesterol ring def.
Triacylglycerol (TCA)	2876	CH2 symmetric stretching
	1744	C=O stretching
	1444	C=C stretching
	1306	C-C, C-H stretching
	1116	C-C, C-H stretching

	1064 847	C-C, C-H stretching C-O stretching

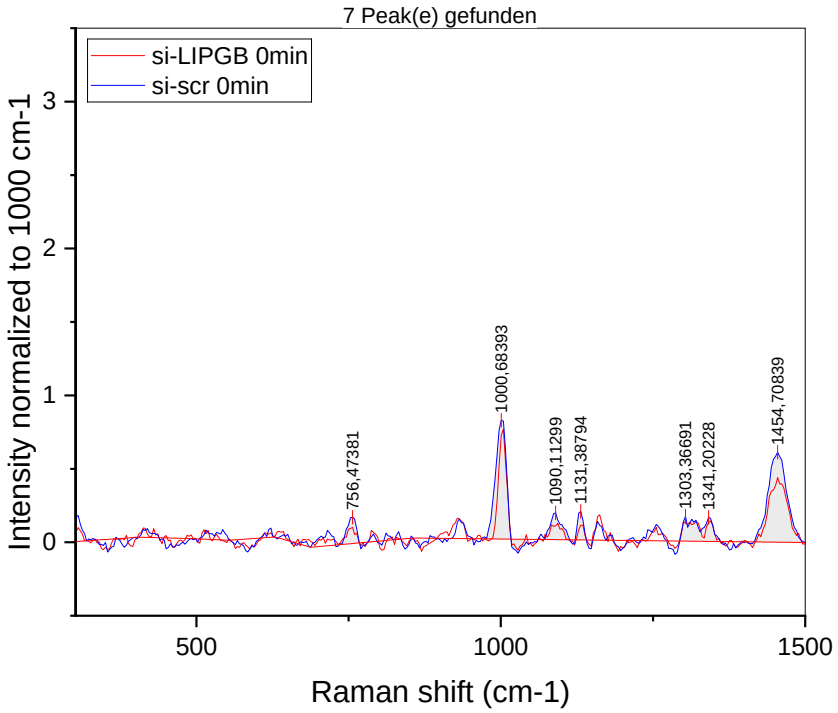

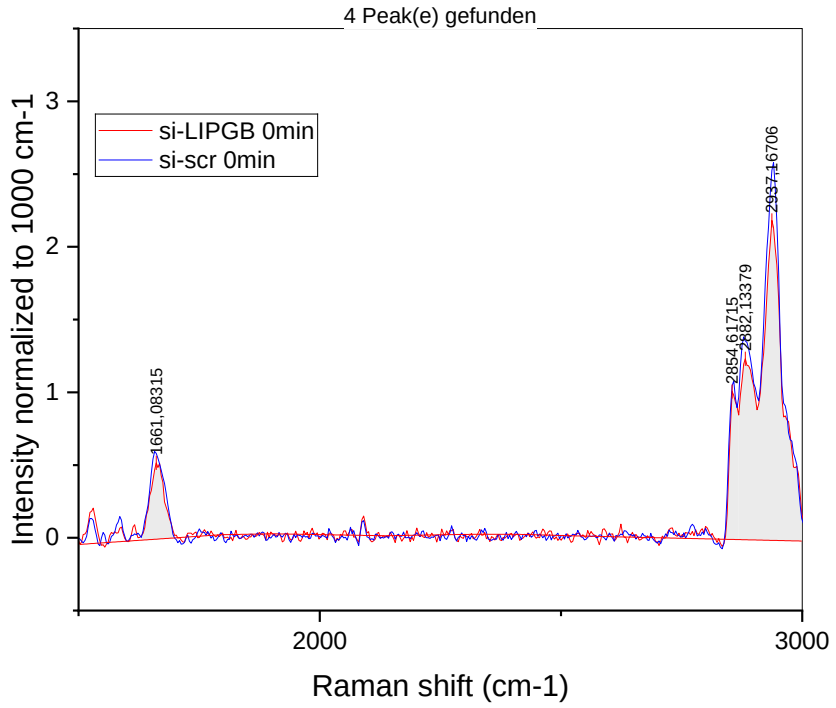

Figure 40: Raman Spectrum after LIPG KD and 24 h starvation in MDA-MB-468. The results represent mean ± SD (n=3).

The Raman Spectrum was assessed after 72 h LIPG KD in MDA-MB-468 and 24 h starvation. Spectral analysis with Origin provided dominant peaks and their respective wavelengths. LIPG KD and si-scr control showed characteristic peaks for cholesteryl palmitate and cholesteryl stearate, especially 2937 cm^{-1} for CPA and 2885/2852 cm^{-1} for CSA. Hereby the si-scr control spectrum (blue line) showed higher intensities, identifying more CPA and CSA in si-scr. The peak at 1661 cm^{-1} was closest to the CPA C=C stretching and showed again higher intensity in the si-scr than in the LIPG KD condition. At around 1302 cm^{-1} and 1131 cm^{-1}, both spectra presented characteristic CSA and CPA C-H or C-C stretching peaks. The 1454 cm-1 was a peak specific for Tricaprin, a Triacylglycerol, which was more prominent in si-scr compared to LIPG KD. The 756 cm^{-1} peak was the closest to a phosphatidylethanolamine peak, which indicated more phosphatidylethanolamine in si-scr compared to si-LIPG B. Spectra characterization showed higher amounts of intracellular CPA and CSA content in si-scr compared to the LIPG KD condition. It showed more phosphatidylethanolamine as well in si-scr compared to LIPG KD.

Upon treatment with HDL for 1 h, the intensity increased of CSA and CPA peaks at 2937 cm^{-1}, 2885 cm^{-1} and 2852 cm^{-1} (Supplementary information). The peak intensities of si-scr at 2937 cm^{-1}, 2885 cm^{-1} and 2852 cm^{-1} increased after 5 h and 24 h treatment (Supplementary information). Also, at 1661 cm^{-1} and 1454 cm^{-1} the peaks showed higher intensity in si-scr. This indicated that CSA, CPA and Tricaprin were increasing after HDL treatment in si-scr control condition. LIPG KD cells after HDL treatment showed less intracellular CSA, CPA and Tricaprin content compared to the respective control. And compared to the initial LIPG KD condition without HDL, the cells seemed to decrease their cellular CSA, CPA and Tricaprin with HDL treatment. Therefore, cells with less LIPG expression may show slowed down cholesterol ester uptake capacities from HDL. LIPG's enzymatic activity seemed to impact cholesterol ester uptake via SCARB1 [(89)], which could influence intracellular cholesterol ester content and distribution. This finding was also observed after quantification of cholesterol esters (CE) using Abcam Kit, where the CE content decreased significantly in LIPG KD after 1 h HDL treatment (Fig. 37). Thus, the results obtained with RAMAN spectroscopy were compatible with those obtained with the Abcam kit. The Raman peaks identified

mostly cholesterol ester and triacylglycerol content; however, free cholesterol should also be analyzed.

6.1.5. HDL signaling properties are impaired by LIPG deficiency in MDA-MB-468 cell

Analysis of HDL exposure up to 24 h in LIPG-deficient cells revealed the accumulation of cholesterol. Moreover, LIPG-deficient breast cancer cells showed a markedly decreased expression of SR-BI, indicating that in the absence of LIPG, breast cancer cells cannot efficiently use HDL-SR-BI-mediated mechanisms to maintain cholesterol levels. In addition to serving as a lipid exchange and trafficking platform, HDL has signaling properties and binding of HDL to its receptor (SR-BI, the SCARB1 product) results in activation of signal transduction pathways such as AKT and MAPK (see chapter 2.5.3.2). Importantly, some studies performed in endothelial cells have demonstrated that pathways that are stimulated by HDL are involved in cell adhesion and migration. One study has even shown that FAK is a target of HDL-signaling via AKT stimulation. [66] Therefore, in a next step it was investigated whether HDL signaling in breast cancer cells leads to similar effects, and whether LIPG KD influences such HDL-signaling effects. To this aim, MDA-MB-468 LIPG KD and si-scr control cells were serum-starved for 24 h and stimulated with 400 µg/mL HDL for 5, 15, 30 and 300 min, and proteins were extracted to investigate activation of proteins involved in cholesterol homeostasis (SCARB1), cell adhesion and migration (FAK) and key signaling kinases (ERK1/2, ERK5 and AKT).

6.1.5.1. HDL-induced SR-BI protein expression is impaired in LIPG knockdown cells

SCARB1 protein expression after incubation with HDL in control and LIPG-silenced MDA-MB-468 cells was analyzed by Western blot. As shown in Figure 41, after serum starvation for 24 h and prior to HDL-stimulation, LIPG KD cells showed decreased SCARB1 expression compared to si-scr cells. In si-scr cells, incubation with HDL resulted in an upregulation of SCARB1 expression. After 300 min (5 h), the expression was comparable to the initial expression. In si-LIPG B cells, incubation with HDL did not lead to upregulation of SCARB1, indicating an impaired HDL-dependent SCARB1 upregulation when LIPG expression is lost.

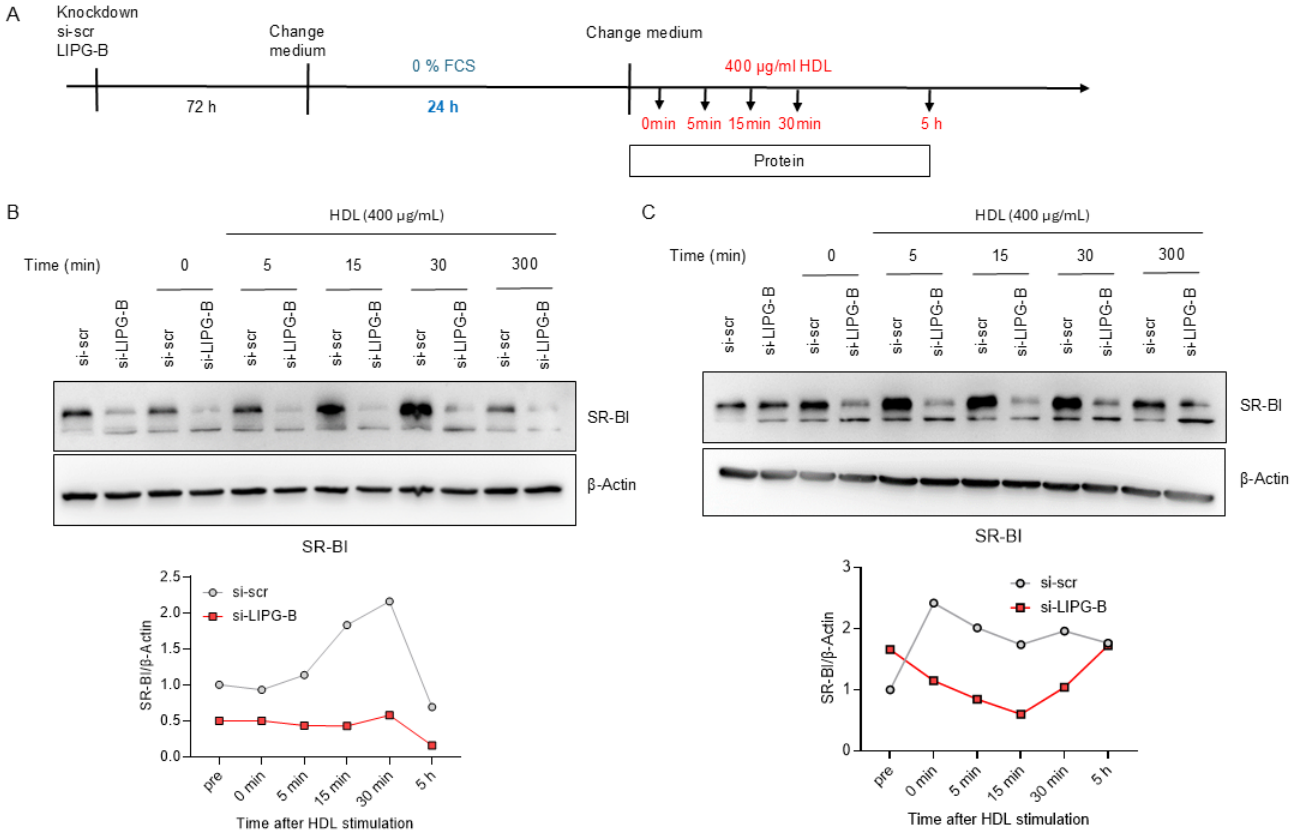

Figure 41: LIPG KD for 72 h in MDA-MB-468 cells, followed by 24 h starvation without FBS. Starved cells were treated with 400 µg/mL HDL for 5 min till 300 min. (A) Illustration of experimental design. (B-C) Immunoblotting of SCARB1 protein expression in cell lysates with β-Actin as a loading control. Two biological replicates are shown.

6.1.5.2 HDL-induced FAK expression and phosphorylation is impaired in LIPG knockdown cells

A study reported activation of FAK in endothelial cells as a result of HDL-signaling. [29] Therefore, in a next step it was investigated whether HDL-signaling in breast cancer also influences FAK expression (total FAK) and activation (phosphorylated FAK at Tyr397) and whether this process is regulated by LIPG. This question was tackled by investigating FAK expression and phosphorylation upon HDL treatment in si-scr and si-LIPG B in MDA-MB-468 cells (Fig. 42).

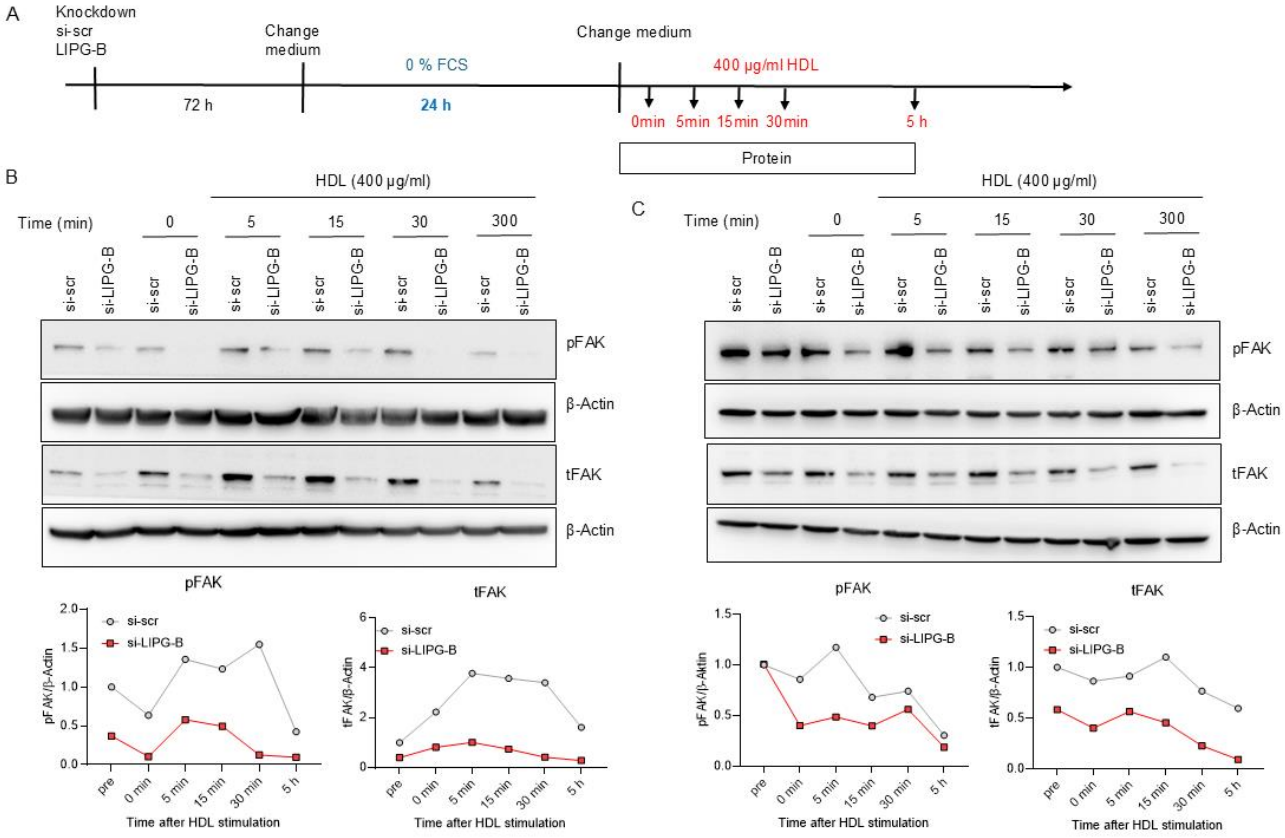

Figure 42: LIPG KD for 72 h in MDA-MB-468 cells, followed by 24 h starvation without FBS. Starved cells were treated with 400 µg/mL HDL for 5 min till 300 min. (A) Illustration of experimental design. (B-C) Immunoblotting of phosphorylated and total FAK protein expression in cell lysates with β-Actin as a loading control. Two biological replicates are shown.

After 72 h LIPG KD, and 24 h FBS starvation higher FAK expression was observed in si-scr compared to si-LIPGB cells. Cultivation of si-scr with 400 µg/mL HDL increased FAK expression, reaching maximal levels 15 min after HDL stimulation. Afterwards, the expression of FAK went down again. Si-LIPG B cells expressed FAK at much lower levels, and HDL treatment did not markedly increase them, indicating an impairment of HDL-dependent FAK upregulation in the absence of LIPG. The decreased FAK expression and lack of FAK upregulation upon HDL (Fig. 42) is in line with the lower adhesion activity in LIPG KD cells after HDL treatment (Fig. 39). In addition to FAK expression, also phosphorylation of FAK was increased by HDL to a higher extent in si-scr as in LIPG knockdown cells (Fig. 42).

6.1.5.3. HDL-induced ERK5 phosphorylation is enhanced in LIPG knockdown cells

HDL binding to SCARB1 was shown to activate the MAPK pathway, which could involve both ERK1/2 and the less well studied MEK5/ERK5 signaling pathway (2.2.3).

Therefore, phosphorylation and total levels of ERK5 were analyzed by Western blot after treatment of LIPG KD and si-scr control MDA-MB-468 with HDL (Fig. 43).

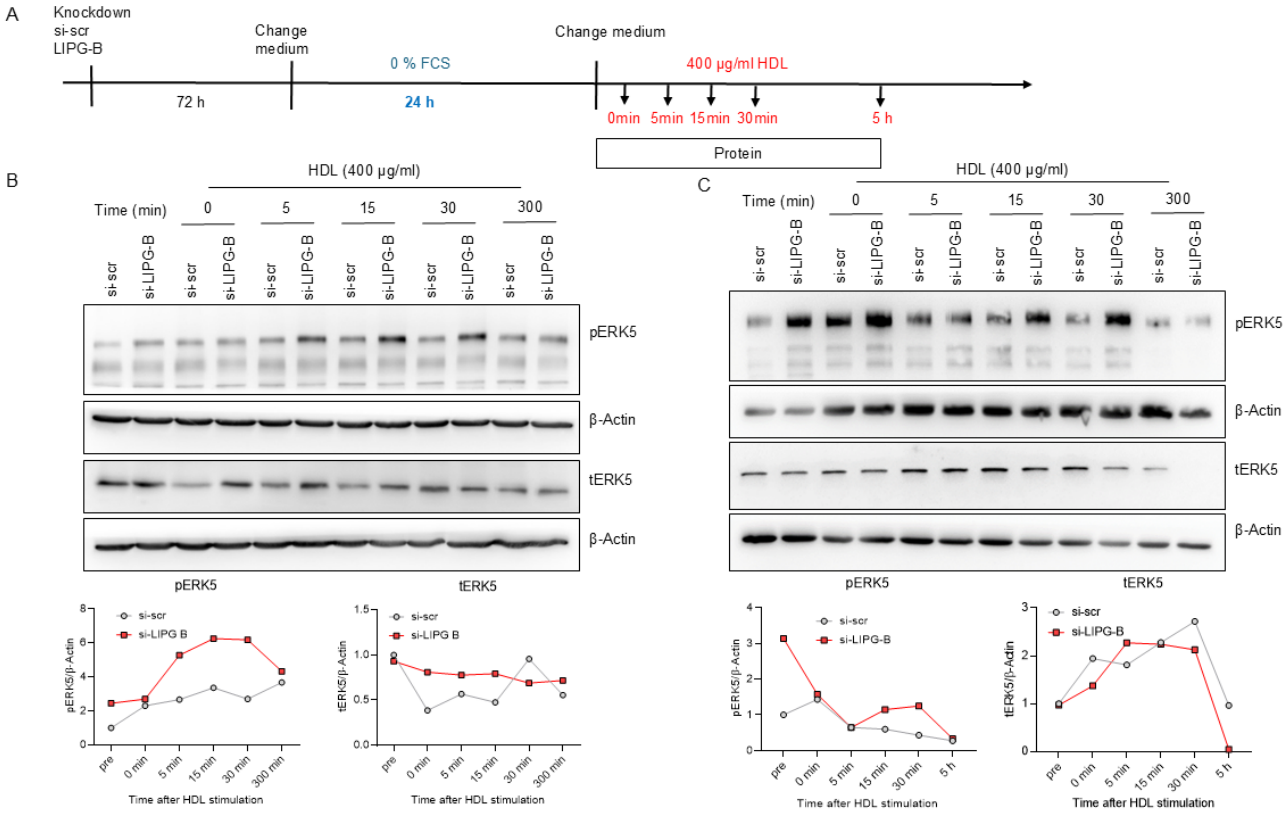

Figure 43: LIPG KD for 72 h in MDA-MB-468 cells, followed by 24 h starvation without FBS. Starved cells were treated with 400 µg/mL HDL for 5 min till 300 min. (A-B) Illustration of experimental design. (B) Immunoblotting of phosphorylated and total ERK5 in cell lysates with β-Actin as a loading control. Two biological replicates are shown.

The phosphorylation of ERK5 was higher after 72 h LIPG KD compared to si-scr control. After serum-starvation for 24 h the phosphorylation of ERK5 was similar in both conditions. Upon HDL treatment, the phosphorylation of ERK5 markedly increased in LIPG KD cells compared to si-scr control cells for until the 30 min time point. 300 min after HDL treatment, similar ERK5 phosphorylation in both conditions was shown. This shows that in the absence of LIPG the MAPK5 signaling pathway is more active. The total ERK5 protein expression was generally lower in the si-scr control compared to the LIPG KD condition. A transient increase in tERK5 was observed 30 min after HDL treatment in si-scr cells, but not in LIPG KD cells.

6.1.5.4. HDL-induced ERK1/2 activation is not markedly affected in LIPG knockdown cells

HDL-induced signaling in endothelial cells is partially mediated by the HDL receptor SCARB1. Thus, in breast cancer cells, the activation of the MAPK pathway in response to HDL could be affected in the LIPG KD condition because of the SCARB1 downregulation. Since ERK1/2 is involved in the MAPK pathway (see chapter 2.5.3), an altered HDL signaling may be reflected in altered phosphorylation or expression levels of this protein. Expression and phosphorylation of ERK1/2 (Thr202/Tyr204) were analyzed by Western blot after treatment with HDL in LIPG KD and si-scr control cells (Fig. 44).

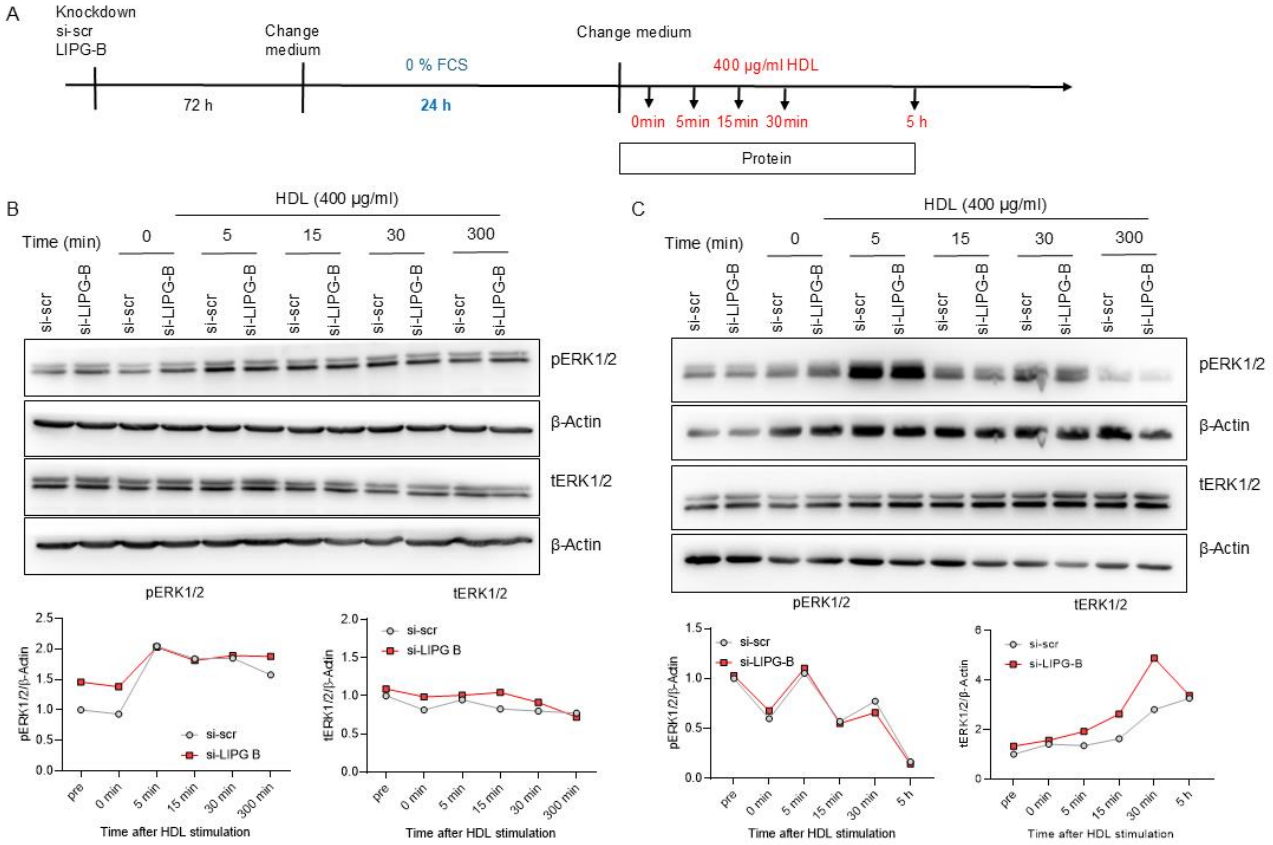

Figure 44: LIPG KD for 72 h in MDA-MB-468 cells, followed by 24 h starvation without FBS. Starved cells were treated with 400 µg/mL HDL for 5 min till 300 min. (A) Illustration of experimental design. (B-C) Immunoblotting of phosphorylated and total ERK1/2 protein expression in cell lysates with β-Actin as a loading control. Two biological replicates are shown.

Silencing LIPG for 72h resulted in only slightly more ERK1/2 phosphorylation compared to the si-scr control, also after serum-starvation. Upon HDL treatment, the phosphorylation of ERK1/2 increased similarly in the LIPG KD condition and the si-scr control, with a peak at 5 min. After 5 h the phosphorylation had decreased for both

conditions. HDL simply activated the MAPK1/2 pathway in general without differentiating between si-LIPG B and si-scr. Thus, silencing LIPG did not seem to interfere with the HDL-induced ERK1/2 signaling.

6.1.5.5. Expression and phosphorylation of AKT is higher in LIPG knockdown cells

Binding of HDL to its receptor SCARB1 has been shown to stimulate AKT in endothelial cells (see chapter 2.5.3). Therefore, it was also investigated whether the activation of the AKT signaling pathway in response to HDL was affected in the LIPG KD condition due to the SCARB1 downregulation. Expression and phosphorylation of AKT at S473 were analyzed by Western blot after treatment with HDL in LIPG KD and si-scr control cells (Fig. 45).

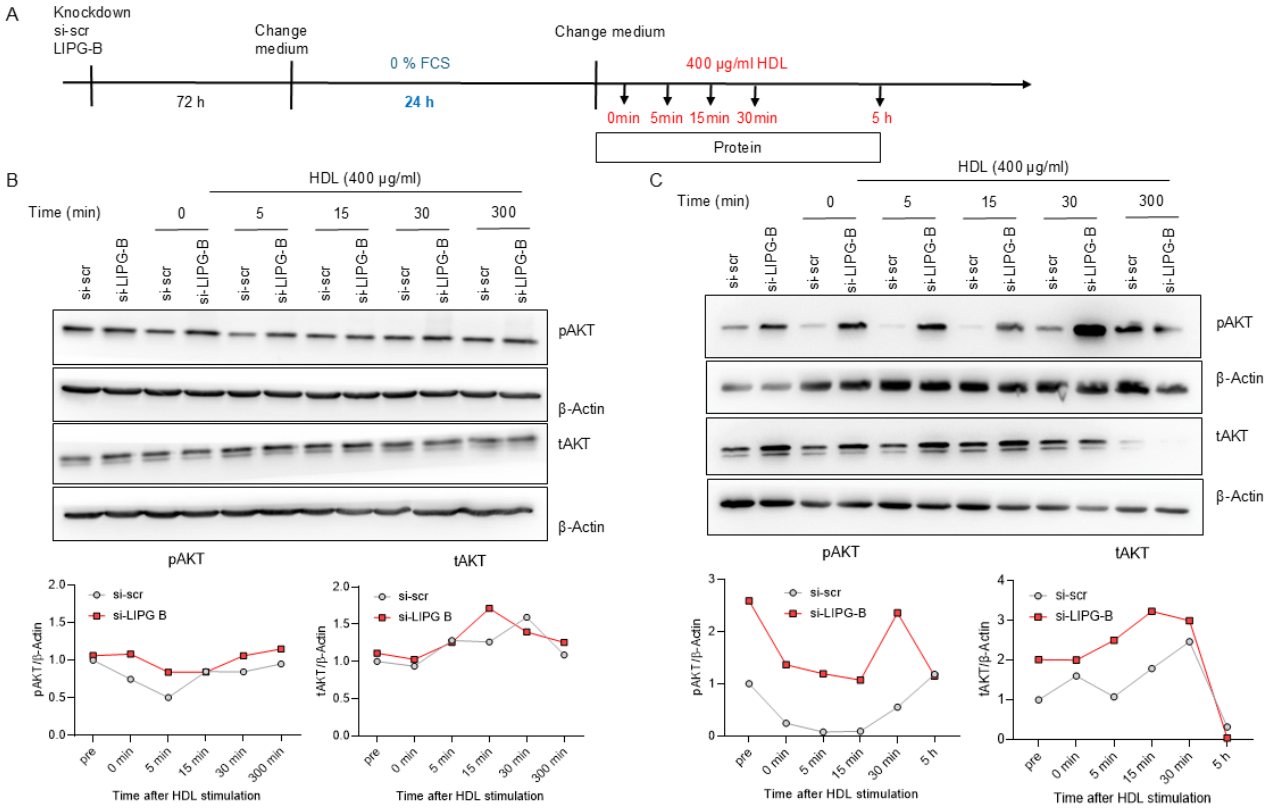

Figure 45: LIPG KD for 72 h in MDA-MB-468 cells, followed by 24 h starvation without FBS. Starved cells were treated with 400 µg/mL HDL for 5 min till 300 min. (A) Illustration of experimental design. (B-C) Immunoblotting of phosphorylated and total AKT in cell lysates with β-Actin as a loading control. Two biological replicates are shown.

Immunoblotting of tAKT presented more AKT expression after 72 h LIPG KD compared to the si-scr control situation. HDL treatment led to higher tAKT expression in both conditions, with a peak in LIPG KD cells after 15 min and in si-scr cells later, after 30 min. Subsequently, the expression of AKT decreased but remained higher in LIPG KD

cells. The phosphorylated AKT was higher after 24 h serum-starvation in LIPG KD cells compared to si-scr control cells. In both LIPG KD and si-scr conditions, HDL treatment led to a transient decrease in phosphorylated AKT, which was more pronounced in the si-scr control condition. From 15 min onwards the AKT phosphorylation levels rose again in both conditions but were higher in the LIPG KD cells. In general, LIPG deficient cells displayed higher AKT expression and phosphorylation.

6.2. Contribution of LIPG to cholesterol regulation in ovarian cancer

Ovarian tumors are diagnosed in advanced stages of disease progression, because of a lack of diagnostic methods and hidden symptoms. Disease progression is mostly caused by rapid and widespread metastasis. Lipid uptake receptors and enzymes as well as lipid synthesis enzymes are involved in ovarian cancer progression. These enzymes altered in cancer development promote tumor development. [125] Several cholesterol metabolism related genes also have been associated with higher ovarian tumor cell proliferation, migration and invasion. Correlations between tumor growth and HMGCR, LDLR, SR-BI and ABCA1 expression have been reported. [126] There is still a need for discovering new therapeutic targets in ovarian cancer. Further exploration of the involvement of lipid and cholesterol metabolism related genes could provide more insights in possible new targets. Therefore, it was explored whether our findings in breast cancer can also be applied to ovarian cancer.

6.2.1 LIPG is highly expressed in a subset of ovarian cancer cell lines

The involvement of LIPG in ovarian tumor development has not been explored so far. The first attempt was to study LIPG expression in several ovarian tumor cell lines. Protein and mRNA expression were compared to non-cancerous ovarian tissue HOSE6-3 (Fig. 46).

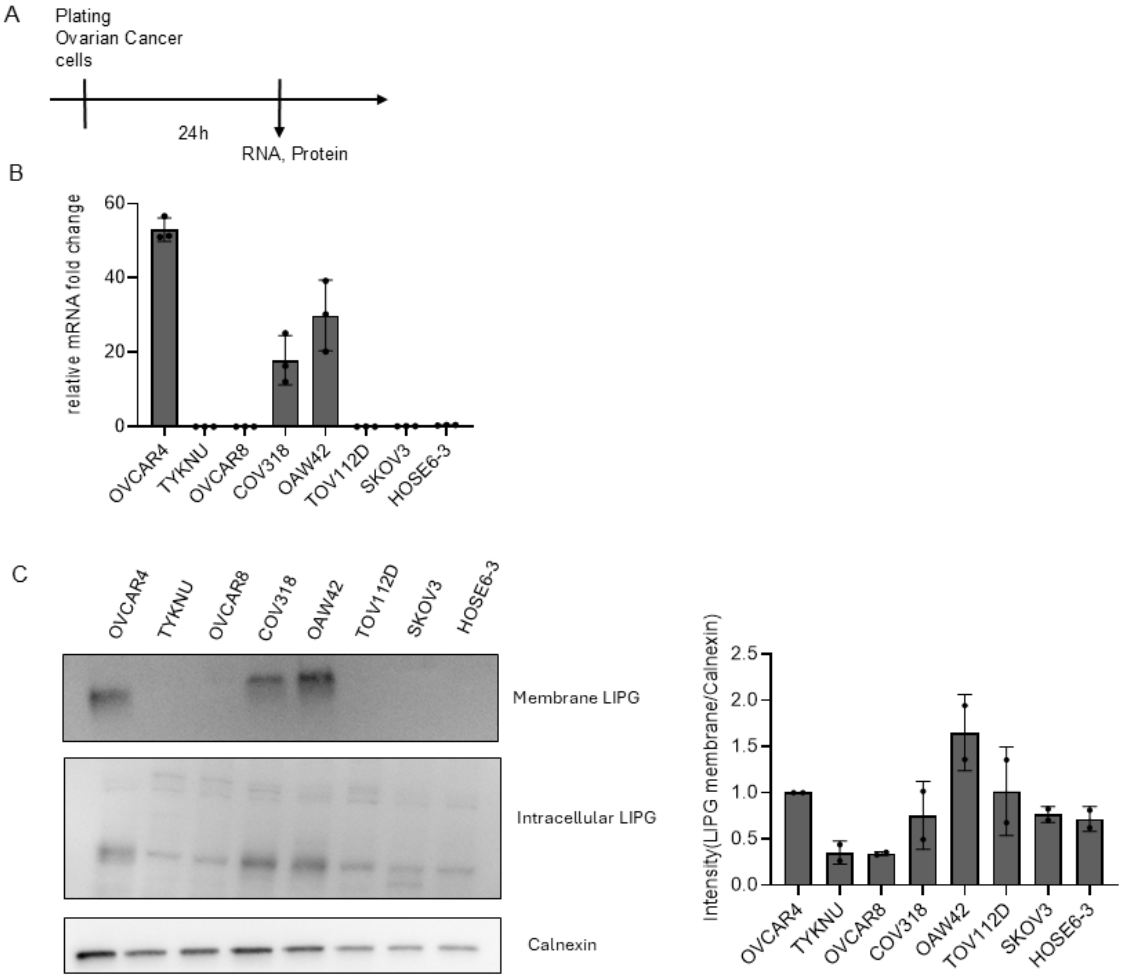

Figure 46: LIPG expression in various ovarian cancer cell lines on mRNA level, protein level and cell triglyceride content. (A) Illustration of experimental design. LIPG expression was analyzed on mRNA level (B) with quantitative RT-PCR and the use of UBC as an endogenous control. The results represent mean ± SD (n=3). Immunoblotting of LIPG protein expression (C) in cell lysates with calnexin as a loading control. The results represent mean ± SD (n=2).

Analysis of LIPG expression in various ovarian cancer cell lines revealed that OVCAR4, OAW42 and COV318 show high LIPG expression on mRNA level compared to the other cell lines (Fig. 46B). This finding is also seen on protein level, where OVCAR4, OAW42 and COV318 showed the highest LIPG protein expression (Fig. 46C). OVCAR4 was chosen for further experiments based on LIPG expression.

6.2.2 LIPG deficiency barely influences the cell adhesion kinetics of OVCAR4Luc cells to fibronectin

The ovarian tumor cell line OVCAR4 was stably transfected with a plasmid encoding the luciferase (luc) reporter gene for future *in vivo* imaging purposes. Therefore, the name OVCAR4Luc is short for OVCAR4 expressing luciferase. LIPG knockdown

experiments were performed in OVCAR4Luc to compare our findings to those obtained with the breast cancer cell lines (Fig. 47-48).

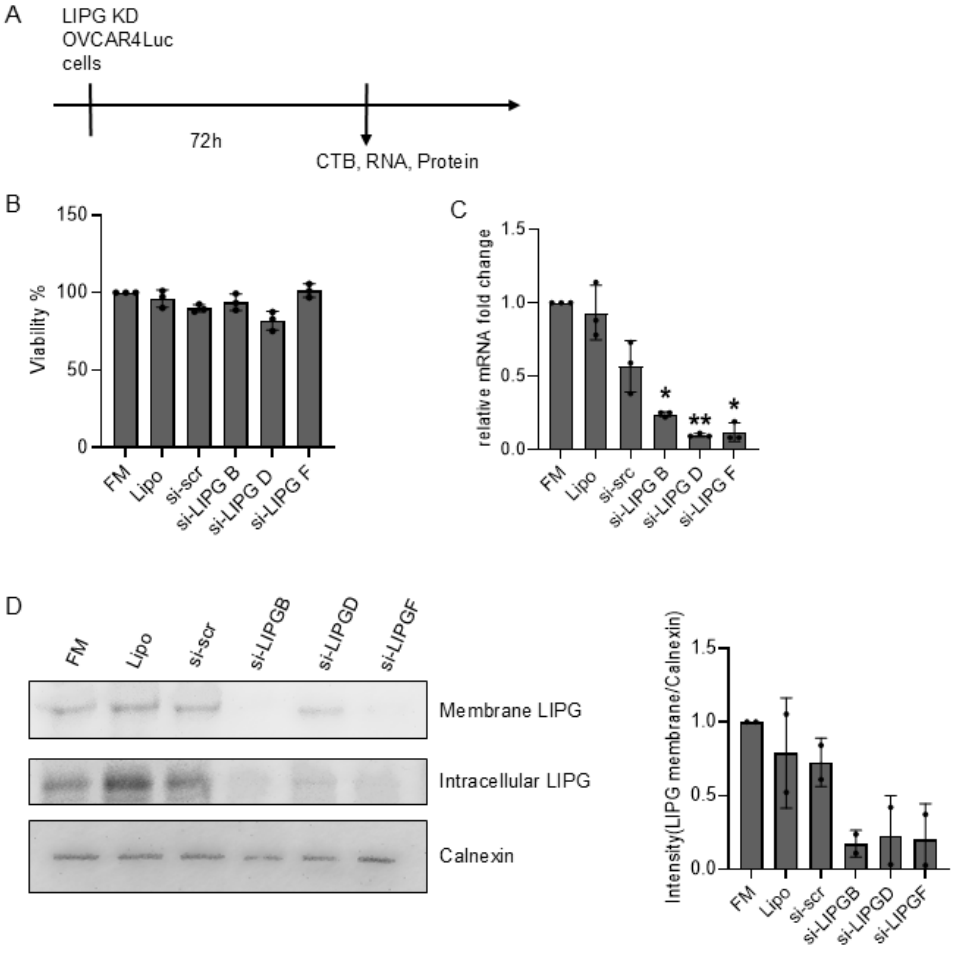

Figure 47: Confirmation of LIPG knockdown in OVCAR4Luc cells with mRNA expression, protein expression and cell viability detection. (A) Illustration of experimental design. Cell viability (B) of all si-RNA were accessed using CTB and fluorescent measurement at 540 nm. LIPG knockdown was analyzed on mRNA level (C) with quantitative RT-PCR and the use of UBC as an endogenous control. The results for CTB and mRNA represent the mean ± SD (n=3). Immunoblotting of LIPG protein expression (D) in cell lysates with calnexin as a loading control. The results represent the mean ± SD (n=2).

As shown in Figure 47B, the cell viability in OVCAR4Luc did not decrease significantly after 72 h LIPG KD. The expression of the LIPG mRNA (Fig. 47C) and protein (Fig. 47D) was significantly reduced for all three knockdown conditions compared to the control conditions indicating a successful knockdown.

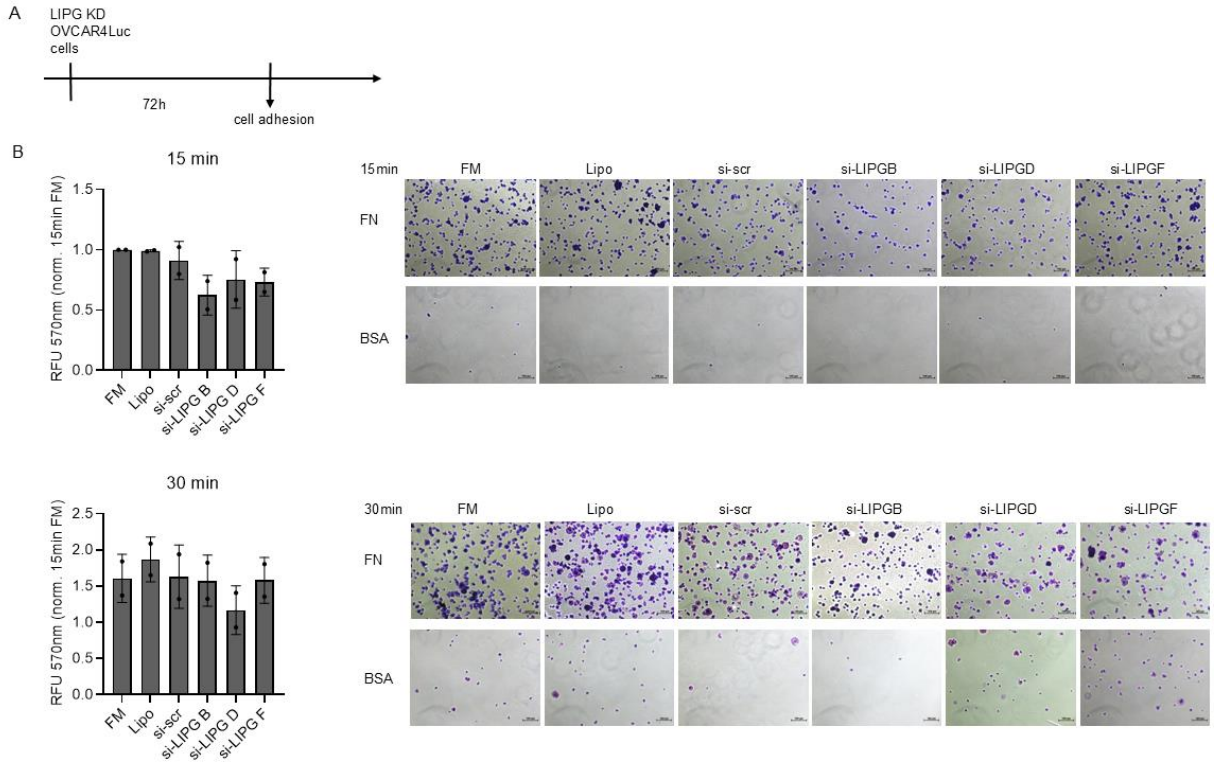

Figure 48: Analysis of cell adhesion on fibronectin after LIPG KD in OVCAR4Luc cells. (A) Illustration of experimental design. (B) Adhesion assessment after 15 min and 30 min in media with 1% FCS. BSA control was subtracted from the fibronectin coated wells and absorption was measured at 570 nm. The results represent mean ± SD (n=2).

The cell adhesion on a fibronectin matrix (Fig. 48B) for all LIPG siRNA knockdown oligos was reduced slightly compared to the controls after 15 min incubation. After 30 min incubation time adhesion for all knockdown conditions was re-established and comparable to the control conditions. Thus, the phenotype resulting from silencing LIPG in this ovarian cancer cell line is milder than that observed in the breast cancer cell lines. The adhesion process of ovarian cancer cells may not be LIPG-dependent.

7. Discussion

7.1. LIPG influences cell adhesion kinetics

The cell adhesion experiments showed a decrease in adhesion to extracellular matrix *in vitro* after LIPG KD for 15 min incubation time. After 30 min incubation time a similar number of cells had attached in LIPG KD and si-scr conditions, indicating that silencing LIPG only provokes a transient effect on cell adhesion. The same observation was made when monitoring attachment of LIPG KD cells on vascular endothelial cells. The transient cell adhesion changes indicate a kinetically slowed down process *in vitro*. Although transient, this effect may be relevant in the metastatic process *in vivo*, since faster attachment may improve the survival chances of metastatic tumor cells. These findings are in line with published data of Slebe et. al. and Lo et. al., who also observed less proliferation, adhesion, migration and invasion *in vitro* and less tumor growth *in vivo* in breast cancer cells lacking LIPG. [98], [99] This provides strong evidence for a possible role for LIPG in metastasis. Extravasation of circulating tumor cells into distant organ sites needs intact cell adhesion properties to metastasize successfully. Therefore, attachment of tumor cells to vascular cells would be expected to be less efficient, if lack of LIPG in breast cancer cells leads to slowed down adhesion. The mechanistic link between the lack of LIPG and the slowed down adhesion kinetics has not been studied so far. The results presented in this thesis showed that LIPG KD is accompanied by slightly decreased expression of the integrin ITGAV and decreased FAK phosphorylation. Downregulation of ITAGV expression and decrease of FAK phosphorylation (pFAK), at least in MDA-MB-468 as a consequence of LIPG silencing has not been previously reported and could provide an explanation for the observed slowed down adhesion processes. This novel mechanistic link would need follow up experiments to distinguish between inside-out or outside-in signaling of the integrins. The contribution of ITAGV in cell adhesion in MDA-MB-468 cells to extracellular matrix, in particularly to fibronectin, was demonstrated in the knockdown experiments in this thesis. The contribution of FAK to cell adhesion and migration processes is well-documented. [127] Altogether, strong evidence for a role of LIPG in different steps of the metastatic process was presented in this study, which justifies further in vivo studies in mice.

7.2. Cholesterol as a regulator of cell adhesion processes

In this thesis, interventions were made to confirm the importance of cholesterol in various cellular processes. Cholesterol addition was shown to successfully increase intracellular cholesterol level and cholesterol depletion successfully decreased intracellular cholesterol level. In agreement with the literature, the cholesterol manipulations affected gene expression of genes involved in cholesterol homeostasis, resulting in significant changes in LDLR (cholesterol uptake) and ABCA1 (cholesterol efflux) mRNA expression. These results revealed that cancer cells respond and adjust their cholesterol metabolism immediately upon changes in their balance. Tight cholesterol regulation is reported as an essential asset for breast cancer migration and proliferation. [31] Moreover, in parallel to gene expression alterations, cholesterol manipulation led to less adhesion after both cholesterol addition and cholesterol depletion. Mohammadalipour et. al. [128], reported decrease of adhesion after cholesterol depletion in non-small lung cancer, which aligns with our previous results. Controversially Fu et. al. [129], reported that cholesterol addition increases adhesion of monocytes. Dorsch et. al. published that inhibition of cholesterol synthesis with Statins causes changes in cell plasticity, which resulted in less metastasis. [130] Different results in adhesion phenotypes upon cholesterol addition or depletion are difficult to explain and may be due to different levels of cholesterol in the cell types analyzed. Alternatively, not the cholesterol amount but its distribution and the kinetics of its trafficking within the cells may be the crucial parameter. Alterations in membrane cholesterol accumulation and distribution could change cell plasticity. This may impair spreading and migration properties as well. In future experiments staining cholesterol and the actin cytoskeleton would be essential to prove the role of cholesterol as an adhesion key regulator.

7.3. LIPG regulates cholesterol exchange with lipoproteins thereby influencing cellular cholesterol levels

A main question of this thesis was to investigate whether LIPG influences cellular cholesterol levels. An increase of mRNA expression of LDLR (cholesterol uptake) and downregulation of SCARB1 (cholesterol exchange), ABCA1 and ABCG1 (cholesterol efflux), indicated an imbalanced cholesterol homoeostasis in the cell after LIPG silencing in breast cancer cells. The loss of expression of SR-BI upon LIPG KD was confirmed at the protein level using different siRNA oligos targeting LIPG, also in a

second breast cancer cell line. These results are novel since changes in gene expression of cholesterol-related genes upon LIPG knockdown have not been reported so far. How LIPG influences gene expression needs further investigation. Based on the observed gene expression changes, an increased cholesterol uptake (*via* LDLR) as well as a decreased cholesterol efflux (*via* SR-BI, ABCA1 and ABCG1) would be expected to occur, leading to elevated cholesterol levels within tumor cells. In agreement with the observed gene expression changes, after knockdown of LIPG and subsequent treatment with lipoproteins (HDL, LDL) and serum (FBS), LIPG KD cells showed accumulated intracellular cholesterol. In this thesis it could not be discriminated whether it is impaired efflux or accelerated uptake of cholesterol, or both, which leads to increased intracellular cholesterol level. Cholesterol efflux assays using labeled cholesterol, would confirm whether the accumulated cholesterol after LIPG knockdown is predominantly caused by perturbed cholesterol efflux. In addition, if loss of SR-BI in LIPG KD cells is the major cause of cholesterol accumulation, a knockdown of SCARB1 could show similar results. Additionally, rescuing SR-BI by overexpression in LIPG KD cells could normalize cholesterol levels, and therefore provide evidence for the hypothesis. In contrast, a knockdown of LDLR would lead to the opposite effect, preventing accumulation of cholesterol. It is also not clear whether LIPG exerts its effects *via* its catalytic or *via* its bridging function. This could be approached using small molecule inhibitors directed against the phospholipase activity of LIPG. An additional remaining question would be the association between cholesterol accumulation and the altered adhesion and migration kinetics in LIPG KD cells. It would be plausible that the accumulation of cholesterol is responsible for slowed down cellular kinetics observed after LIPG KD, since addition of cholesterol leads to similar effects. This could be tackled by cholesterol and actin cytoskeleton staining to visualize cholesterol localization and filament structure. Although, analysis of baseline cholesterol level after LIPG KD and FBS starvation in MDA-MB-468 did not show any changes using the Abcam Cholesterol Quantification Kit, RAMAN Spectroscopy was a promising tool to study cellular cholesterol composition in more detail. Indeed, studying the cholesterol content after LIPG KD and FBS starvation using RAMAN Spectroscopy showed that different species of cholesterol esters (cholesteryl palmitate and cholesteryl stearate) can be distinguished and revealed less cholesterol ester accumulation in breast cancer cells lacking LIPG compared to control cells. These findings indicate intracellular cholesterol ester changes upon LIPG KD, indicating a role for LIPG in selective

cholesterol ester uptake from HDL lipoproteins in breast cancer cells. This was substantiated by the fact that after treatment with HDL the triacylglycerol, cholesterol and cholesterol ester content did increase in the control cells but decreased in the LIPG KD condition in a time dependent manner. These results are also in agreement with the results obtained using the Abcam Cholesterol Quantification Kit, although the quantification of cholesterol esters in the cellular lysates only revealed a significant effect 1h after HDL incubation. The Raman Spectra reveals a kinetic dependency of intracellular cholesterol changes *via* selective HDL-cholesterol ester uptake, which depends on LIPG.

7.4. LIPG influences HDL-mediated signaling

In addition to its role in reverse cholesterol transport, HDL can also activate signaling pathways after binding to its cellular receptors. Such studies have been conducted in endothelial cells, where functional effects of HDL-induced signaling pathway included endothelial cell migration, tube formation and angiogenesis. (94) The impact of HDL-signaling in breast cancer cells has not been studied in detail. In fact, only scarce data are available concerning the signaling pathways activated or repressed by SR-BI in cancer cells. The study of Danilo et al. reported activation of both PI3K and Erk1/2 pathways by HDL binding to SR-BI in the MDA-MB-231 and MCF7 breast cancer cell lines. [(131)]

In this thesis, it was explored whether HDL can induce signaling pathways (AKT, ERK1/2, ERK5, FAK), as well as expression of its receptor SR-BI in MDA-MB-468 breast cancer cells, and whether silencing LIPG influences such events. Interestingly, it was shown that not only SR-BI protein levels increased after HDL signaling but also that this upregulation is impaired in the LIPG KD condition. These results reveal new aspects of HDL-signaling effects, such as the fact that HDL can upregulate its own receptor and that cells without LIPG are refractory to this effect. Moreover, the downregulation of SR-BI observed after LIPG KD cannot be rescued by HDL treatment, indicating that LIPG is essential for adequate expression or stability of the SR-BI.

HDL was able to enhance FAK protein expression and activity (phosphorylation) in MDA-MB-468 cells, and this was impaired in LIPG KD cells. The influence of HDL-signaling on FAK reveals a link between HDL and the various functions that can be regulated by FAK, including cell adhesion and migration (see chapter 2.3). Interestingly, FAK has been reported to be involved in efficient cholesterol delivery to

the plasma membrane via FAK/Integrin recycling endosomes. This accelerates the recycling of active integrins and stimulates FA dynamics and cell migration. [132] LIPG silencing was shown to affect HDL-induced FAK expression and activation and this, in turn could explain both the altered adhesion and migration kinetics of LIPG-deficient cells as well as their increase cholesterol levels. Therefore, this study also revealed a requirement for LIPG in HDL-dependent FAK expression and activation.

It was surprising that despite the observed downregulation of SR-BI upon LIPG KD, two signaling pathways (ERK1/2 and AKT) that are known to be activated by HDL-SR-BI interaction were not repressed. ERK1/2 phosphorylation in response to HDL was comparable between control and LIPG-silenced MDA-MB468 cells while AKT and ERK5 expression and phosphorylation were even generally higher. The reason for the higher activity of these signaling proteins in the absence of LIPG remains unknown but could be related to the accumulation of cholesterol. Other signaling pathways activated by HDL may play a role and should be investigated.

Sawhney *et. al.* have reported a contribution of ERK5 to FAK expression. ERK5 overexpression led to increased FAK phosphorylation and increased adhesion. [71] In contrast, in this thesis, an upregulation of ERK5 expression and phosphorylation upon HDL treatment in LIPG KD cells was observed, where FAK expression and phosphorylation are decreased, and adhesion and migration are slowed down. This finding disputes the role of ERK5 in FAK regulation. A connection between S1P and FAK has been reported in other studies [133], where S1P was shown to activate FAK in prostate cancer cells. Importantly, HDL is a well-known carrier of S1P, and LIPG is shown to be a critical determinant in S1P signaling. [94] Therefore, LIPG knockdown may be affecting HDL-S1P-signaling via S1PR in this study, leading to impaired FAK actions. This should be investigated in detail next.

7.5 The importance of LIPG in ovarian cancer

Disease progression in ovarian cancer is caused by rapid and widespread metastasis. [6] Metastasis formation and tumor growth in ovarian cancer has been associated with cholesterol metabolism and cholesterol related gene expression (HMGCR, LDLR, SR-BI and ABCA1). [134] However, a role for LIPG in ovarian cancer disease progression has not been reported. Based on the results obtained in breast cancer, the importance of LIPG in ovarian cancer should also be explored. The results of this study revealed that LIPG is highly expressed in a subset of ovarian cancer cell lines. OVCAR4 is a

high-grade serous ovarian adenocarcinoma, which are characterized by their migration/invasion ability and tumorigenicity. [135] Therefore, adhesion properties after LIPG silencing were analyzed in OVCAR4Luc and the data revealed that the slowed down adhesion observed in breast cancer was much less pronounced in ovarian cancer. At first glance, this implies that LIPG is more relevant in breast cancer adhesion and metastasis formation than in ovarian cancer. However, the kinetically slowed down adhesion in OVCAR4Luc might still affect metastasis formation *in vivo*, which should be investigated in the future. If LIPG silencing would prevent *in vivo* metastasis formation of both breast cancer and ovarian cancer cell lines, then LIPG would function as a relevant prognostic factor in metastasis by possible alterations in cholesterol homeostasis in multiple cancer subtypes.

7.6 Limitations of this study

Despite extensively investigating the influence of LIPG on cellular cholesterol homeostasis, this study reveals some limitations in regard to technical difficulties and employment of new techniques. For instance, all cholesterol analyses were performed with whole cell lysates using the Abcam Cholesterol Quantification Kit. These analyses were able to reveal clear changes in the intracellular cholesterol content but could not reveal in which cellular compartments the cholesterol is accumulated. Cholesterol could be accumulating in the plasma membrane or alternatively could be trapped in the endolysosomal compartment on its way to the plasma membrane. However, cholesterol localization and trafficking, which are important aspects of maintaining cholesterol homeostasis, were not investigated so far. For further studies fluorescent visualization of cholesterol and cholesterol trafficking proteins could provide more insights into the exact role of LIPG in maintaining cholesterol homeostasis. A technical difficulty was the variability between different HDL lots used for the experiments. The HDL, provided by a company, was derived from human plasma samples pooled from different donors and it was not always possible to obtain the same lot. This could be responsible for variabilities between replicate experiments. Indeed, human plasma HDL particles are very heterogeneous and encompass various HDL- subclasses which differ in density, size, shape and lipid and protein composition. In addition, their stability is very limited, since HDL is known to oxidize; therefore, HDL functionality decreases after long-term storage, and this also affected the experiments. Another technical difficulty was the detection of important proteins (e.g. LDLR) by immunoblotting, which

was not possible due to lack of signal using various commercially available antibodies. Due to this constraint, the study focused on the downregulation of SR-BI observed after LIPG knockdown only, neglecting other possibly important alterations that were observed at the mRNA levels, such as upregulation of LDLR.

8. Conclusion

In conclusion, this research clearly demonstrates that LIPG influences both metastatic processes and cholesterol homeostasis in breast cancer cells, the latter by regulating the cholesterol exchange between cells and lipoproteins as well lipoprotein-induced signaling pathways. However, to clearly understand how these processes are connected, i.e. how LIPG´s influence on tumor cell cholesterol exactly modulate adhesion and migration, further research is needed. Silencing LIPG slows down tumor cell adhesion kinetics and migration in breast cancer cells and to a lesser extent in ovarian cancer cells, which are processes relevant to metastasis formation. A possible link between LIPG and metastasis formation could be by modulating integrin expression, trafficking or signaling. When looking at ITAGV expression, only a slight reduction in LIPG knockdown conditions in MDA-MB-468 cells was observed. However, FAK phosphorylation (activation) was significantly reduced in MDA-MB-468 cells and silencing LIPG in HCC1954Luc cells revealed less expression of FAK in the LIPG knockdown condition with oligo B. From this set of experiments, it could be concluded that LIPG expression influences metastatic processes by controlling FAK in different ways dependent on the cell line. From the studies on the role of LIPG on cholesterol homeostasis, one key finding was the downregulation of the HDL receptor SR-BI after LIPG knockdown. The loss of SR-BI from the plasma membrane would be expected to influence many processes, including cholesterol exchange with HDL particles as well as HDL-mediated activation of signaling pathways that involve SR-BI. Both processes were shown to be affected by silencing LIPG in this study: 1) LIPG KD cells accumulate more cholesterol in the presence of lipoproteins (especially HDL); 2) various HDL-mediated signaling events were altered in LIPG-silenced cells. Most worth mentioning here were a compromised HDL-induced upregulation of SR-BI and a phosphorylation/expression of FAK. This observation reveals that some of the signaling properties of HDL that affect FAK function depend on LIPG. This, in turn links LIPG and adhesion *via* a HDL-SRBI-FAK pathway. It is also possible that cholesterol transfer from and to HDL modulates the signaling pathways as well. Altogether, high LIPG expression may be an advantage in tumors in many ways: 1) to rapidly adjust their cholesterol levels to their requirements and so to avoid toxicity by its excessive accumulation, 2) to fine-tune cholesterol at focal adhesions and so to promote metastasis. It remains to be experimentally confirmed whether the influence of LIPG

on cell adhesion and migration is mediated by the ability of LIPG to regulate cellular cholesterol.

9. Outlook

This study has demonstrated that LIPG regulates various cellular processes relevant to the metastatic cascade *in vitro*. As a next step, *in vivo* experiments should be performed to confirm the relevance of these findings. To this aim, mouse models of peritoneal or lung metastasis will be employed, in which metastasis of injected tumor cells can be traced by *in vivo* imaging, using the generated luciferase-expressing HCC1954Luc and OVCAR4Luc cell lines. In addition, this study has revealed a novel role for LIPG in influencing tumor cell cholesterol homeostasis by multiple ways, including (i) regulation of cholesterol exchange with lipoproteins, particularly with HDL, (ii) control of cholesterol-related gene expression (SR-BI), and (iii) modulation of signaling pathways that are cholesterol-dependent and affect multiple biological processes (expression and activation of FAK). More work will be needed to prove the hypothesis that these are mechanisms underlying the effects of LIPG on cell adhesion and migration. Complementary experiments to the already performed LIPG-silencing experiments would be to investigate LIPG overexpression and its impact on adhesion and cholesterol homeostasis, as well as the use of small molecule inhibitors that inhibit the catalytical activity of LIPG. Further research is also needed to explore the influence of LIPG on the integrin signaling pathway and to differentiate between in-and-out or out-and-in signaling. Currently, experiments are ongoing to clarify if a knockdown of SCARB1 would lead to similar effects on cholesterol accumulation as those seen after LIPG knockdown. Or if the lack of LIPG has more broader effects and influences additional signaling pathways independent of SR-BI. Finally, the accumulation of intracellular cholesterol in LIPG-silenced cells resulting from lipoprotein interaction needs more exploration to tackle the question if it is due to increased cholesterol uptake or impaired cholesterol efflux. A possible experiment would be to trace cholesterol efflux by treating cells with fluorescent-labeled cholesterol and observing the process *via* imaging. Understanding the importance of LIPG-lipoprotein interactions for tumor progression may identify a target for anti-tumor strategies.

10. Supplemental

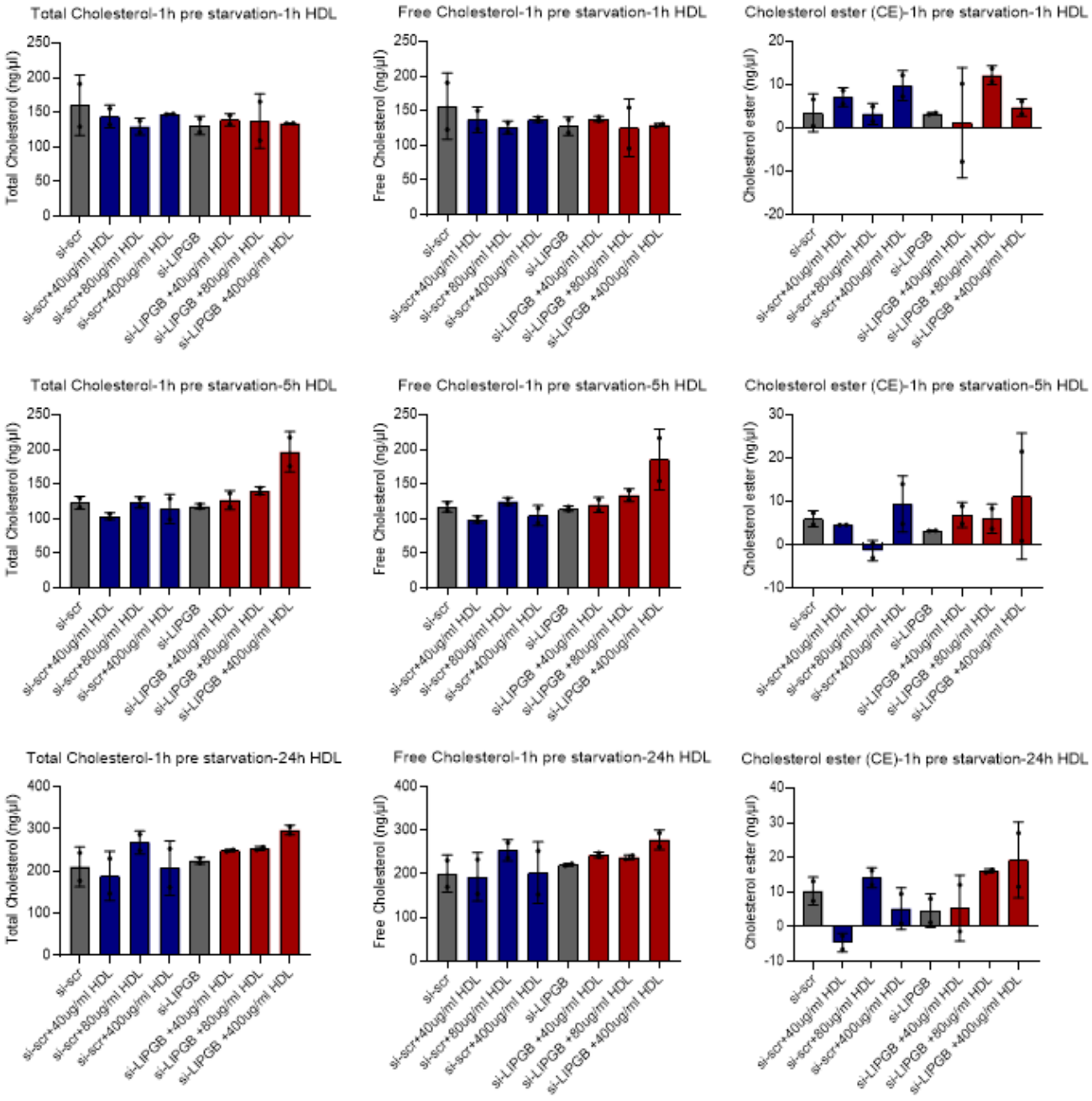

Figure S1: LIPG KD for 72 h in MDA-MB-468, followed by 1 h starvation without FBS. Starved cells were treated with 40 µg/mL, 80 µg/mL or 400 µg/mL HDL for 1 h, 5 h or 24 h. Cholesterol content was measured using Abcam Quantification Kit and fluorescence detection at 590 nm. The results represent mean ± SD (n=2).

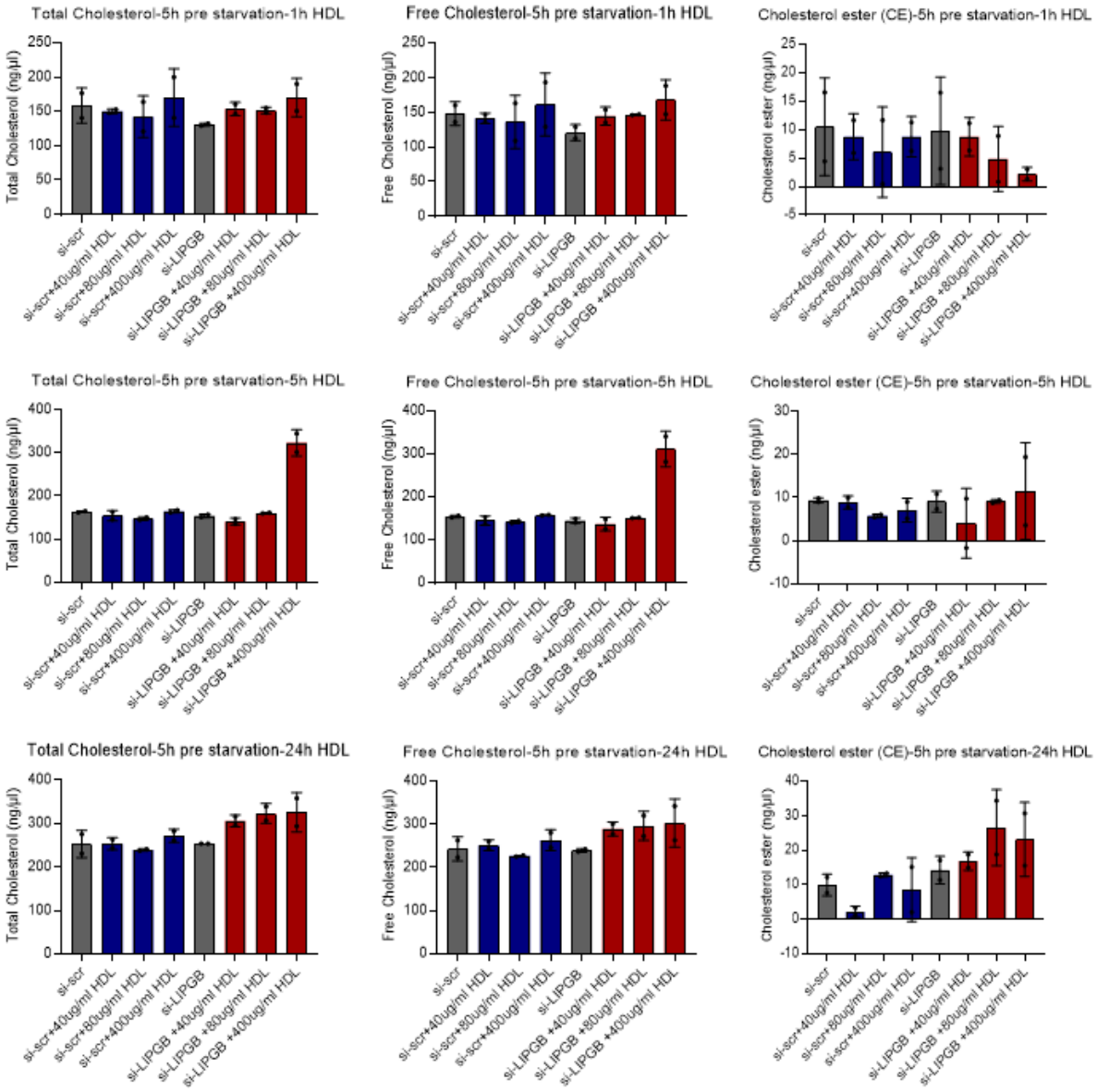

Figure S2: LIPG KD for 72 h in MDA-MB-468, followed by 5 h starvation without FBS. Starved cells were treated with 40 µg/mL, 80 µg/mL or 400 µg/mL HDL for 1 h, 5 h or 24 h. Cholesterol content was measured using Abcam Quantification Kit and fluorescence detection at 590 nm. The results represent mean ± SD (n=2).

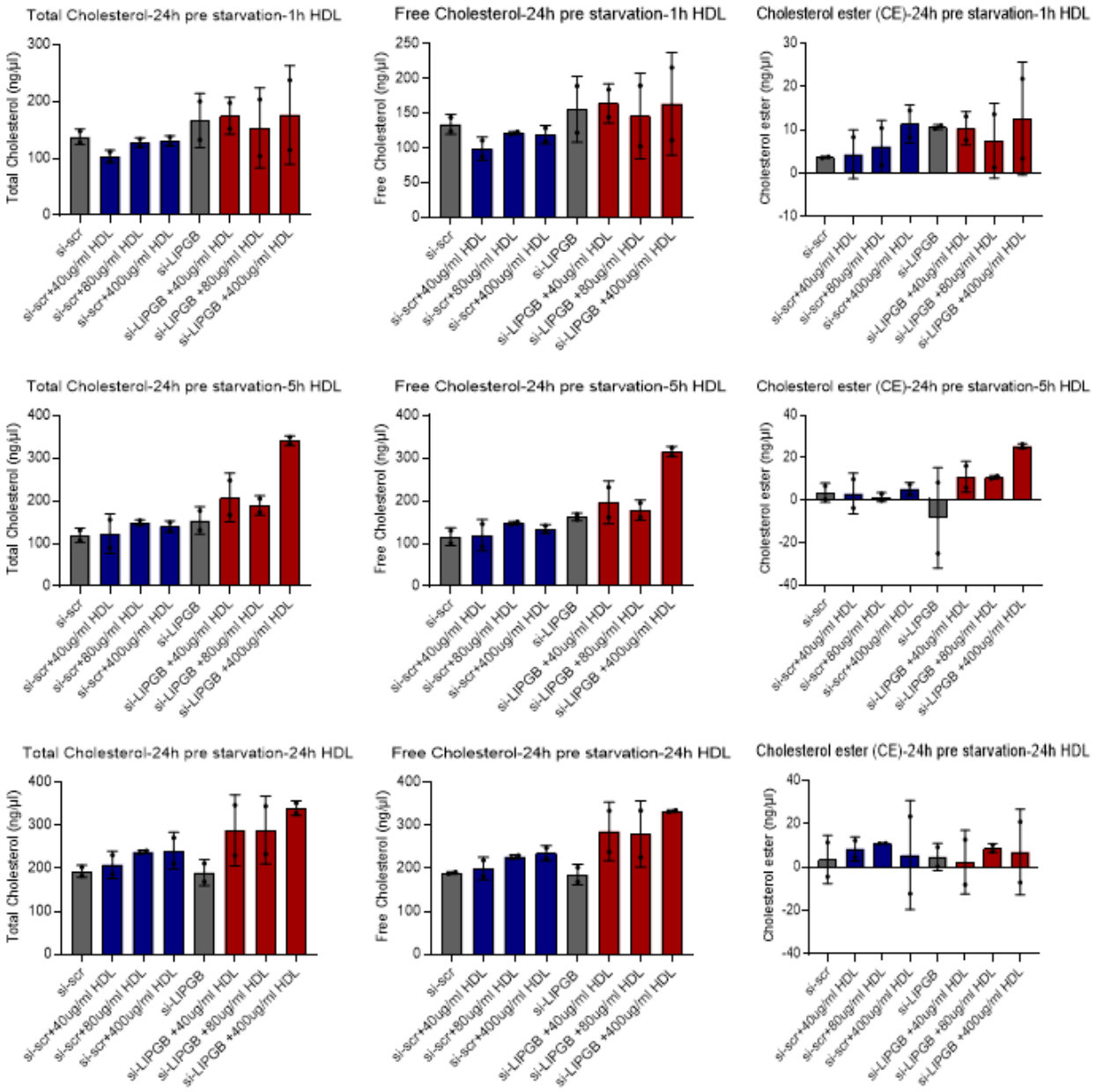

Figure S3: LIPG KD for 72 h in MDA-MB-468, followed by 24 h starvation without FBS. Starved cells were treated with 40 µg/mL, 80 µg/mL or 400 µg/mL HDL for 1 h, 5 h or 24 h. Cholesterol content was measured using Abcam Quantification Kit and fluorescence detection at 590 nm. The results represent mean ± SD (n=2).

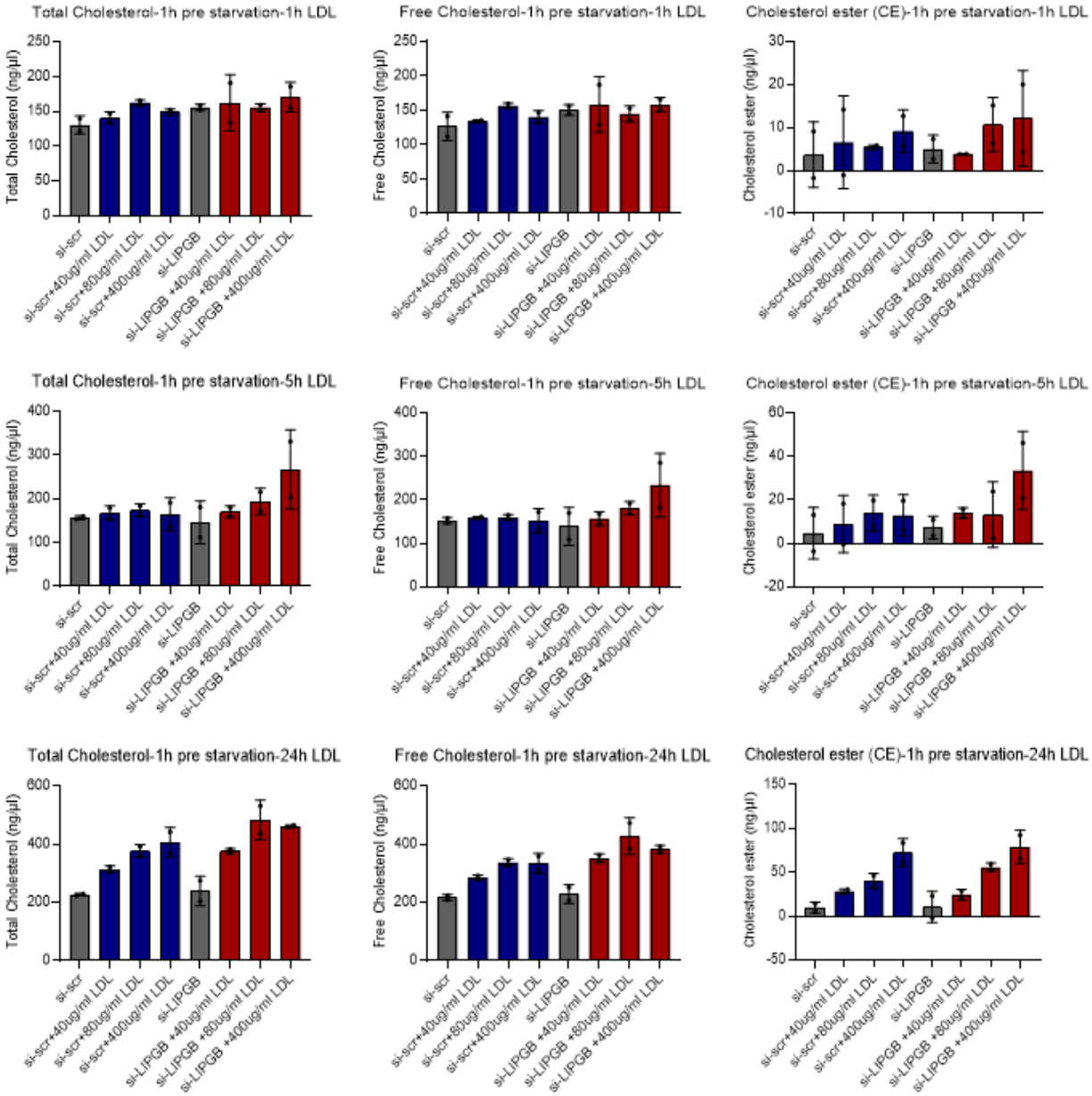

Figure S4: LIPG KD for 72 h in MDA-MB-468, followed by 1 h starvation without FBS. Starved cells were treated with 40 µg/mL, 80 µg/mL or 400 µg/mL LDL for 1 h, 5 h or 24 h. Cholesterol content was measured using Abcam Quantification Kit and fluorescence detection at 590 nm. The results represent mean ± SD (n=2).

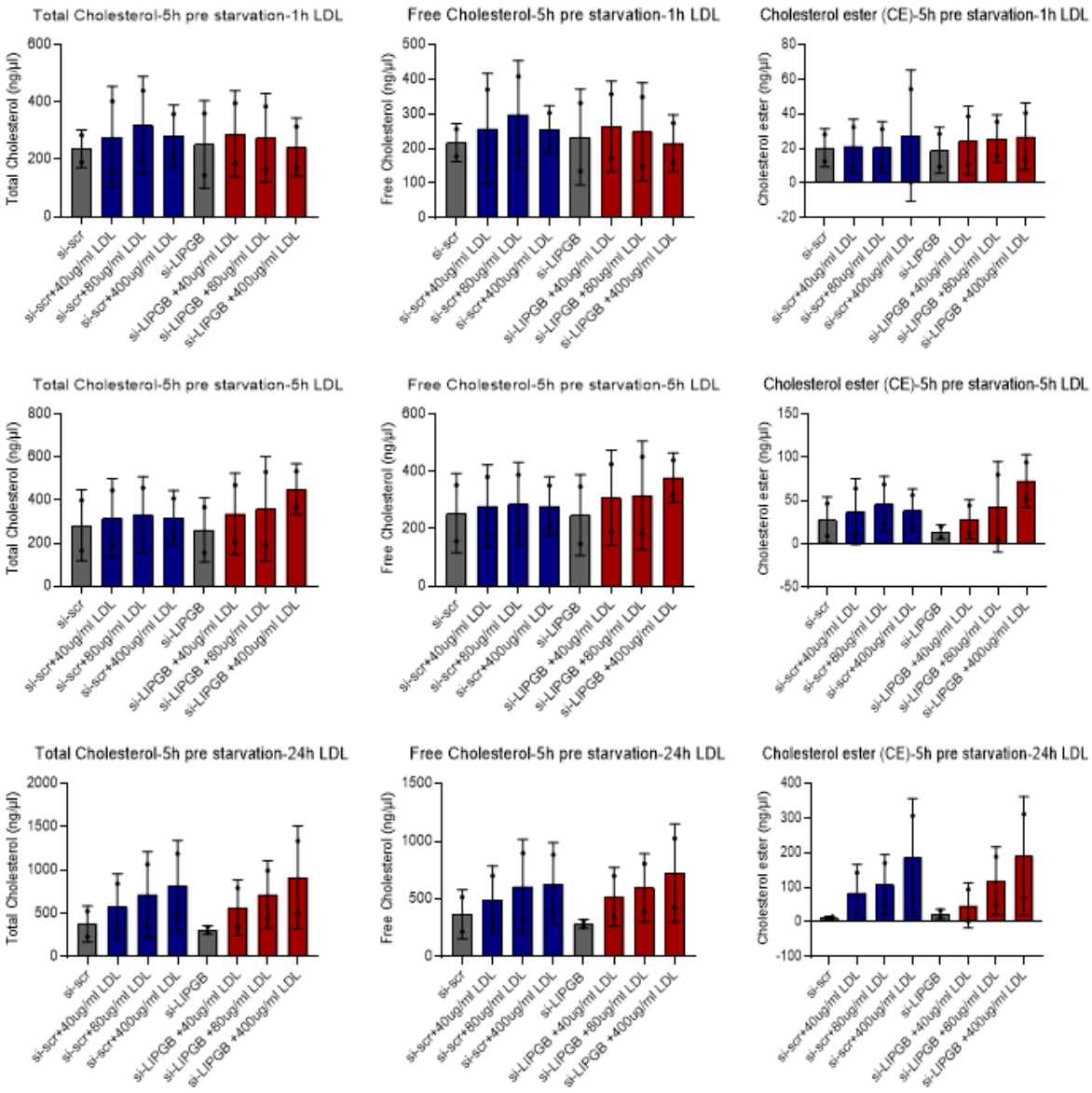

Figure S5: LIPG KD for 72 h in MDA-MB-468, followed by 5 h starvation without FBS. Starved cells were treated with 40 µg/mL, 80 µg/mL or 400 µg/mL LDL for 1 h, 5 h or 24 h. Cholesterol content was measured using Abcam Quantification Kit and fluorescence detection at 590 nm. The results represent mean ± SD (n=2).

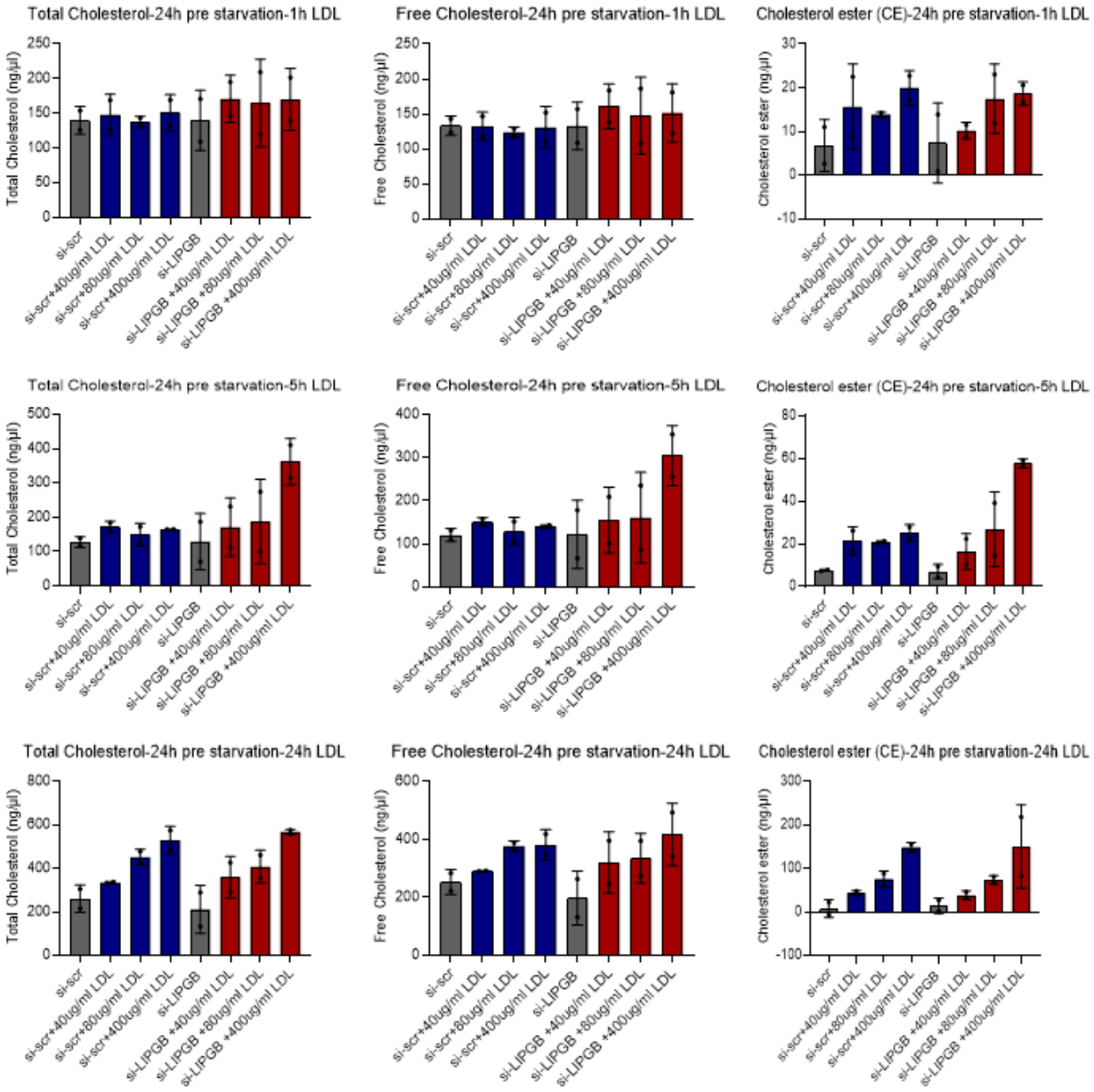

Figure S6: LIPG KD for 72 h in MDA-MB-468, followed by 24 h starvation without FBS. Starved cells were treated with 40 µg/mL, 80 µg/mL or 400 µg/mL LDL for 1 h, 5 h or 24 h. Cholesterol content was measured using Abcam Quantification Kit and fluorescence detection at 590 nm. The results represent mean ± SD (n=2).

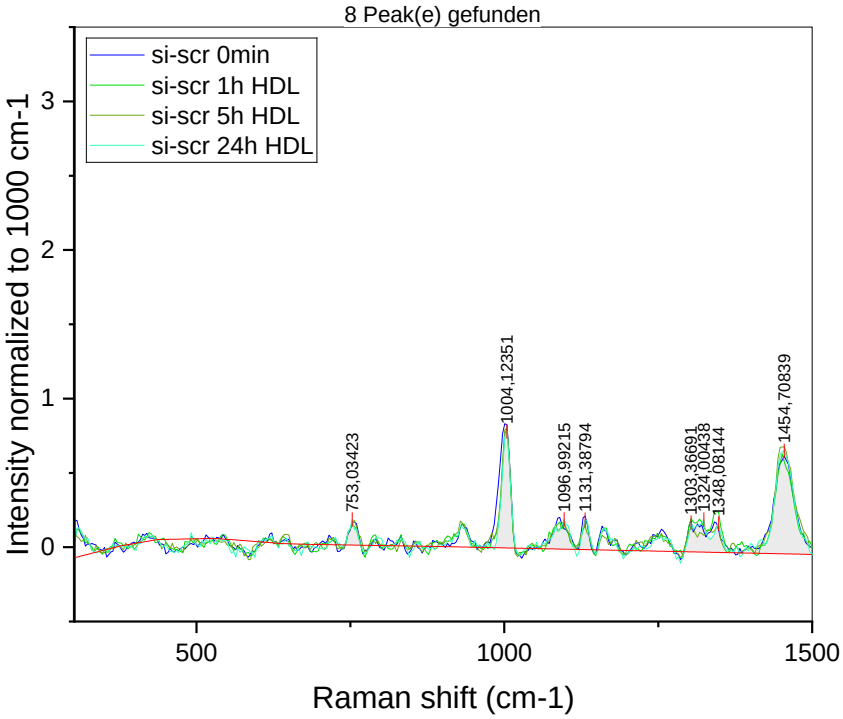

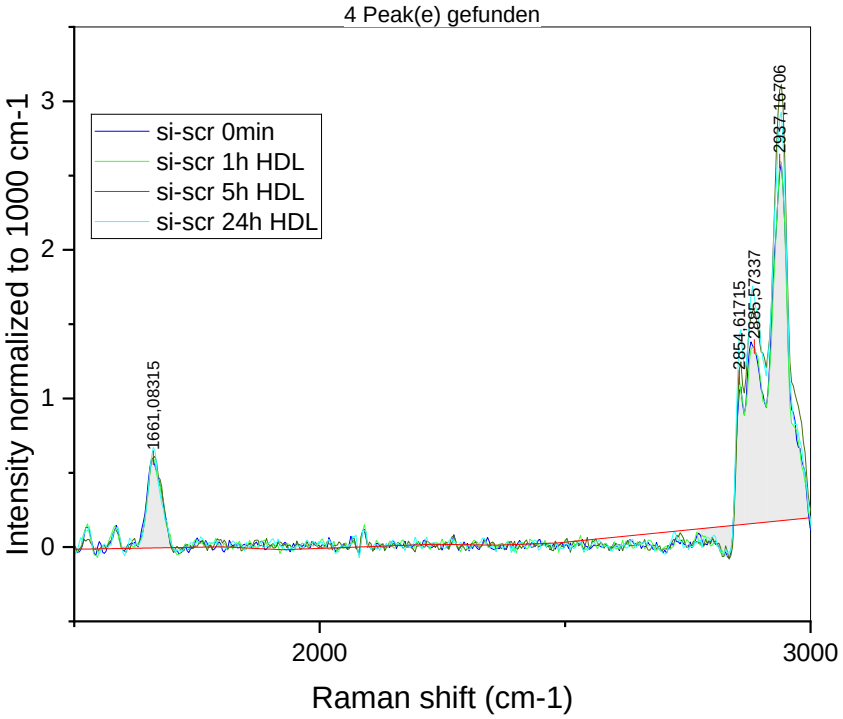

Figure S7: Raman Spectrum in si-scr control cells, 24 h serum starvation and HDL treatment for 1 h, 5 h and 24 h. The results represent mean ± SD (n=3).

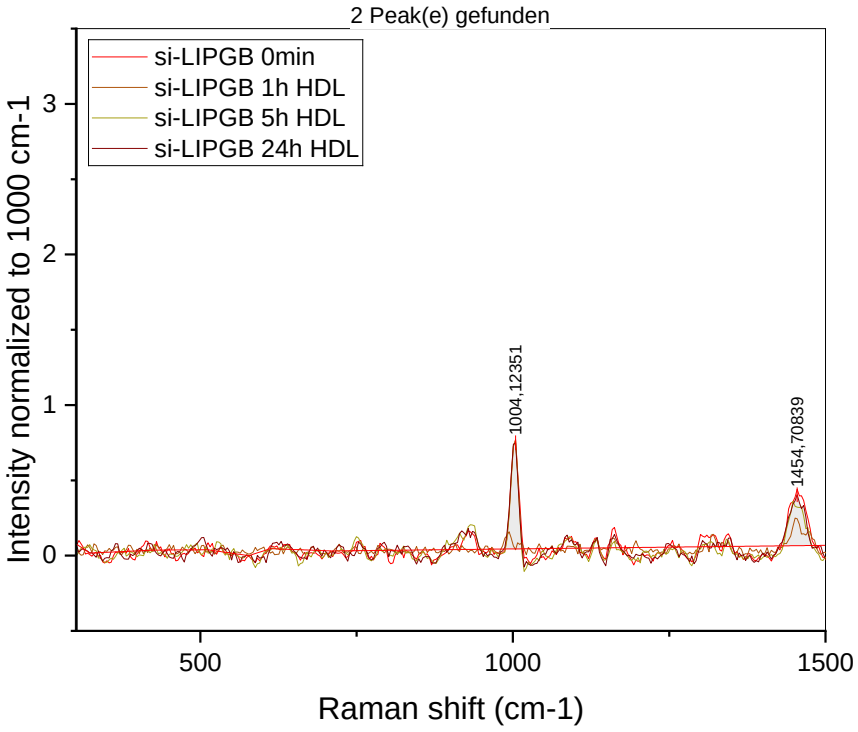

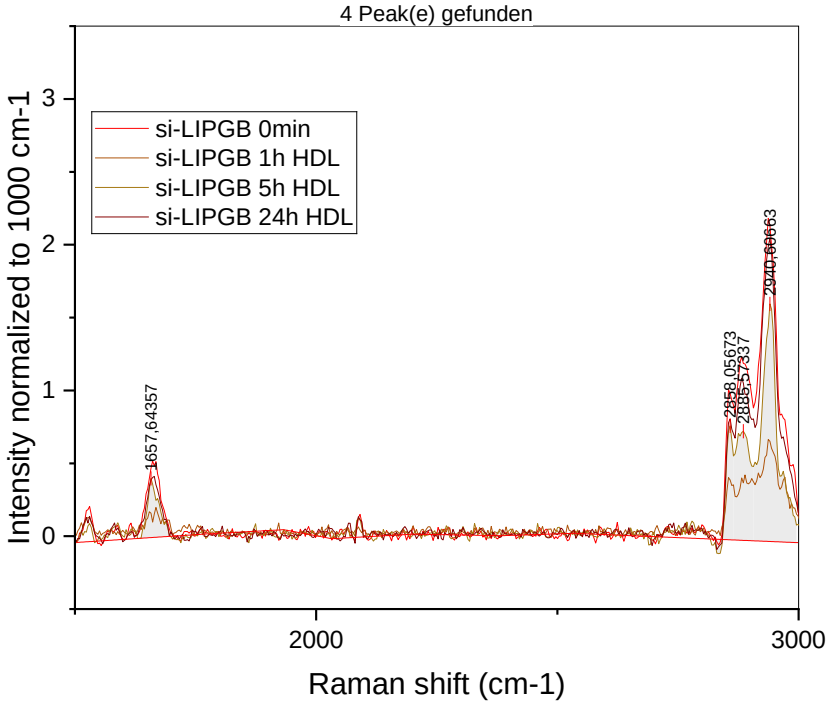

Figure S8: Raman Spectrum after LIPG KD, 24 h serum starvation and HDL treatment for 1 h, 5 h and 24 h. The results represent mean ± SD (n=3).

11. Literature

(1) Cadenas *et. al*., LIPG-promoted lipid storage mediates adaptation to oxidative stress in breast cancer, *Int. J. Cancer*, **2019**, *145(4)*, 901-915

(2) https://www.cancer.org/cancer/types/breast-cancer/about/how-common-is-breast-cancer.html 05.06.24

(3) Guo *et. al.,* Different breast cancer subtypes show different metastatic pattern: A study from a large public data base*, Asian Pac J Cancer Prev.*, **2020**, *21(12)*, 3587–3593

(4) Dai X, Li T, Bai Z *et al*., Breast cancer intrinsic subtype classification, clinical use and future trends. *Am J Cancer Res*., **2015**, 5(10), 2929-2943

(5) https://seer.cancer.gov/statfacts/html/ovary.html 05.06.24

(6) Koshiyama *et. al.,* Subtypes of Ovarian Cancer and Ovarian Cancer Screening, *Diagnostics*, **2017**, *7(1)*, 12

(7) Zhou *et. al*., The Effect of Histological Subtypes on Outcomes of Stage IV Epithelial Ovarian Cancer, *Front. Oncol*., **2018***, 8*, 577

(8) Mitra, Ovarian Cancer Metastasis: A Unique Mechanism of Dissemination, *Tumor Metastasis*, **2016**

(9) Compagni and Christofori, Recent advances in research on multistage tuheregenesis, *British Journal of Cancer*, **2022**, *83(1)*, 1-5

(10) Sidiqui *et. al.,* Resveratrol nanoformulation for cancer prevention and therapy, ANNALS, **2015**, 1348(1)

(11) Seyfried and Huysentruyt, On the Origin of cancer metastasis, *Crit. Rev. Oncog.*, **2013**, *18(1-2)*, 43-37

(12) Valastyan and Weinberg, Tumor Metastasis: Molecular Insights and Evolving Paradigms, *Cell*, **2011**, *147(2),* 275-292

(13) Martin et. al., Cancer Invasion and Metastasis: Molecular and Cellular Perspective, *Madame Curie Bioscience Database*, **2013**

(14) Chambers *et. al*., Dissemination and growth of cancer cells in metastatic sites, *Nat. Rev. Cancer*, **2002**, *2(8)*, 563-572

(15) Paschos *et. al.*, The role of cell adhesion molecules in the progression of colorectal cancer and the development of liver metastasis, *Cellular Signalling*, **2009**, *5(21)*, 665-674

(16) Bendas and Borsig, Cancer Cell Adhesion and Metastasis: Selectins, Integrins, and the Inhibitory Potential of Heparins, *Int. J. Cell Biology*, **2012**

(17) Moorwood *et. al*., The Role of Extracellular Matrix (ECM) Adhesion Motifs in Functionalised Hydrogels, *Molecules*, **2023**, *28(12)*, 4616
(18) Walma and Yamada, The extracellular matrix in development, *Development*, **2020**, *147(10)*
(19) Hynes, Integrins: Bidirectional, Allosteric Signaling Machines, *Cell*, **2002**, *110(6)*, 673-687
(20) Hastings *et. al.*, The extracellular matrix as a key regulator of intracellular signaling networks, *Br. J. Pharmacol*., **2019**, *176(1)*, 82-92
(21) Khalili and Ahmad, A Review of cell adhesion studies for biomedical and biological applications, *Int. J. Mol. Sci*., **2015**, *16(8)*, 18149-18184
(22) Braga, Cell-cell adhesion and signaling, *Current Opinion in Cell Biology*, **2002**, *14(5)*, 546-556
(23) Alberts *et. al*., Molecular Biology of the Cell, *Garland Science*, **2002**
(24) Klezovitch and Vasioukhin, Cadherin signaling: keeping cells in touch, *F1000Res.*, **2015**, *4(550)*
(25) Perez-Moreno *et. al*., Sticky Business: Orchestrating Cellular Signals at Adherens Junctions, *Cell*, **2003**, *112(4)*, 535-548
(26) Murai, The Role of Lipid Rafts in Cancer Cell Adhesion and Migration, *Int. J. Cell Biol.*, **2012**
(27) Lietha and Izard, Roles of Membrane Domains in Integrin-Mediated Cell Adhesion, *Int. J. Mol. Sci*., **2020**, *21(15)*, 5531
(28) Felsenfeld *et. al*., Selective regulation of integrin–cytoskeleton interactions by the tyrosine kinase Src, *Nature Cell Biology*, **1999**, *1*, 200-2006
(29) Leitinger and Hogg, The involvement of lipid rafts in the regulation of integrin function, *J. Cell Sci*., **2002**, *115(5)*, 963-972
(30) Gliozzi *et. al*., Cholesterol homeostasis: Researching a dialogue between the brain and peripheral tissues, *Pharmacological Research*, **2021**, *163*
(31) Coradini, Impact of De Novo Cholesterol Biosynthesis on the Initiation and Progression of Breast Cancer, *Biomolecules*, **2024**, *14(1)*, 64
(32) Kumar *et. al*., Cholesterol Homeostasis, Mechanisms of Molecular Pathways, and Cardiac Health: A Current Outlook, *Current problems in cardiology*, **2024**, *49(1B)*
(33) Afonso *et. al.*, Molecular Pathways Underlying Cholesterol Homeostasis, *Nutrients*, **2018**, *10(6)*, 760

(34) Duan *et. al*., Regulation of cholesterol homeostasis in health and diseases: from mechanisms to targeted therapeutics, *Signal Transduction and Targeted Therapy*, **2022**, *7(265)*

(35) Feingold, Introduction to Lipids and Lipoproteins*, Endotext*, **2024**

(36) Cox and Garcia-Palmieri, Cholesterol, Triglycerides, and Associated Lipoproteins, *Clinical Methods*, **1990**, *31*

(37) Villiers *et. al*., Lipoprotein receptors, *Principles and treatment of lipoprotein disorders*, **1994**, 53-87

(38) Miller *et. al.*, Role of N-linked glycosylation in the secretion and activity of endothelial lipase, *JLR*, **2004**, *45(11)*, 2080-2087

(39) Furi *et al*., Cell Free DNA of Tumor Origin Induces a 'Metastatic' Expression Profile in HT-29 Cancer Cell Line, *PLoS One*, **2015**, *10(7)*

(40) Brown and Goldstein, Receptor-mediated endocytosis: insights from the lipoprotein receptor system*, Proc. Natl. Acad. Sci. USA*, **1979**, *76(7)*, 3330-3337

(41) Gonen and Miller, From Inert Storage to Biological Activity—In Search of Identity for Oxidized Cholesteryl Esters, *Front. Endocrinol*., **2020**, *11*

(42) Chang *et. al*., Acyl-Coenzyme A: cholesterol acyltransferases, *Am. J. Physiol. Endocrinol. Metab*., **2009**, *297(1)*

(43) Favari *et. al*., Cholesterol Efflux and Reverse Cholesterol Transport, *High Density Lipoproteins*, **2014**, 181-206

(44) Segrest *et. al.,* ABCA1 is an extracellular phospholipid translocase, *nature communications*, **2022**, *13(4812)*

(45) Yazdi *et. al*., The role of ATP-binding cassette transporter G1 (ABCG1) in Alzheimer's disease: A review of the mechanisms, *BCDT*, **2024**, *134(4)*, 423-438

(46) Gutierrez-Pajares *et. al*., SR-BI: Linking Cholesterol and Lipoprotein Metabolism with Breast and Prostate Cancer, *Front. Pharmacol*., **2017**, *7*, 338

(47) Marques *et. al*., Reverse Cholesterol Transport: Molecular Mechanisms and the Non-medical Approach to Enhance HDL Cholesterol, *Front. Physiol*., **2018**, *9*, 582

(48) Choi *et. al*., New Strategies to Promote Macrophage Cholesterol Efflux, *Frontiers in Cardiovascular Medicine*, **2021**, *8*

(49) Hanahan and Weinberg, Hallmarks of Cancer: The next Generation, *Cell Press*, **2011**, *144(5)*, 646-674 7(265)

(50) Jin *et. al.,* Lipid metabolic reprogramming in tumor microenvironment: from mechanisms to therapeutics, *Journal of Hematology and Oncology*, **2023**, *16(103)*

(51) Yang et. al., Role of *de novo* cholesterol synthesis enzymes in cancer, J. Cancer, 2020, 11(7), 1761-1767

(52) Giacomini *et. al*., Cholesterol Metabolic Reprogramming in Cancer and Its Pharmacological Modulation as Therapeutic Strategy, *Front. Oncol*., **2021**

(53) Wang *et. al.*, Pre-metastatic niche: formation, characteristics and therapeutic implication, *Signal Transduction and Targeted Therapy*, **2024**, *9(236)*

(54) Ganguli and Kimmelman, Reprogramming of tissue metabolism during cancer metastasis, *Trends Cancer*, **2023**, *9(6)*, 461-471

(55) Perswani *et. al*., Rethinking HDL-C: An In-Depth Narrative Review of Its Role in Cardiovascular Health, *Current Problems in Cardiology*, **2024**, *49(2)*

(56) Santana *et. al.*, Proteomic Profiling of HDL in Newly Diagnosed Breast Cancer Based on Tumor Molecular Classification and Clinical Stage of Disease, *Cells*, **2024**, *13(16)*

(57) Ohashi *et. al*., Reverse cholesterol transport and cholesterol efflux in atherosclerosis, *International Journal of Medicine*, **2005**, *12(98)*, 845-856

(58) Phillips, Molecular Mechanisms of Cellular Cholesterol Efflux, *J. Biol. Chem*., **2014**, *289(35)*, 24020–24029

(59) Brites *et. al*., Antioxidative activity of high-density lipoprotein (HDL): Mechanistic insights into potential clinical benefit, *BBA Clinical*, **2017**, *8*, 66-77

(60) Soran *et. al*., Antioxidant properties of HDL, *Front. Pharmacol*., **2015**, *6(222)*

(61) Eckardtstein and Kardassis, Functionality of HDL: Antioxidation and Detoxifying Effects, *High Density Lipoproteins Springer*, **2014**, 207-228

(62) Weber and Lanci, Lipid peroxidation and cancer, *Cancer Advances*, **2021**, *4(6)*

(63) Krieger, Charting the fate of the "good cholesterol": identification and characterization of the high-density lipoprotein receptor SR-BI, *Annu. Rev. Biochem*., **1999**, *68*, 523-558

(64) Al-Jarallah *et. al*., High density lipoprotein stimulated migration of macrophages depends on the scavenger receptor class B, type I, PDZK1 and

Akt1 and is blocked by sphingosine 1 phosphate receptor antagonists, *PLoS One*, **2014**, *9*, e106487

(65) Trigatti and Fuller, HDL signaling and protection against coronary artery atherosclerosis in mice, *J. Biomed. Res*., **2016**, *30(2)*, 94-100

(66) Eckardstein and Kardassis,: From Biological Understanding to Clinical Exploitation, *High Density Lipoproteins Springer*, **2014**, 229-256

(67) Nishimoto and Nishida, MAPK signaling: ERK5 versus ERK1/2, *EMBO Rep*., **2006**, *7(8)*, 782-786

(68) Paudel *et. al.,* The MEK5/ERK5 Pathway in Health and Disease, *Int. J. Mil. Sci*., **2021**, *22(14)*

(69) Nithianandarajah-Jones *et. al*., ERK5: Structure, regulation and function, *Cellular Signalling*, **2012**, 24(11), 2187-2196

(70) Stecca and Rovida, Impact of ERK5 on the Hallmarks of Cancer, *Int. J. Mol. Sci*., **2019**, *20(6)*, 1426

(71) Sawhney *et. al*., A novel role of ERK5 in integrin-mediated cell adhesion and motility in cancer cells via Fak signaling, *Journal of Cellular Physiology*, **2008**, *219(1)*, 152-161

(72) Takabe *et. al*., “Inside-Out” Signaling of Sphingosine-1-Phosphate: Therapeutic Targets, Pharmacol. Rev., **2008**, *60(2)*, 181–195

(73) Lee *et. al*., S1P in HDL promotes interaction between SR-BI and S1PR1 and activates S1PR1-mediated biological functions: calcium flux and S1PR1 internalization, *J. Lipid. Res*., **2017**, *58(2)*, 325-338

(74) Nofer, Signal Transduction by HDL: Agonists, Receptors, and Signaling Cascades, *Handbook of Experimental Pharmacology*, **2015**, *224*, 229-256

(75) Rebsamen *et. al*., Role of cyclooxygenase 2, p38 and p42/44 MAPK in the secretion of prostacyclin induced by epidermal growth factor, endothelin-1 and angiotensin II in rat ventricular cardiomyocytes, *J. Mol. Cell Cardiol*., **2003**, *35(1)*, 81-89

(76) Comita *et. al*., Regulation of STAT3 and its role in cardioprotection by conditioning: focus on non-genomic roles targeting mitochondrial function, *Basic Res. Cardiol*., **2021**, *116(1)*, 56

(77) Cristea *et. al*., The MEK5-ERK5 kinase axis controls lipid metabolism in small cell lung cancer, *Cancer Res*., **2020**, *80(6)*, 1293-1303

(78) Khan *et. al*., The PDK1 Inhibitor Dichloroacetate Controls Cholesterol Homeostasis Through the ERK5/MEF2 Pathway, *Sci. Rep*., **2017**, *7*

(79) Skropeta *et. al.*, *N*-Glycosylation regulates endothelial lipase-mediated phospholipid hydrolysis in apoE- and apoA-I-containing high-density lipoproteins, *JLR*, **2007**, *48(9)*, 2047-2057

(80) Gauster *et. al*., Endothelial lipase is inactivated upon cleavage by the members of the proprotein convertase family, *JLR*, **2005**, *46(5)*, 977-987

(81) Griffon *et. al.,* Identification of the Active Form of Endothelial Lipase, a Homodimer in a Head-to-Tail Conformation, *J. Biol. Chem*., **2009**, *284(35)*, 23322-23330

(82) Choi *et. al.*, Endothelial lipase, *JLR*, **2002**, *43(11)*, 1763-1769

(83) Arora *et. al*., Structure of lipoprotein lipase in complex with GPIHBP1, *PNAS*, **2019**, *116(21)*, 10360-10365

(84) McGoy *et. al.*, Characterization of the lipolytic activity of endothelial lipase, *JLR*, **2002**, *43(6)*, 921-929

(85) Patricia G. Yancey *et. al*., High Density Lipoprotein Phospholipid Composition Is a Major Determinant of the Bi-directional Flux and Net Movement of Cellular Free Cholesterol Mediated by Scavenger Receptor BI, *The Journal of Biological Chemistry*, **2000**, *275(47)*, 6596 –36604

(86) Strauss *et. al.*, Endothelial cell-derived lipase mediate275(47)s uptake and binding of high-density lipoprotein (HDL) particles and the selective uptake of HDL-associated cholesterol esters independent of its enzymic activity, *Biochem. J.*, **2002**, *368(1)*, 69-79

(87) Pagler *et. al.*, SR-BI-mediated High-Density Lipoprotein (HDL) Endocytosis Leads to HDL Resecretion Facilitating Cholesterol Efflux, *Journal of biological chemistry*, **2006**, *281(16)*, 11193-11204

(88) Power and Sahoo, SR-B1's Next Top Model: Structural Perspectives on the Functions of the HDL Receptor, *Vascular Biology*, **2022**, *24*, 277-288

(89) Nijstad *et. al.*, Scavenger Receptor BI-mediated Selective Uptake Is Required for the Remodeling of High-Density Lipoprotein by Endothelial Lipase, *JBC*, **2009**, *284(19)*, 6093-6100

(90) Lewis and Rader, New Insights into the Regulation of HDL Metabolism and Reverse Cholesterol Transport, *Circulation Research*, **2005**, *96(12)*, 1221-1232

(91) Gauster *et. al*., Endothelial lipase-modified high-density lipoprotein exhibits diminished ability to mediate SR-BI (scavenger receptor B type I)-dependent free-cholesterol efflux, *Biochem. J.*, **2004**, *282(1)*, 75-82

(92) Takaguchi *et. al*., Hepatic Overexpression of Endothelial Lipase Lowers High-Density Lipoprotein but Maintains Reverse Cholesterol Transport in Mice: Role of Scavenger Receptor Class B Type I/ATP-Binding Cassette Transporter A1-Dependent Pathways, *Arterioscler. Thromb. Vasc. Biol*., **2018**, *38(7)*,1454-1467

(93) Qiu G, Hill JS, Endothelial lipase promotes apolipoprotein AI-mediated cholesterol efflux in THP-1 macrophages, *Arterioscler. Thromb. Vasc. Biol*., **2009**, *29(1)*, 84-91

(94) Tatematsu *et. al*., Endothelial lipase is a critical determinant of HDL-stimulated sphingosine 1-phosphate-dependent signaling in vascular endothelium, *Arterioscler. Thromb. Vasc. Biol*., **2013**, *33(8)*, 1788–1794

(95) Zho *et. Al*., Reprogramming of fatty acid metabolism in breast cancer: a narrative review, *TBCR*, **2021**

(96) Havas KM *et al*., Metabolic shifts in residual breast cancer drive tumor recurrence, *J Clin Invest,* **2017**,*127*, 2091-105

(97) Justine *et. al*., The Role of Endothelial Lipase in Lipid Metabolism, Inflammation, and Cancer, *Histol. Histopathol*., **2018**, *33(1)*, 1-10

(98) Slebe *et. al*., FoxA and LIPG endothelial lipase control the uptake of extracellular lipids for breast cancer growth, *Nature Communications*, **2016**, *7*, 11199

(99) Lo *et. al*., LIPG signaling promotes tumor initiation and metastasis of human basal-like triple-negative breast cancer, *Elife*, **2018**, *7*, e31334

(100) Yuan Y *et al*., The Functional Roles of ISG15/IS Gylation in Cancer, *Molecules*, **2023**, *28(3)*, 1337

(101) Santos *et. al*., The impact of lipid metabolism on breast cancer: a review about its role in tumorigenesis and immune escape, *Cell Communication and Signaling*, **2023**, *21(161)*

(102) Vona *et. al*., Role of Cholesterol and Lipid Rafts in Cancer Signaling: A Promising Therapeutic Opportunity?, *Front. Cell Dev. Biol*., **2021**, *9*

(103) Linton *et. al*., The Role of Lipids and Lipoproteins in Atherosclerosis, *Endocrinology*, **2019**

(104) Dana *et. al*., Molecular Mechanism and Biological Functions of si-RNA, *Int. J. Biomed. Sci*., **2017**, *13(2)*, 48-57

(105) thermofisher.com/de/de/home/life-science/pcr/real-time-pcr/real-time-pcr-learning-center/real-time-pcr-basics/essentials-real-time-pcr.html

(106) Orlando *et. al*., A Comprehensive Review on Raman Spectroscopy Applications, *Chemosensors*, **2021**, *9(9)*, 262

(107) thermofisher.com/de/de/home/life-science/pcr/real-time-pcr/real-time-pcr-learning-center/real-time-pcr-basics/essentials-real-time-pcr.html

(108) Orlando *et. al*., A Comprehensive Review on Raman Spectroscopy Applications, *Chemosensors*, **2021**, *9(9)*, 262

(109) Schneeweiss *et. al.*, Diagnosis and Therapy of Triple-Negative Breast Cancer (TNBC) – Recommendations for Daily Routine Practice, *Geburtshilfe Frauenheilkd.*, **2019**, 79(6), 605-617

(110) Exman and Tolaney, HER2-positive metastatic breast cancer: a comprehensive review, *Clin. Adv. Hematol. Oncol*., **2021**, *19(1)*, 40-50

(111) Mahmoud, The role of LIPG in cell adhesion in breast cancer, *Master thesis*, **2019**

(112) Cerqueira *et. al*., Prognostic value of integrin αV expression and localization pattern in invasive breast carcinomas, *Neoplasia*., **2022**, *30*, 100803

(113) Liu *et. al.*, Integrins in cancer: Emerging mechanisms and therapeutic opportunities, *Pharmacology and Therapeutics*, **2023**, *247*, 109458

(114) Provenzano and Keely, The role of focal adhesion kinase in tumor initiation and progression, *Cell Adh. Migr*., **2009**, *3(4)*, 347-350

(115) Haake *et. al*., Integrating integrins with the hallmarks of cancer, *Matrix Biology*, **2024**, *130*, 20-35

(116) Gomez-Cuadrado *et. al.*, Mouse models of metastasis: progress and prospects, *Dis. Model. Mech*., **2017**, *10(9)*, 1061-1074

(117) Leblond *et. al*., Pre-clinical whole-body fluorescence imaging: Review of instruments, methods and applications, *Journal of Photochemistry and Photobiology*, **2010**, *98(1)*, 77-94

(118) Fan *et. al*., The overall process of metastasis: From initiation to a new tumor, *Biochimica et Biophysica Acta*, **2022**, *1877(4)*, 188750

(119) Norman *et. al*., Modification of Cellular Cholesterol Content Affects Traction Force, Adhesion and Cell Spreading, *Cell Mol. Bioeng*., **2010**, *3(2)*, 151-162

(120) Sun *et. al*., The effect of cellular cholesterol on membrane-cytoskeleton adhesion, *J. Cell Sci*., **2007**, *120(13)*

(121) Sohn *et. al*., Influence of cholesterol/caveolin-1/caveolae homeostasis on membrane properties and substrate adhesion characteristics of adult human mesenchymal stem cells, *Stem Cell Research and Therapy*, **2018**, *9(86)*

(122) Langan and Chou, Synchronization of mammalian cell cultures by serum deprivation, *Methods Mol. Biol*., **2011**, *761*, 75-83

(123) de Cássia Fernandes Borges *et. al*., Detecting alterations of glucose and lipid components in human serum by near-infrared Raman spectroscopy, *Res. Biomed. Eng*., **2015**, *31(2)*

(124) Czamara et. al., Raman spectroscopy of lipids: a review, J. Raman Spectros., 2015, 46, 4-20

(125) Ji *et. al*., Deregulation of Lipid Metabolism: The Critical Factors in Ovarian Cancer, *Front. Oncol*., **2020,** *10*

(126) He *et. al*., Aberrant Cholesterol Metabolism in Ovarian Cancer: Identification of Novel Therapeutic Targets, *Font. Oncol*., **2021**, *11*, 738177

(127) Mohammadalipour *et. al*., Cholesterol depletion decreases adhesion of non-small cell lung cancer cells to E-selectin, *Am. J. Physiol. Cell Physiol*., **2023**, *325(2)*, 471-482

(128) Fu *et. al*., Cholesterol increases adhesion of monocytes to endothelium by moving adhesion molecules out of caveolae, *BBA-Molecular and Cell Biology of Lipids*, **2010**, 702-710

(129) Dorsch *et. al*., Statins affect cancer cell plasticity with distinct consequences for tumor progression and metastasis, *Cell Reports*, **2021**

(130) Danilo *et. al*., Scavenger receptor class B type I regulates cellular cholesterol metabolism and cell signaling associated with breast cancer development, *Breast Cancer Res*, **2013**, *15(5)*

(131) Takahashi *et. al*., ORP2 couples LDL-cholesterol transport to FAK activation by endosomal cholesterol/PI(4,5)P2 exchange, *EMBO J*., **2021**, *40(14)*, e106871

(132) Gibbs *et. al*., Signal transduction responses to lysophosphatidic acid and sphingosine 1-phosphate in human prostate cancer cells, *Prostate*, **2009**, *69(14)*, 1493-506

(133) He *et. al*., Aberrant Cholesterol Metabolism in Ovarian Cancer: Identification of Novel Therapeutic Targets, *Front. Oncol*., **2021**, *11*, 738177

(134) Henkels and Turchi, Induction of apoptosis in cisplatin-sensitive and -resistant human ovarian cancer cell lines, *Cancer Res.,* **1997**, *57(20)*, 4488-4492

12. Eidesstaatliche Versicherung/Affidavit

NAME: Zhwan Mahmoud **Matrikelnummer:** 177249

Ich versichere hiermit an Eides statt, dass ich die vorliegende Dissertation mit dem folgenden Titel:

The role of LIPG in regulating cholesterol homeostasis in cancer.

selbstständig und ohne unzulässige fremde Hilfe erbracht habe. Ich habe keine anderen als die angegebenen Quellen und Hilfsmittel benutzt sowie wörtliche und sinngemäße Zitate kenntlich gemacht. Die Arbeit hat in gleicher oder ähnlicher Form noch keiner Prüfungsbehörde vorgelegen.

_____ _____

Ort, Datum **Unterschrift**

Belehrung: Wer vorsätzlich gegen eine die Täuschung über Prüfungsleistungen betreffende Regelung einer Hochschulprüfungsordnung verstößt, handelt ordnungswidrig. Die Ordnungswidrigkeit kann mit einer Geldbuße von bis zu 50.000,00 € geahndet werden. Zuständige Verwaltungsbehörde für die Verfolgung und Ahndung von Ordnungswidrigkeiten ist der Kanzler/die Kanzlerin der Technischen Universität Dortmund. Im Falle eines mehrfachen oder sonstigen schwerwiegenden Täuschungsversuches kann der Prüfling zudem exmatrikuliert werden. (§ 63 Abs. 5 Hochschulgesetz - HG -). Die Abgabe einer falschen Versicherung an Eides statt wird mit Freiheitsstrafe bis zu 3 Jahren oder mit Geldstrafe bestraft. Die Technische Universität Dortmund wird gfls. elektronische Vergleichswerkzeuge (wie z.B. die Software „turnitin“) zur Überprüfung von Ordnungswidrigkeiten in Prüfungsverfahren nutzen.

Die obenstehende Belehrung habe ich zur Kenntnis genommen:

_____ _____

Ort, Datum **Unterschrift**